Sudan University of Science and Technology

College of Graduate Studies

Estimation of Non-Small Cell Lung Carcinoma Gross Target Volume Using Fluorine-18 Fluorodeoxyglucose Positron Emission Tomography

تقدير الحجم الاجمالي المستهدف لسرطان الرئة ذو الخلايا غير الصغيرة باستخدام فحص التصوير المقطعي بالانبعاث البوزيتروني بالفلور

A thesis Submitted for the Fulfillment of Ph.D. Degree in Medical Radiation Physics

By:

Sami Yahia Ibrahim Awadain

Supervisors:

Prof. Dr. Mohammed Elfadil Mohamed Gar Elnabi

2021

قال تعالي:

فَتَعَالَى اللَّهُ الْمَلِكُ الْحَقُّ ۗ وَلَا تَعْجَلْ

بِالْقُرْآنِ مِن قَبْلِ أَن يُقْضَىٰ إِلَيْكَ

وَحْيُهُ ۖ وَقُل رَّبِّ زِدْنِي عِلْمًا

سورة طه الآية{114}

Dedication

To my family

To soul of my mother

Acknowledgements

Firstly I would like to thank Prof Mohamed Elfadil for giving me the wonderful opportunity to complete my Ph.D. thesis under his supervision, it is truly an honor. Thank you for all the advice, ideas, moral support and patience in guiding me through this project. Thank you for your enthusiasm for the study. Your wealth of knowledge in the field and medical physics in particular is inspiring. Special thanks should also be given to Dr Suhaib Alameen. Thank you for your all efforts and help without it I will not reach this point

Abstract

The aim of the study is to estimate and identify the GTV of NSCLC with fluorine-18 fluorodeoxyglucose (^{18}F-FDG) positron emission tomography (PET) scan instead of using the CT imaging, The PET scan so useful in estimation of sub mucosal extension of the tumor as well as in staging and restaging of lung carcinomas and changing in gross target volume either positively (+) or negatively (-).

This study was conducted in Kuwait Cancer Control Center (kccc) in Kuwait City, during the period 2016 to 2018.

The study sample included 156 patients with non- small cell lung carcinoma underwent whole body PET/CT scan.

The features extracted from PET/CT images using Second order statistic and All these features were calculated for all images and then the data were ready for discrimination which was performed using step-wise technique in order to select the most significant feature that can be used to classify the lung cells from PET/CT images and the results show that The classification showed that the lung cells were classified well from the rest of the tissues although it has characteristics mostly similar to surrounding tissue. The classification score matrix generated by linear discriminate analysis and the overall classification accuracy of lung cells 96.0%, were the classification accuracy of cardiac 91.6%, lung accuracy 100%, the tumor 99.6%, While the submucosal showed a classification accuracy of 91.2%.

Texture analysis depending on the relative attenuation coefficient of tissues and can used to avoid invasive technique if the base line for individual tissues being determined and algorithmic aided computer have been applied.

الخلاصة

الهدف من الدراسة هو تقدير وتحديد الحجم الهدف لسرطان الرئة ذو الخلايا غير الصغيرة باستخدام فحص التصوير المقطعي النووي البوزيترونى المدمج مع عنصر الفلور المشع 18 بدلا عن التصوير المقطعي المحوسب. والمسح النووي البوزيتروني مفيد جدا في تقدير امتداد الغشاء المخاطي الفرعي للورم وكذلك في تنظيم وتكرار سرطانات الرئة والتغيير في الحجم الإجمالي المستهدف اما بشكل إيجابي (+) او سلبا (-)

أجريت هذه الدراسة في مركز الكويت لمكافحة السرطان (kccc) في مدينة الكويت، خلال الفترة من 2016 إلى 2018.

تضمنت عينة الدراسة 156 مريضًا مصابًا بسرطان الرئة ذو الخلايا غير الصغيرة وخضعوا لفحص المسح النووي البوزيترونى المدمج مع التصوير المقطعي المحوسب لكامل الجسم.

الميزات المستخرجة من صور المسح النووي البوزيترونى المدمج مع التصوير المقطعي المحوسب باستخدام إحصائية من الدرجة الثانية وتم حساب كل هذه الميزات لجميع الصور ثم أصبحت البيانات جاهزة للتمييز الذي تم إجراؤه باستخدام تقنية التدرج من أجل تحديد أهم ميزة يمكن استخدامها يصنف خلايا الرئة من صور المسح النووي البوزيترونى المدمج مع التصوير المقطعي المحوسب وأظهرت النتائج أن التصنيف أظهر أن خلايا الرئة تم تصنيفها جيدًا من باقي الأنسجة على الرغم من أن لها خصائص مشابهة في الغالب للأنسجة المحيطة. مصفوفة درجات التصنيف الناتجة عن تحليل التمييز الخطي ودقة التصنيف الكلية لخلايا الرئة 96.0٪، دقة تصنيف القلب 91.6٪، دقة الرئة 100٪، الورم 99.6٪، بينما الغشاء المخاطي أظهر دقة تصنيف 91.2٪.

يعتمد تحليل النسيج على معامل التوهين النسبي للأنسجة ويمكن استخدامه لتجنب التقنية الغازية إذا تم تحديد خط الأساس للأنسجة الفردية وتم تطبيق الكمبيوتر بمساعدة الخوارزمية.

List of tables

List of Figures

List of abbreviation

PET	Positron Emission Tomography
CT	Computerized Tomography
^{18}F	Flourine-18
FDG	Fluoro-Deoxy-Glucose
RT	Radiotherapy
MRI	Magnetic Resonance imaging
ICRU	International Commission on Radiation
GTV	Gross Tumour Volume
CTV	Clinical Target Volume
PTV	Planning Target Volume
MTV	Metabolic Tumor Volume
EPIDs	Electronic Portal Imaging Devices
IGRT	Image-Guided Radio-Therapy
ROI	Region Of Interest
NSCLC	Non-Small Cell Lung Carcinoma
SCLC	Small Cell Lung Carcinoma
SPN	Solitary Pulmonary Nodule
EOS	End Of Synthesis
RLD	Reference Listed Drug
MBq	Mega-Becquerel
mci	Milli-Curie

rem	Roentgen Equivalent Man
mGy	milligray
ml	milliliter
mR	milli-Roentgen
rad	Absorbed Radiation Dose
Sv	Sieverts
mSv	milli-Sieverts
MSCT	Multi-Slice Computerizes Tomography
SSCT	Single-Slice Computerized Tomography
MDCT	Multi-Detector Computerized Tomography
mA	Milliampere
mAs	milliampere-seconds
MPR	Multi-Planar Reformation
kV	Kilo-voltage
kVp	Kilo-Voltage Peak
AEC	Automatic Exposure Control
ATCM	Automatic Tube Current Modulation
ECG	Electro Cardio Graphy
ALARA	As Low As Reasonably Achievable
AAPM	American Association of Physicists in Medicine
SSP	Slice Sensitivity Profile

CTDI Computerized Tomography Dose Index

$CTDI_{100}$ Computerized Tomography Dose Index 100

$CTDI_{w}$ Computerized Tomography Dose weighted Index

$CTDI_{vol}$ Computerized Tomography Dose Index volume

TLD Thermo Luminescence Dosimeter

MSAD Multiple Scan Average Dose

DLP Dose Length Product

FOV Field Of View

CTA CT angiography

SNR Signal-to-Noise Ratio

LET Linear Energy Transfer

SUV Standardized Uptake Values

OSEM Ordered Subset Expectation Maximization

AC Attenuation Correction

PACS Picture Archiving and Communication System

DICOM Digital Imaging and Communications in Medicine

BMI Body Mass Index

IDL Interactive Data Language

FBS Fasting Blood Sugar

CHAPTER ONE

1.1 Introduction

Positron emission tomography (PET) is a nuclear imaging technique that uses the unique decay characteristics of radionuclides that decay by positron emission. These radionuclides are produced in a cyclotron and are then used to label compounds of biological interest. The labeled compound (typically 10^{13}-10^{15} labeled molecules) is introduced into the body, usually by intravenous injection, and is distributed in tissues in a manner determined by its biochemical properties. A PET scan play great role in measuring important body functions, such as blood flow, oxygen use, and sugar (glucose) metabolism, to show and evaluate how well organs and tissues are functioning .When the radioactive atom on a particular molecule decays, a positron is ejected from the nucleus, ultimately leading to the emission of high-energy photons that have a good probability of escaping from the body. A PET scanner consist of a set of detectors that surround the object to be imaged and are designed to convert these high-energy photons into an electrical signal that can be fed to subsequent electronics. In a typical PET scan, 10^6 to 10^9 events (decays) will be detected. These events are corrected for a number of factors and then reconstructed into a tomographic image using mathematical algorithms. The output of the reconstruction process is a three-dimensional (3-D) image volume, where the signal intensity in any particular image voxel (is a volume element in a three-dimensional image array. It is analogous to a pixel in a two-dimensional image array) is proportional to the amount of the radionuclide (and, hence, the amount of the labeled molecule to which it is attached) in that voxel. Thus, PET images allow the spatial distribution of radiolabeled tracers to be mapped quantitatively in a living human. By taking a time sequence of images, the tissue concentration of the

radiolabeled molecules as a function of time is measured, and with appropriate mathematical modeling, the rate of specific biological processes can be determined (Michael E. Phelps 2006).

Radiation therapy or radiotherapy is therapy using ionizing radiation as one of the three established cancer treatment modalities is used to treat most types of solid tumors and selected hematologic malignancies. It is used almost entirely to treat malignant disease, although it has a small role in preventing proliferation in benign disease, Radiation therapy may be curative in a number of types of cancer if they are localized to one area of the body. Radiation therapy is routinely combined with surgery, chemotherapy, or both to improve therapeutic results. It is often used with surgery to destroy microscopic regions of tumor extension and with chemotherapy to more effectively destroy the primary tumor. An understanding of the therapeutic use of ionizing radiation requires a basic comprehension of both the physics of radiation therapy delivery and the biological effects of the interaction of radiation with matter.The toxic biological effects of ionizing radiation, although complex, varied, and incompletely understood, form the basis for the use of radiation therapy as a cancer treatment. These biological effects are initiated when packets of energy are deposited in a volume of tissue and remove electrons from constituent atoms through a process called ionization. Ionizing radiation works by damaging the DNA of cancerous tissue leading to cellular death. Accordingly, the physics of radiation oncology is focused on the details of how, where, and how much energy can be deposited in diseased tissue in the hopes of eradicating it, while simultaneously minimizing the energy released in healthy tissue. This process requires an understanding of the nature of the radiation and the matter through which it passes and how that matter is changed as a result of the energy deposition events (Elaine et al 2014).

To spare normal tissues (such as skin or organs which radiation must pass through to treat the tumor), shaped radiation beams are aimed from several angles of exposure to intersect at the tumor, providing a much larger absorbed dose there than in the surrounding, healthy tissue. Besides the tumor itself, the radiation fields may also include the draining lymph nodes if they are clinically or radio logically involved with tumor, or if there is thought to be a risk of subclinical malignant spread. It is necessary to include a margin of normal tissue around the tumor to allow for uncertainties in daily set-up and internal tumor motion. These uncertainties can be caused by internal movement (for example, respiration and bladder filling) and movement of external skin marks relative to the tumor position. So radiotherapy is, by its nature, a localized treatment for localized tumors, following staging radiotherapy planning requires very specific definition of the location and extent of the primary tumor. Information is also required about the extent of spread around the tumor itself, and the location of regional lymph node spread. Knowledge of anatomy and an understanding of the pathology of tumor spread are essential. Better imaging produces better staging, it is clear that diagnostic imaging guides the definition of the tumor extent in almost all sites. However, for a successful outcome after radiotherapy, every single tumor cell must be eradicated, including those which have invaded beyond gross, palpable or image able disease. In radiotherapy planning, therefore, a margin must be added to account for this microscopic spread. This margin extends outside the gross tumor, sometimes for a surprisingly large distance. (Michael I. Lewis et al 2010)

A common international language for describing target volumes is found in

International Commission on Radiation Units (ICRU) published recommendations Report 50 (1993), 62 (1999) and 71 (2004). These contain clear definitions to enable centers to use the same criteria for delineating tumours for radiation so that their treatment results can be compared.

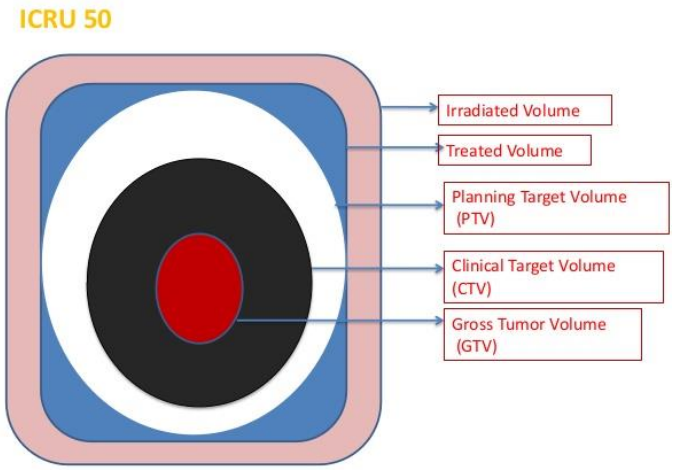

Figure 1.1 ICRU target volume definitions GTV, CTV, PTV, treated and irradiated volume. Reproduced with permission from ICRU (1993) Prescribing, Recording and Reporting Photon Beam Therapy. ICRU report 50.

Gross tumour volume

Gross tumour volume (GTV) is the primary tumour or other tumour mass shown by clinical examination, at examination under anaesthetic (EUA) or by imaging.

GTV is classified by staging systems such as TNM (UICC), AJCC or FIGO.

Tumour size, site and shape may appear to vary depending on the imaging technique used and an optimal imaging method for each particular tumour site must therefore also be specified. A GTV may consist of primary tumour (GTV-T)

and/or metastatic lymphadenopathy (GTV-N) or distant metastases (GTV-M). GTV always contains the highest tumour cell density and is absent after complete surgical resection.

Clinical target volume

Clinical target volume (CTV) contains the GTV when present and/or subclinical microscopic disease that has to be eradicated to cure the tumour. CTV definition is based on histological examination of post mortem or surgical specimens assessing extent of tumour cell spread around the gross GTV, as described by Holland et al. (1985) for breast cancer. The GTV-CTV margin is also derived from biological characteristics of the tumour, local recurrence patterns and experience of the radiation oncologist. A CTV containing a primary tumour may lie in continuity with a nodal GTV/CTV to create a CTV-TN (e.g. tonsillar tumour and ipsilateral cervical nodes). When a potentially involved adjacent lymph node which may require elective irradiation lies at a distance from the primary tumour, separate CTV-T and CTV-N are used (Fig. 1.2), e.g. an anal tumour and the inguinal nodes.

CTV can be denoted by the dose level prescribed, as for example, CTV-T50 for a particular CTV given 50 Gy. For treatment of breast cancer, three CTVs may be used for an individual patient: CTV-T50 (50 Gy is prescribed to the whole breast); CTV-T66 (66 Gy to the tumour bed); and CTV-N50 (50 Gy to regional lymph nodes). Variation in CTV delineation by the clinician (‘doctor’ s delineation error’) is the greatest geometrical uncertainty in the whole treatment process. Studies comparing outlining by radiologists and oncologists have shown a significant inter-observer variability for both the GTV and/or CTV at a variety of tumour sites. This is greater than any intra-observer variation. Published results for nasopharynx, brain, lung, prostate, medulloblastoma and breast all show significant discrepancies in the volumes outlined by different clinicians. Improvements can be

made with training in radiological anatomy which enables clinicians to distinguish blood vessels from lymph nodes and to identify structures accurately on computed tomography (CT) and magnetic resonance imaging (MRI). Joint outlining by radiologists and oncologists can improve consistency and ensure accurate interpretation of imaging of the GTV. Consensus guidelines such as those for defining CTV for head and neck nodes (Gregoire et al. 2000) and pelvic nodes (Taylor et al. 2005) have improved CTV delineation greatly. Protocols for outlining GTV and CTV at all tumour sites are needed and suggestions are made in each individual chapter.

Planning target volume

When the patient moves or internal organs change in size and shape during a fraction of treatment or between fractions (intra- or inter-fractionally), the position of the CTV may also move. Therefore, to ensure a homogeneous dose to the CTV throughout a fractionated course of irradiation, margins must be added around the CTV. These allow for physiological organ motion (internal margin) and variations in patient positioning and alignment of treatment beams (set-up margin), creating a geometric planning target volume. The planning target volume (PTV) is used in treatment planning to select appropriate beams to ensure that the prescribed dose is actually delivered to the CTV. (Ann Barrett et al 2009).

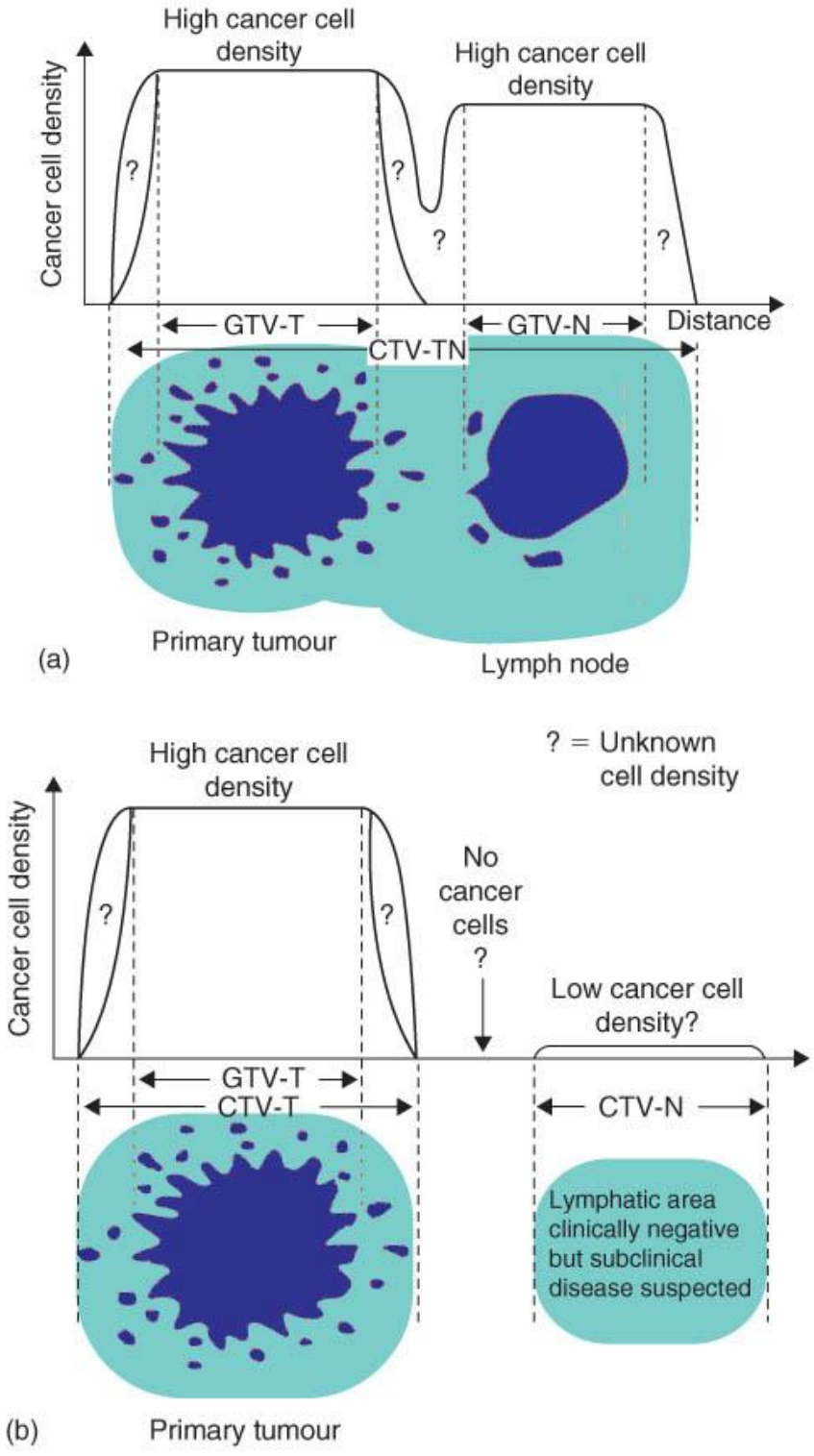

Figure 1.2 ICRU illustrations to show (a) GTV-T plus GTV-N in continuity (CTV-TN) and (b) CTV-T and CTV-N at a distance. Reproduced with permission from ICRU (2004) Prescribing, Recording and Reporting Electron Beam Therapy. ICRU report 71.

When treating lung tumours, the displacement of the CTV caused by respiration can be dealt with in several ways: by increasing the CTV-PTV margin eccentrically to include all CTV positions during a respiratory cycle; by using suspended respiration with a technique such as the active breathing control (ABC) device; or by delivery of radiation using gating or respiratory correlated CT scanning and treatment. Protocols for minimizing effects on the CTV of variations in bladder and rectal filling are described in relevant chapters. Uncertainties from organ motion can also be reduced by using fiducial markers, and published results are available for lung, prostate and breast tumours. Radio-opaque markers are inserted and imaged at localization using CT or MRI, and at treatment verification, using portal films, electronic portal imaging devices (EPIDs) or online cone beam CT image-guided radiotherapy (IGRT). The internal margin therefore allows for inter- and intra-fractional variations in organ position and shape which cannot be eliminated (Ann Barrett et al 2009).

1.2 Problem of the study:

Identification of gross target volume (GTV) using CT scan sometimes underestimate region of interest (ROI) because of sub mucosal extension around the tumor. The PET scan so useful in estimation of sub mucosal extension of the tumor as well as in staging and restaging of lung carcinomas and changing in gross target volume either positively (+) or negatively (-) .

1.3 Objectives:

1.3.1 ***The general objective*** of this study is to estimate non-small cell lung carcinoma gross target volume with ^{18}F-FDG PET scan.

1.3.2 Specific objectives:

- To measure the GTV in CT image.
- To measure the GTV in PET image.
- To find sub mucosal extension using PET and CT fused image.
- To correlate between sub mucosal extension and GTV.
- To predict sub mucosal extension using the GTV measured in CT.
- To find the effect of the sub mucosal extension in grading and staging.

1.4 Importance of the study:

To establish a database for treating the non- small cell lung tumor with all safe margin and sub mucosal extension, and to prevent the chances of disease recurrence, and also to make a rule of sub mucosal extension can be used for the countries that haven't PET.

1.4.1 Overview of the study:

This study will fall into five chapters with chapter one is an introduction, problem of the study, objectives and overview. Chapter two include literature review while chapter three include material used and the method of data collection and analysis. Chapter four presents the result of the study in a line graphs and table and finally chapter five which include the discussion, conclusion, recommendation and references.

CHAPTER TWO

2.1 Anatomy

2.1.1Introduction

The anatomy and physiology of the respiratory tract is quite complex. Each anatomic segment performs in concert with the others and is accountable for a wide variety of physiological responsibilities. These responsibilities vary with rest or exercise, disease or health. the respiratory tract is a delicate and complicated system that can be involved in a number of disease processes. An understanding of the anatomy and physiology of the respiratory tract is critical to understanding this elaborate system to maintain respiratory health and treat respiratory diseases (2). Lung is a major organ of the respiratory system; each lung houses structures of both the conducting and respiratory zones. The main function of the lungs is to perform the exchange of oxygen and carbon dioxide with air from the atmosphere. To this end, the lungs exchange respiratory gases across a very large epithelial surface area—about 70 square meters—that is highly permeable to gases (J. GORDON BETTS 2013).

2.1.2 Gross Anatomy of the Lungs

The respiratory system is comprised of several elements including the central nervous system, the chest wall, the pulmonary circulation, and the respiratory tract. The respiratory tract can be divided into four distinct segments: the naso oropharynx, the conducting airways, the respiratory bronchioles, and the alveoli (Matthew. L. Mintz 2006).

The lungs are pyramid-shaped, paired organs that are connected to the trachea by the right and left bronchi; on the inferior surface, the lungs are bordered by the

diaphragm. The diaphragm is the flat, dome-shaped muscle located at the base of the lungs and thoracic cavity. The lungs are enclosed by the pleurae, which are attached to the mediastinum. The right lung is shorter and wider than the left lung, and the left lung occupies a smaller volume than the right. The cardiac notch is an indentation on the surface of the left lung, and it allows space for the heart (Figure 1). The apex of the lung is the superior region, whereas the base is the opposite region near the diaphragm. The costal surface of the lung borders the ribs. The mediastinal surface faces the midline (J. GORDON BETTS 2013).

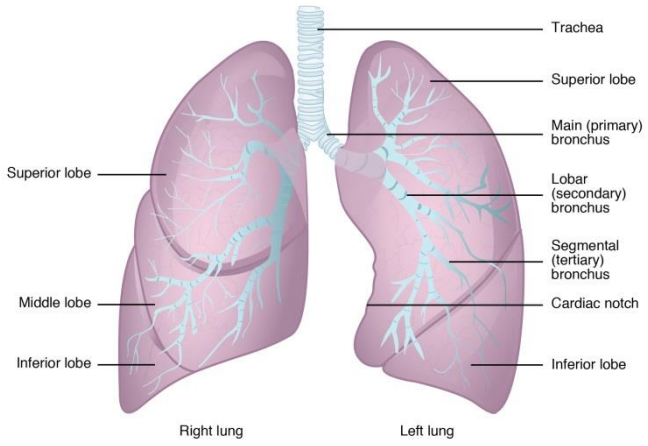

Figure 2.1 Gross Anatomy of the Lungs

Each lung is composed of smaller units called lobes. Fissures separate these lobes from each other. The right lung consists of three lobes: the superior, middle, and inferior lobes. The left lung consists of two lobes: the superior and inferior lobes. The lungs can also be divided into the conducting airways and the units of respiration. The trachea, bronchi, and bronchioles conduct and transport air from the outside world and deliver it to the respiratory units—the alveoli. Gas-exchange occurs at the level of the alveoli, providing the necessary oxygen for the body's

daily functions (Matthew. L. Mintz 2006), a bronchopulmonary segment is a division of a lobe, and each lobe houses multiple bronchopulmonary segments. Each segment receives air from its own tertiary bronchus and is supplied with blood by its own artery. Some diseases of the lungs typically affect one or more bronchopulmonary segments, and in some cases, the diseased segments can be surgically removed with little influence on neighboring segments. A pulmonary lobule is a subdivision formed as the bronchi branch into bronchioles. Each lobule receives its own large bronchiole that has multiple branches. An interlobular septum is a wall, composed of connective tissue, which separates lobules from one another (J. GORDON BETTS 2013).

The next segment is the conducting airways, beginning with the trachea, which branches repeatedly to form approximately 14 generations of conduits for air reaching several distinct pulmonary segments. The trachea bifurcates at the carina into the right and left main-stem bronchi. Aspiration occurs more commonly at the right main bronchus because of its gentler angle off the trachea. The right lung is divided into upper, middle, and lower lobes, each of which is further subdivided into segments and each with its own conducting airway. The upper lobe contains three segments: the apical, posterior, and anterior. The middle lobe consists of the lateral and medial segments. The lower lobe has five segments: the superior, medial basal, anterior basal, lateral basal and posterior basal. The right lung has 10 segments, as opposed to 8 found in the left lung. The left main bronchus has two divisions serving the left upper lobe. The superior division of the bronchus leads to the apical–posterior and anterior segments. The inferior division of the bronchus leads to the superior and inferior lingular segments. The left lower lobe consists of the superior, anteromedial basal, lateral basal, and posterior basal segments. Each

bronchopulmonary segment is supplied by an individual branch of the pulmonary artery (Matthew. L. Mintz 2006)

2.1.2 Blood Supply and Nervous Innervation of the Lungs

The blood supply of the lungs plays an important role in gas exchange and serves as a transport system for gases throughout the body. In addition, innervation by the both the parasympathetic and sympathetic nervous system provides an important level of control through dilation and constriction of the airway.

2.1.2.1Blood Supply

The major function of the lungs is to perform gas exchange, which requires blood from the pulmonary circulation. This blood supply contains deoxygenated blood and travels to the lungs where erythrocytes, also known as red blood cells, pick up oxygen to be transported to tissues throughout the body. The pulmonary artery is an artery that arises from the pulmonary trunk and carries deoxygenated, arterial blood to the alveoli. The pulmonary artery branches multiple times as it follow the bronchi, and each branch becomes progressively smaller in diameter. One arteriole and an accompanying venule supply and drain one pulmonary lobule. As they near the alveoli, the pulmonary arteries become the pulmonary capillary network. The pulmonary capillary network consists of tiny vessels with very thin walls that lack smooth muscle fibers. The capillaries branch and follow the bronchioles and structure of the alveoli. It is at this point that the capillary wall meets the alveolar wall, creating the respiratory membrane. Once the blood is oxygenated, it drains from the alveoli by way of multiple pulmonary veins, which exit the lungs through the hilum. (J. GORDON BETTS 2013).

2.1.1.2 Nervous Innervation

Dilation and constriction of the airway are achieved through nervous control by the parasympathetic and sympathetic nervous systems. The parasympathetic system causes bronchoconstriction, whereas the sympathetic nervous system stimulates bronchodilation. Reflexes such as coughing, and the ability of the lungs to regulate oxygen and carbon dioxide levels, also result from this autonomic nervous system control. Sensory nerve fibers arise from the vagus nerve, and from the second to fifth thoracic ganglia. The pulmonary plexus is a region on the lung root formed by the entrance of the nerves at the hilum. The nerves then follow the bronchi in the lungs and branch to innervate muscle fibers, glands, and blood vessels. (J. GORDON BETTS 2013).

Pleura of the Lungs

Each lung is enclosed within a cavity that is surrounded by the pleura. The pleura (plural = pleurae) is a serous membrane that surrounds the lung. The right and left pleurae, which enclose the right and left lungs, respectively, are separated by the mediastinum. The pleurae consist of two layers. The visceral pleura is the layer that is superficial to the lungs, and extends into and lines the lung fissures (Figure 2). In contrast, the parietal pleura is the outer layer that connects to the thoracic wall, the mediastinum, and the diaphragm. The visceral and parietal pleurae connect to each other at the hilum. The pleural cavity is the space between the visceral and parietal layers. (J. GORDON BETTS 2013).

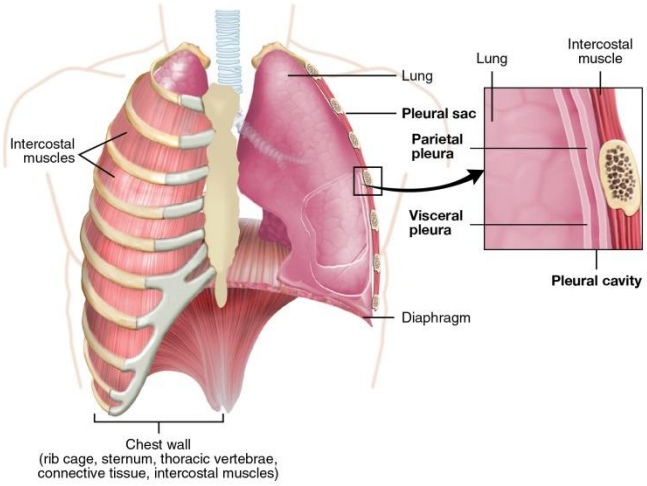

Figure 2.2: Parietal and Visceral Pleurae of the Lungs.

The pleurae perform two major functions: They produce pleural fluid and create cavities that separate the major organs. Pleural fluid is secreted by mesothelial cells from both pleural layers and acts to lubricate their surfaces. This lubrication reduces friction between the two layers to prevent trauma during breathing, and creates surface tension that helps maintain the position of the lungs against the thoracic wall. This adhesive characteristic of the pleural fluid causes the lungs to enlarge when the thoracic wall expands during ventilation, allowing the lungs to fill with air. The pleurae also create a division between major organs that prevents interference due to the movement of the organs, while preventing the spread of infection (J. GORDON BETTS 2013).

2.2 Physiology

The physiological makeup of the lungs maintains the delicate balance between these disparate anatomic entities. Several terms have been developed to describe the various physiological capacities of the respiratory tract. Total lung capacity is defined as the volume of gas in the lungs following maximal inspiration.

Functional residual capacity is the volume of gas in the lungs at the end of normal expiration. The functional residual capacity is comprised of the expiratory reserve volume (the amount of air that can be expelled with maximal expiratory effort) and the residual volume (the volume of air in the lungs after maximal expiration). Tidal volume is the volume of gas in any normal breath (generally around 500–800 mL), whereas vital capacity is the maximal volume of air that can be expelled following maximal inspiration. These volumes can be measured by spirometry.

The three main physiological functions of the respiratory tract are ventilation, perfusion, and diffusion. Ventilation is the process of procuring air from the external environment via inspiration to supply the alveolus, after which it is subsequently returned to the outside of the body through expiration. The elastic nature of the lungs and chest wall permit pressure differentials without which inspiration and expiration could not occur. The lungs are distended by pressure exerted by the airways and alveoli (positive internal pressure) or by pressure outside the lungs (negative external pressure). The chest wall's elasticity allows it to act as a spring. When the pressures exerted on it are altered, the chest wall moves and breathing occurs. The stimulus for respiration comes mainly from the medulla and pons, which constantly receive neural inputs from several sources.

The carotid bodies detect changes in PaO2, PaCO2, and pH, whereas the medullary chemo-receptor monitors PaCO2 and pH alone. Muscle spindles and Golgi tendon organs monitor chest wall muscles and stretch. All of this information is combined to determine ventilatory needs, which increase in illness, exercise, or other physiological states in which tissue oxygen needs are increased. The responses of these receptors can be blunted and lead to decreased ventilation as well. This can occur with obesity, severe chronic bronchitis, or severe metabolic alkalosis.

The ventilatory drive is stimulated by PaO2 and PaCO2 levels, although the body demonstrates far greater sensitivity to PaCO2 levels. In normal individuals at rest,

the $PaCO_2$ level is tightly controlled. If the $PaCO_2$ level raises slightly, to 42 mmHg, the rate of ventilation quickly increases. However, the PaO_2 generally must decrease to around 65 mmHg for a similar ventilatory response to be initiated via hypoxemic stimulus. Hypercapnia is therefore the primary drive for ventilation.

Distribution of inhaled air also varies. In a normal, upright individual intra-pleural pressure is most negative at lung apices and least negative at lung bases.

At rest, therefore, the alveoli are least distended at the bases of the lungs, and this area receives greater ventilation as a result.

Another main physiological responsibility of the respiratory tract is diffusion. This is measured by diffusion capacity for carbon monoxide, which tests how well the gas in inspired air can cross the wall of the alveolus and enter the capillary. This entails crossing the alveolar type 1 epithelial cells, the interstitial space, and the vascular endothelial cells. Carbon monoxide is used for measuring the diffusing capacity of the lung, generally by use of the single breath determination.

Adjustments must be made for those with altered lung volumes, those with increased carbon monoxide levels (such as smokers), and those who are anemic or who are being tested at high altitudes. Elevated values may be found in asthmatics or those with pulmonary hemorrhage, whereas decreased values are found in emphysema, interstitial lung diseases, or any other process that may disturb the integrity of the alveoli (Anna Person 2006).

2.3 Lung pathology

2.3.1 Lung disease

Whenever you see an area of increased density within the lung, it must be the result of one of these four patterns.

1. **Consolidation** - any pathologic process that fills the alveoli with fluid, pus, blood, cells (including tumor cells) or other substances resulting in lobar, diffuse or multifocal ill-defined opacities. Pneumonia is by far the most common cause of consolidation. The disease usually starts within the alveoli and spreads from one alveolus to another. When it reaches a fissure the spread stops there.

2. **Interstitial** - involvement of the supporting tissue of the lung parenchyma resulting in fine or coarse reticular opacities or small nodules. There are four patterns: reticular, nodular, high and low attenuation

3. **Nodule or mass** - any space occupying lesion either solitary or multiple.

Solitary Pulmonary Nodule (SPN):

A solitary pulmonary nodule or SPN is defined as a discrete, well-marginated, rounded opacity less than or equal to 3 cm in diameter. It has to be completely surrounded by lung parenchyma, does not touch the hilum or mediastinum and is not associated with adenopathy, atelectasis or pleural effusion. The differential diagnosis of SPN is basically the same as of a mass except that the chance of malignancy increases with the size of the lesion. Lesions smaller than 3 cm, i.e. SPN's are most commonly benign granulomas, while lesions larger than 3 cm are treated as malignancies until proven otherwise and are called masses.

Metastases:

Metastases are the most common cause of multiple pulmonary masses. Usually they vary in size and are well-defined. They predominate in the lower lobes and in the sub-pleural region.

4. **Atelectasis** - collapse of a part of the lung due to a decrease in the amount of air in the alveoli resulting in volume loss and increased density, with subsequent volume loss due to airway obstruction or compression of the lung by pleural fluid or a pneumothorax.

In many cases atelectasis is the first sign of a lung cancer. Evidently it is very important to recognize the various presentations of atelectasis, since some of them can be easily misinterpreted.

2.3.2 Lung cancer

Lung cancer is a significant public health problem and is of particular interest to primary care physicians because smoking, major attributable cause is a modifiable risk factor. Despite the fact that the death rate from lung cancer has decreased modestly in recent years, the annual incidence of lung cancer, in the worldwide, continues to rise. As a result, lung cancer is now the leading cause of cancer death in both men and women. This is more than the combined mortality from colorectal, breast, and prostate cancer. Bronchogenic carcinoma is by far the most common form of lung cancer and is responsible for approximately 1 million deaths worldwide each year. This includes one-third of all cancer-related deaths in men and approximately 5 to 10% of all cancer deaths in women. As population size increases and ages, it is likely that the number of new lung cancer cases per year will continue to rise. Of all lung cancers, 35 to 40% are adenocarcinoma, 20 to 30% are squamous cell carcinoma, 10% are large carcinoma, and 15 to 20% are SCLC. Bronchogenic carcinoma is divided into two groups: non-small cell lung cancer (NSCLC) and SCLC. NSCLC is further categorized as adenocarcinoma, squamous cell carcinoma, and large cell carcinoma. SCLC is further categorized as oat cell, mixed cell, intermediate, and undifferentiated carcinoma. Approximately

75% of all lung cancers represent NSCLC. Classification of primary malignant tumors of the lung, specifically bronchogenic carcinomas, is extremely useful because the various neoplastic diseases in a subgroup share a similar natural history, prognosis, and expected response to therapy. For example, the cancers grouped as NSCLC have different clinical presentations and histopathologies, but share similar prognoses and treatment approaches. SCLC, on the other hand, has a markedly different prognosis and treatment approach than NSCLC. (Harsh Mohan 2010).

Neoplastic diseases of the lung, specifically malignant neoplasms, is most commonly arising in response to carcinogenic insult or irritation. The mucosal lining of the lung parenchyma is vulnerable to chemical injury. Cigarette smoke alone has been found to contain more than 1000 chemical entities, many of which can initiate and/or promote carcinogenesis. A complex process initiated by exposure to carcinogens results in a transformation of normal mucosal cells into malignant cells. There are many different theories that explain how this transformation occurs, most revolving around genetic alteration caused by carcinogens, such as activation and implication of oncogenes and inactivation of tumor suppressor genes, and several investigations have found that most pulmonary neoplastic lesions contain many of these genetic alterations. Enzo pyrene from tobacco smoke has been shown to cause inactivation of p53, one of the most commonly inactivated tumor suppressor genes in bronchogenic carcinoma. The molecular pathogenesis of NSCLC is believed to be mutations in the ras oncogenes and, to a lesser extent, aberrant anti-apoptotic pathways and mutations causing abnormal activation of epithelial growth factor receptor. (Harsh Mohan 2010).

Adenocarcinomas are the most common lung cancers among nonsmokers and include bronchial-derived adenocarcinoma and bronchi alveolar carcinoma. The difference between these two subtypes of adenocarcinomas, as their names imply, is the specific epithelial location from which the lesions arise. These are usually

slower growing as compared with other forms of NSCLC and tend to be peripherally located in the lung. Histologically, adenocarcinomas range from well differentiated glandular structures to poorly differentiated papillary lesions and masses (Harsh Mohan 2010).

2.4 Imaging

Lung cancer, in theory, should lend itself to screening. The disease is very common and in its earliest stages¡70% of cases can be cured by surgery. Despite this, lung cancer has an overall prognosis so dismal that incidence exceeds prevalence. The main risk factor, smoking, is easily identifiable and noninvasive screening tests such as chest radiography and sputum cytology are widely available. (N. Hollings et al 2002).

2.4.1 Chest radiography.

Due to its widespread availability, including to primary care physicians, the chest radiograph is often the first imaging modality to suggest the diagnosis of bronchogenic carcinoma. Lung cancer may present as a straightforward speculated mass but its presence may also be inferred from other appearances such as un-resolving pneumonia or lobar collapse.

In some situations, no further imaging will be necessary when bulky contralateral mediastinal adenopathy is present or when an obvious bony lesion is identified.

However, CT scanning of the chest is often needed because of the lack of sensitivity of the chest radiographs in detecting mediastinal lymph node metastases and chest wall and mediastinal invasion. (N. Hollings et al 2002).

2.4.2 Chest Computed tomography (CT).

CT can identify specific features in lung nodules that are diagnostic, e.g. arteriovenous fistulae, rounded atelectasis, fungus balls, mucoid impaction and infarcts. High-resolution scanning further refines this diagnostic process. The ability of CT scanning to evaluate the entire thorax at the time of nodule assessment is of further benefit. Spiral or helical CT is advantageous as small nodules are not missed between slices as may happen on older, nonspiral machines. It also increases the detection rate of nodules v5 mm in diameter, especially when viewed in cine-format on a workstation. The acquisition of continuous volume data sets permits three-dimensional image reconstruction and multiplanar (i.e. nonaxial) reformatting. These techniques have been shown to improve the detection of pleural invasion by tumour and clarify the origin of peri-diaphragmatic tumors respectively. Further manipulation of raw data sets enables the technique of virtual bronchoscopy. An interactive, simulated bronchoscopy can be performed with the added benefit of simultaneous information on adjacent mediastinal structures. This technique has far reaching potential both as a teaching tool and as a means of evaluating patients9 thoracic and bronchial anatomy prior to interventional procedures and stent placement. The recent advent of multislice scanners has seen advances in image resolution with a substantial reduction in both tube loading and scanning time as up to four slices can be acquired simultaneously. Both spiral and multislice machines suffer less from respiratory motion artefact due to their shorter scanning times. Spiral CT with a bolus injection of intravenous iodinated contrast medium affords "dynamic scanning". (N. Hollings et al 2002).

2.4.3 Chest Magnetic resonance imaging (MRI)

Magnetic resonance imaging (MRI) is becoming more available but pressure on MRI scanning time is so intense that it is usually used for problem solving and where administration of contrast media is contraindicated. MRI can be more accurate than CT in separating stage IIIa (resectable) from IIIb (generally un-resectable) tumours in selected patients due to its ability to detect invasion of major mediastinal structures, i.e. T4 disease. The advantages MRI has over CT include: better soft tissue contrast, multiplanar imaging capability, and therefore useful for superior sulcus tumours and evaluation of the aorto-pulmonary window, and cardiac gating which enables excellent delineation of the heart and great vessels and removes cardiac pulsation artifact. MRI is also useful in the assessment of mediastinal and chest wall invasion by virtue of its ability to determine fat-stripe invasion and involvement of the diaphragm and spinal canal. In addition, it has been shown to aid in differentiating lymph nodes from hila vessels due to the "flow void" phenomenon. MRI has disadvantages compared to CT, being slower and more expensive with poorer spatial resolution and providing limited lung parenchyma information. MRI can overestimate lymph node size because of respiratory movement, causing the blurring together of discrete nodes into a larger, conglomerate mass. MRI is also poorly tolerated by claustrophobic patients and is contra-indicated in patients with indwelling electromagnetic devices and some prosthetic heart valves. T1-weighted sequences are used for the visualization of fat planes and improved spatial resolution. T2-weighted sequences are useful for detection of high-signal tumour infiltration. Gadolinium enhancement can further enhance the diagnostic yield (N. Hollings et al 2002).

2.4.4 Positron Emission Tomography (PET)

2.4.4.1 History of PET

The name "PET" comes from Positron Emission Tomography. It is a new scanning technique in medical research. PET allows us, for the first time, to measure in detail the functioning of distinct areas of the human brain while the patient is comfortable, conscious and alert. We can now study the chemical process involved in the working of healthy or diseased human brains in a way previously impossible. Before the advent of the PET scanner, we could only infer what went on within the brain from post-mortems (dissections after death) or animal studies (Sorensen and Phelps, 1987)

In the 1970's PET scanning was formally introduced to the medical community. At that time it was seen as an exciting new research modality that opened doors through which medical researchers could watch, study, and understand the biology of human disease. In 1976, the radiopharmaceutical fluorine-18-2-fluoro-2-deoxyglucose (FDG), a marker of sugar metabolism with a half-life of 110 minutes, enabled tracer doses to be administered safely to the patient with low radiation exposure. The development of radiopharmaceuticals like FDG made it easier to study living beings, and set the groundwork for more in-depth research into using PET to diagnose and evaluate the effect of treatment on human disease. To perform PET studies in the late 1970's, a large staff was needed: physicists to run the cyclotron that produces the F-18 and to oversee the scanner, chemists to make the tracers such as FDG, and dedicated, specialist physicians. During the 1980's the technology that underlies PET advanced greatly. Commercial PET scanners were developed with more precise resolution and images. As a result, many of the steps required for producing a PET scan became automated and able to be performed by a trained technician and experienced physician, thereby reducing the cost and complexity of

the procedure. Smaller, self-shielded cyclotrons were developed, making it possible to install cyclotrons at more locations. Positron Emission Tomography (PET) is rapidly becoming a major diagnostic imaging modality used predominantly in determining the presence and severity of cancers, neurological conditions, and cardiovascular disease. It is currently the most effective way to check for cancer recurrences. Studies demonstrate that PET offers significant advantages over other forms of imaging such as CT or MRI scans in diagnosing disease. Last year more than 200,000 PET scans were performed at more than 700 sites around the country. If you're interested in learning how a PET scan can benefit you and need additional information, talk with your local health care provider or referring physician. At the end of this page are links to other sites with PET information to. PET images demonstrate the chemistry of organs and other tissues such as tumors. A radiopharmaceutical, such as FDG (fluorodeoxyglucose), which includes both sugar (glucose) and a radionuclide (a radioactive element) that gives off signals, is injected into the patient and its emissions are measured by a PET scanner.

A PET scanner consists of an array of detectors that surround the patient as shown in Fig.4.1. Using the gamma ray signals given off by the injected radionuclide, PET measures the amount of metabolic activity at a site in the body and a computer reassembles the signals into images. Cancer cells have higher metabolic rates than normal cells, and show up as denser areas on a PET scan. PET is useful in diagnosing certain cardiovascular and neurological diseases because it highlights areas with increased, diminished or no metabolic activity, thereby pinpointing problems (Karp et al, 1991).

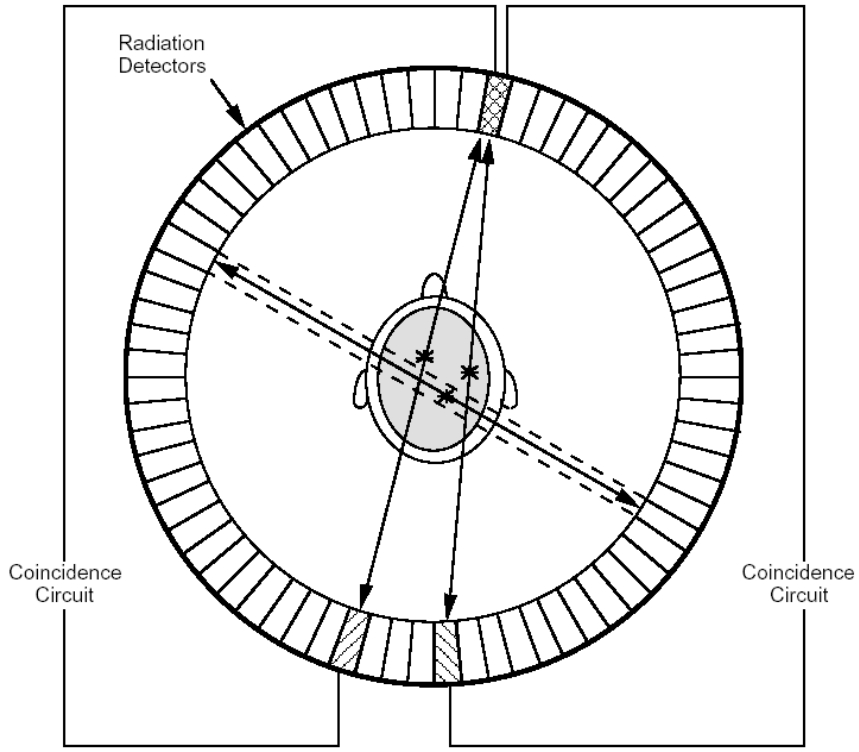

Figure 2.3: Detectors array of PET systems

PET and CT or MRI

Because PET measures metabolism, as opposed to MRI or CT, which "see" structure, it can be superior to these modalities, particularly in separating tumor from benign lesions, and in differentiating malignant from non-malignant masses such as scar tissue formed from treatments like radiation therapy. PET is often used in conjunction with an MRI or CT scan through "fusion" to give a full three-dimensional view of an organ and the location of cancer within that organ. Newer PET scanners are being made that are a combination of PET/CT devices (Wienhard et al 1994).

2.4.4.2 Basic principle of PET

Proton-rich isotopes can decay by positron emission or electron capture. The positron (β+) is the anti-particle to the electron. It has the same properties as an electron except that is has positive charge. In positron emission, the positron

undergoes inelastic collisions with atomic electrons. After it reaches thermal energies, the positron annihilates with an electron, converting the mass of the two particles into radiation in the form of gamma rays.

To conserve energy and momentum, two annihilation photons of 511 keV are emitted in opposite directions as depicted below. Detecting these photons is crucial for the image.

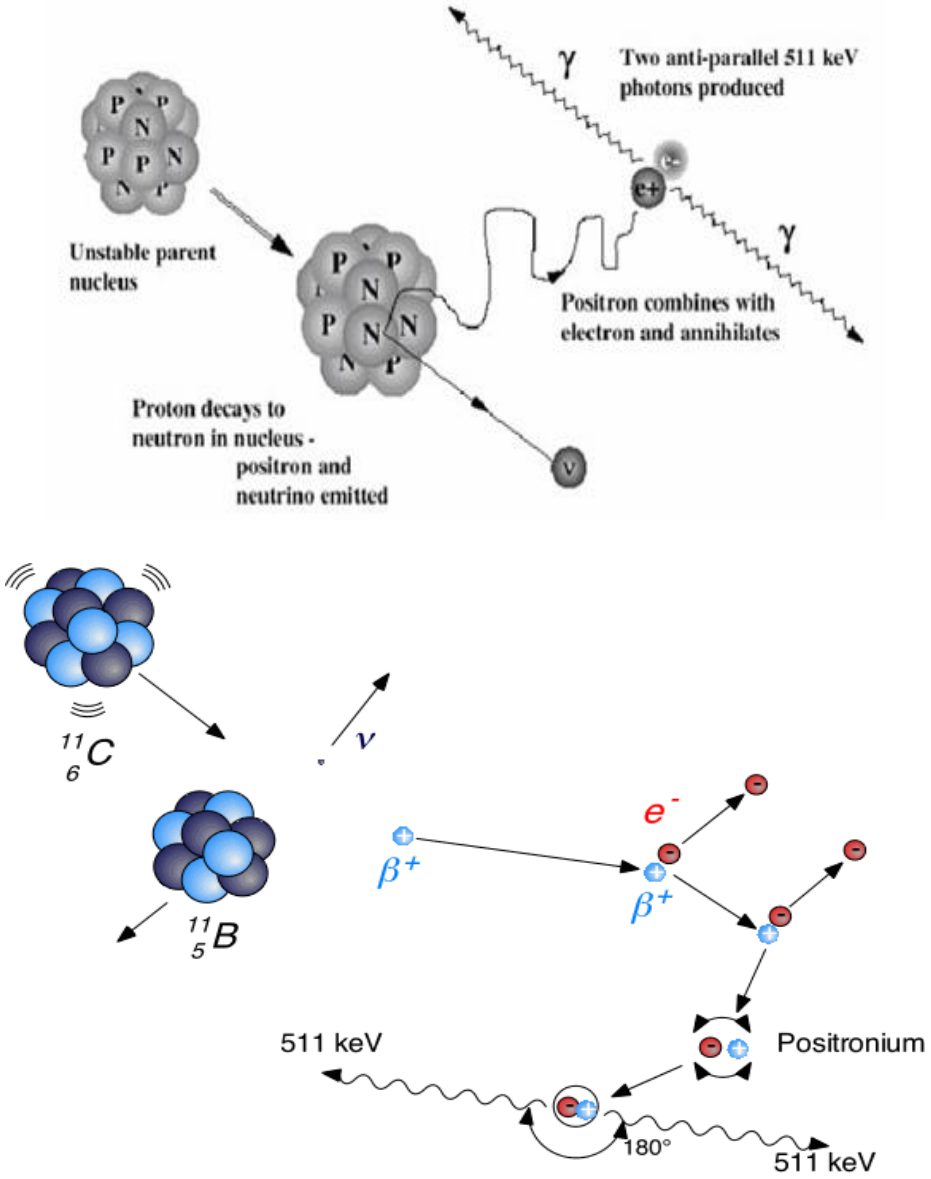

Figure.2.4: Positron emission and annihilation

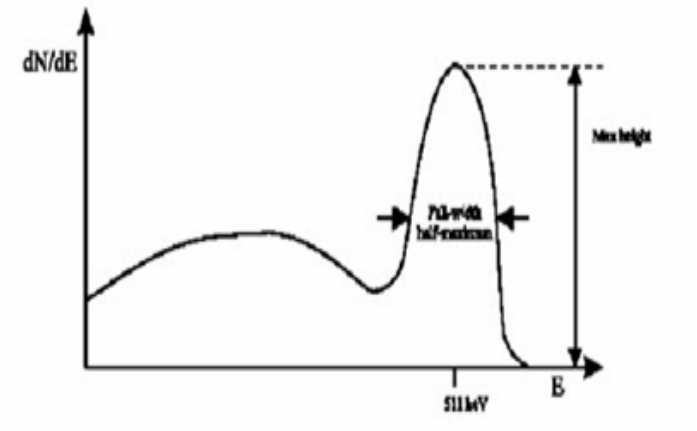

Figure 2.5: Energy distribution measured by scintillation detector exposed to 511KeV photons

2.4.4.3 Important Parameters in PET

Detector Efficiency: It is the probability that the detector registers an event when a gamma ray path intersects the detector.

System Sensitivity: It is the number of events registered by the scanner per unit activity.

Time resolution: It is the ability to accurately determine coincidence events.

Count-Rate Capability: It is the ability of the scanner to record events at high count rates.

Spatial Resolution: The ability to distinguish closely spaced objects.

2.4.4.4 Preparation and Quality Assurance of ^{18}F-Radiopharmaceuticals

2.4.4.4.1 Introduction

Positron Emission Tomography (PET) which employs radiotracers to observe cell metabolism in vivo is fast becoming a highly useful diagnostic technique. The most commonly used radiotracer is Fluorine-18 labelled 2-Fluoro-2-deoxy-D-glucose (^{18}FDG). FDG is naturally absorbed by cells just like glucose, but cannot be metabolized. It accumulates in cancer cells because of their characteristic high metabolic rate.

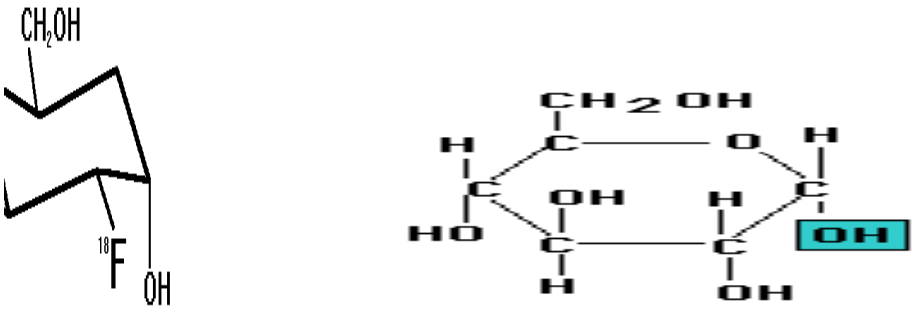

^{18}F-2-fluor-2-deoxy-glucose **Glucose (ring form)**

Figure 2.6: ^{18}F-FDG chemical form

F-18 emits a positron of relatively low energy disintegrating and emitting 511 keV gamma rays. It has a half-life of 109 minutes which is long enough for the chemical labelling, transport, and to carry out the PET examination. F-18 is a small atom its addition to a molecule does not deform it to the point where it is not recognized by the body anymore.

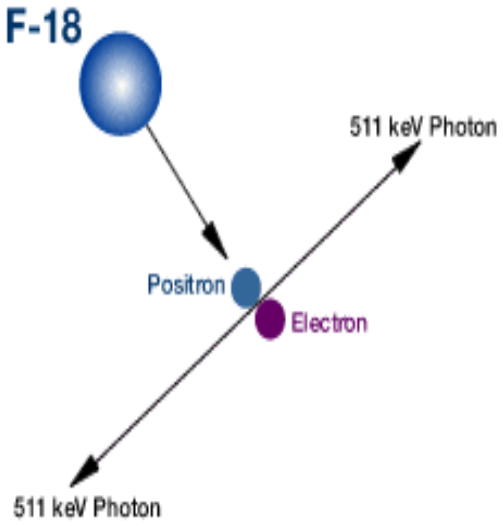

Figure 2.7: Positron emission annihilation process

A limiting factor of ^{18}FDG use is the relatively short half-life (~100 minutes) of the ^{18}F atom. The entire process from creation of ^{18}F to synthesis of ^{18}FDG through injection into a patient must occur within several hours. This has led to the creation of several automated ^{18}FDG synthesizers that utilize kits to aid the process.

2.4.4.4.2 Development of [^{18}F] FDG

2-Deoxy-2-[^{18}F] fluoro-D-glucose ([^{18}F] FDG) is a widely used radiotracer developed in the Brookhaven National Laboratory in 1976 and used to measure glucose metabolism. The first synthesis of [^{18}F] FDG utilized the electrophilic fluorination of glucal with [^{18}F] F2. The addition to the least hindered face of the molecule was preferred yielding [^{18}F] FDG and its 2-epimer (mannose type) in the ratio of 4:1. A few years later an improved synthesis was reported in which acetyl [^{18}F] hypo fluorite prepared from [^{18}F] F2 was used as [^{18}F] F+ source. The selectivity was improved to 95:5. A nucleophilic substitution with [^{18}F] fluoride was developed in 1986. It gave significantly higher yields and has largely replaced the electrophilic route.

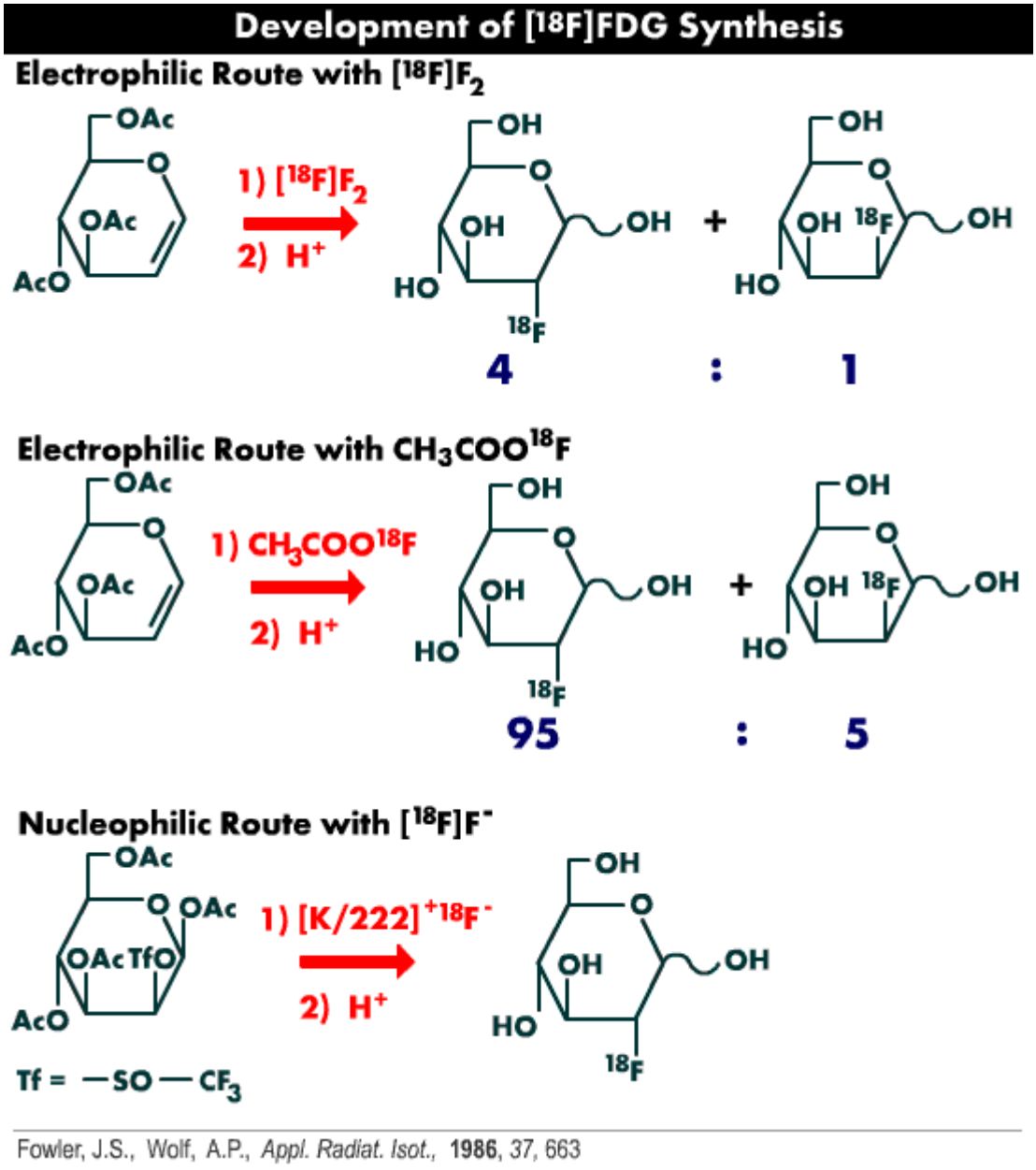

Figure 2.8: Development of (^{18}F) FDG synthesis

Mannose Triflate Procedure

ß-D-Mannopyranose1,3,4,6-tetra-O-acetate2-O-trifluoromethanesulfonate. This is a new product used for manufacturing commercial quantities of ^{18}FDG as shown below:

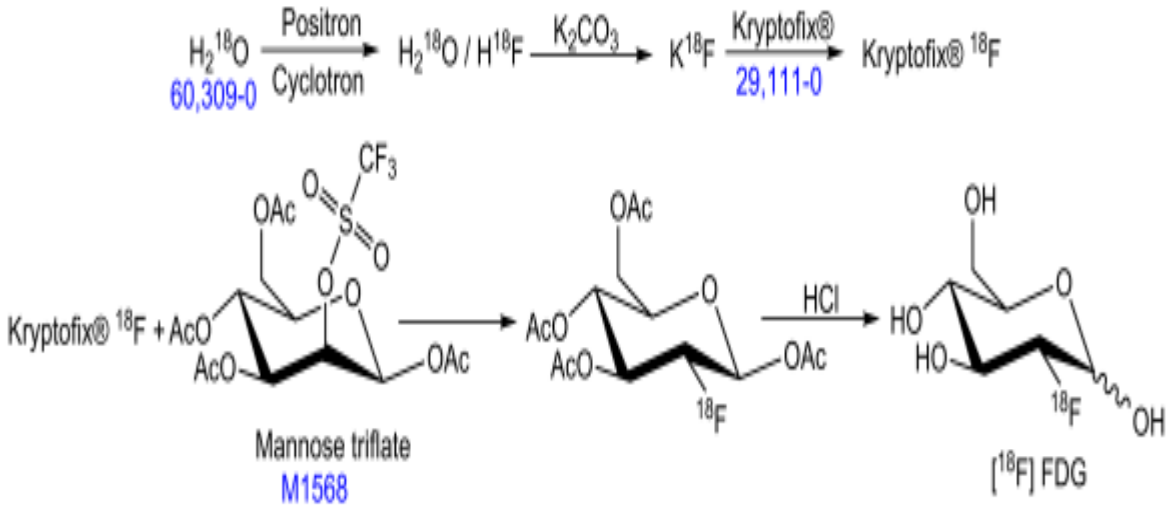

Figure 2.9: Cyclotron Production of 2-[^{18}F]-FDG Using Gems FDG Micro lab and a Gems Target

Cyclotron Production of 2-[^{18}F]-FDG Using Gems FDG Microlab and a Gems Target:

The synthesis of ^{18}FDG requires the use of a cyclotron to produce ^{18}F from 18O enriched water and typically utilizes an ^{18}FDG synthesizer. Sigma-Aldrich supplies many key components used in ^{18}FDG synthesis and supplies raw materials used in ^{18}FDG synthesizer kits. Catalog number, chemical abstract registry numbers of these raw materials are given in Table (2.1).

Table 2.1: Catalog number, chemical abstract registry numbers of some raw materials used for synthesis of ^{18}FDG

Catalog No.	CAS Rn	Material
60,309-0	14314-42-2	Water-^{18}O
M1568	92051-23-5	Mannose Triflate (FDG precursor)
29,111-0	23978-09-8	Krypto fix® 222 (Phase transfer catalysts) (4,7,13,16,21,24-Hexaoxa-1,10-diazabicyclo [8.8.8] hexaoxane)
F5006	29702-43-0	2-Fluoro-2-deoxy-D-glucose (FDG reference standard)
C203	14685-79-1	2-Chloro-2-deoxy-D-glucose (2-ClDG reference standard)

For the production of ^{18}F by bombarding an $H_2{}^{18}O$-target with H- ions, the 120 M cyclotron has been used. Fluorine-18 is produced under the irradiation conditions allowing the average beam current up to 20 mA. The effective target yield is 1.5 GBq ^{18}F-/mAh. Using this method, approximately 60 GBq^{18}F may be produced for the synthesis within the period of 160 minutes. The radiopharmaceutical, 2-[^{18}F]-FDG in the "injection quality", is then produced by the GMP rules (Good Manufacturing Procedures). (Fowler, 1986)

In 1999 the product was registered in the Czech Republic. In its Czech Pharmacopoeia article (identical to European Pharmacopoeia -Third Edition, supplement 1999) the product has been declared as a sterile, isotonic, bacterial endotoxins free aqueous solution, suitable for intravenous administration (Fowler, 1986)

The 2-[^{18}F]-FDG is routinely produced using an FDG Micro Lab equipment (called PET trace FDG Micro lab) with maximum 40% efficiency (including correction). The Micro Lab production method utilizes a unique method which used solid-phase trapping of the ^{18}F- anion on a resin and a subsequent reaction of this anion with the 2-[^{18}F]-FDG -precursor. All steps take place inside a disposable cassette. The system is exposed to small amounts of radioactive compounds only. The synthesis of 2-[^{18}F]-FDG can be described by the following steps:

1. Trapping of ^{18}F on a resin (trapping agent is 4-(4-methylpiperidinyl) pyridinium cation). The resin is placed in a column, in the cassette.

2. Replacement of water by acetonitrile as a mobile phase.

3. Reaction of the trapped fluoride anion with 1,3,4,6-tetra-O-acetyl-2-O-trifluoromethanesulfolyl-2-D-mannose-pyranose on the column and transfer of the formed protected 2-[^{18}F]-FDG analog to the hydrolytic vessel.

4. Evaporation of the acetonitrile, hydrolysis of the acetyl groups with hydrochloric acid, and neutralization of the hydrochloric acid with a phosphate buffered sodium hydroxide solution.

5. Purification of the 2-[^{18}F]-FDG by passing through a C18-reversed phase column and alumina column.

6. Transfer of final 2-[^{18}F]-FDG via sterile filter into a vial in a separate radiation shielded container. The average activity of 2-[^{18}F]-FDG for shipping is 8 to 12 GBq, which can be used for 8 cardiology examinations - PET imaging of the myocardial perfusion.

Injection of 2-deoxy-2 [^{18}F] fluoro-D-glucose was used clinically for administration and investigation of 600 patients with ischemic heart disease. By the end of 1999 more than 180 batches of the product were prepared. The quality control process is carried out during the time of transportation and the results are routinely announced by fax or e-mail to the hospital. The quality control tests include the determinations of purity, radiochemical purity, chemical purity, pyrogenetic and sterility (first control integrity of the 0.22 mm sterile filter). (Fowler, 1986)

2.4.4.4.3 Indications and Usage of ^{18}FDG

Fluorodeoxyglucose ^{18}F-injection is indicated in positron emission tomography (PET) imaging for:

(1) An assessment of abnormal glucose metabolism to assist in the evaluation of malignancy in patients with known or suspected abnormalities found by other testing modalities, or in patients with an existing diagnoses of cancer.

(2) Patients with coronary artery disease and left ventricular dysfunction, when used together with myocardial perfusion imaging, for the identification of left ventricular myocardium with residual glucose metabolism and reversible loss of systolic function.

(3) Patients for the identification of regions of abnormal glucose metabolism associated with foci of epileptic seizures. (Fowler, 1986)

2.4.4.4.4 Dosage and Administration

The recommended dose of Fluorodeoxyglucose ^{18}F-injection for an adult (70 kg) is 185-370 MBq (5-10 mCi), as an intravenous injection for studies of malignancy, cardiology, and epilepsy.

In general, Fluorodeoxyglucose F-18 injection should be administrated after patients have fasted for 4-6 hours. For cardiac use, Fluorodeoxyglucose F-18 injection may be administered either to patients who have fasted or to patients who have received a glucose load.

The optimum rates of administration and upper safe dose for Fluorodeoxyglucose F-18 injection have not been established. The time interval between doses of Fluorodeoxyglucose F-18 injection should be long enough to allow substantial decay (physical and biological) of previous administration.

The final dose for the patient should be calculated using proper decay factors from the time of the end of synthesis (EOS), and measured by a suitable radioactivity calibration system before administration taking into account decay correction factors. (Fowler, 1986)

2.4.4.4.4.5 Patient Preparation

Blood glucose levels should be stabilized before Fluorodeoxyglucose F-18 injection is administered. In non-diabetic patients this may be accomplished by fasting 4-6 hours before Fluorodeoxyglucose F-18 injection. Diabetic patients may need stabilization of blood glucose on the day preceding and on the day of the Fluorodeoxyglucose F-18 injection. For cardiac imaging, administration of Fluorodeoxyglucose F-18 injection to fasting patients limits the accumulation of Fluorodeoxyglucose F-18 to ischemic

myocardium. This may make localization of the ischemic region difficult because the surrounding myocardium will not be well-visualized. Conversely, administration of Fluorodeoxyglucose F-18 injection to patients who have received a glucose load (e.g., 50-75 grams, 1-2 hours before Fluorodeoxyglucose F-18 administration) allows the surrounding, non-ischemic myocardium to be seen and facilitates localization of ischemic areas. (Fowler, 1986)

2.4.4.4.4.6 Imaging

Optimally, it is recommended that positron emission tomography (PET) imaging be initiated within 40 minutes of administration of Fluorodeoxyglucose F-18 injection. Static emission scans are acquired after 30-100 minutes from the time of injection.

2.4.4.4.4.7 Drug handling

Fluorodeoxyglucose F-18 injection, like other parenteral drug products, should be inspected visually for particulate matter and discoloration before administration, whenever solution and container permit. Fluorodeoxyglucose F-18 injection preparations containing particulate matter or discoloration should not be administered. They should be disposed of in a safe manner, in compliance with applicable regulations. Aseptic techniques and effective shielding should be employed in withdrawing doses for administration to patients. Waterproof gloves and effective shielding should be worn when handling the product. The contents of each vial are sterile and non-pyrogenic. To maintain sterility, aseptic technique must be used during all operations involved in the manipulation and administration of Fluorodeoxyglucose F-18 injection.

The current Reference Listed Drug (RLD) states the Fluorodeoxyglucose F-18 should be used within 8 hours of the end of synthesis (EOS). (Fowler, 1986)

As with any other radioactive material, appropriate shielding should be used to avoid unnecessary radiation exposure to the patient, occupational workers, and other persons. Fluorodeoxyglucose F-18 injection, like other radioactive drugs, must be handled with care and appropriate safety measure should be used to minimize radiation exposure to clinical personnel. Care should be taken to minimize exposure to the patient consistent with proper patient management. Radiopharmaceuticals should be used by or under the control of physicians who are qualified by specific training and experiences in the safe use and handling of radionuclides, and whose experience and training have been approved by the appropriate governmental agency authorized to license the use of radionuclides. (Fowler, 1986)

2.4.4.4..4.8 Radiation dosimetry

The estimated absorbed radiation doses (rem/mCi) to a 1-year (9.8 kg), 5-year (19kg), 10-year (32kg), 15-year (57kg), and a human adult (70kg) from intravenous injection of Fluorodeoxyglucose F-18 are shown in Table 3.2. These estimates were calculated based on human date and using the data published by the International Commission on Radiological Protection for Fluorodeoxyglucose F-18. The dosimetry data obtained and presented in this table show that there are slight variations in absorbed radiation dose for various organs in each of the age groups. These dissimilarities in absorbed radiation dose are understood to be due to developmental age variations (e.g., organ size, location, and overall metabolic rate for each age group). The identified critical organs (in descending order) across all age groups evaluated (i.e., newborn, 1, 5, 10, 15 year(s) and adults) are the urinary bladder, heart, pancreas, spleen, and lungs. The absolute values for absorbed radiation in each of these organs vary in each of the age groups. (Fowler, 1986)

Table 2.2: **Estimated absorbed radiation doses (rem/mCi) after intravenous administration of 2-deoxy-2-[^{18}F] fluoro-D-glucose, Fluorodeoxyglucose F-18 injection**.

Organ	New born (3.4 kg)	1 y old (9.8 kg)	5-y old (19 kg)	10-y old (32 kg)	15y old (57 kg)	Adults (70 kg)
Bladder Wall[2]	4.3	1.7	0.93	0.60	0.40	0.32
Heart wall	2.4	1.2	0.70	0.44	0.29	0.22
Pancreas	2.2	0.68	0.33	0.25	0.13	0.096
Spleen	2.2	0.84	0.46	0.29	0.19	0.14
Lungs	0.96	0.38	0.20	0.13	0.092	0.064
Kidneys	0.81	0.34	0.19	0.13	0.089	0.074
Ovaries	0.80	0.8	0.19	0.11	0.058	0.053
Uterus	0.79	0.35	0.19	0.12	0.076	0.062
LLI wall	0.69	0.28	0.15	0.097	0.060	0.051
Liver	0.69	0.31	0.17	0.11	0.076	0.058
Gallbladder wall	0.69	0.26	0.14	0.093	0.059	0.019
Small Intestine	0.68	0.29	0.15	0.096	0.060	0.047
ULI wall	0.67	0.27	0.15	0.090	0.057	0.046
Stomach wall	0.65	0.27	0.14	0.089	0.057	0.047
Adrenals	0.65	0.28	0.15	0.095	0.061	0.048
Tests	0.64	0.27	0.14	0.085	0.052	0.041
Red Marrow	0.62	0.26	0.14	0.089	0.057	0.047
Thymus	0.61	0.26	0.14	0.086	0.056	0.044
Thyroid	0.61	0.26	0.13	0.080	0.049	0.039
Muscle	0.58	0.25	0.13	0.078	0.049	0.039
Bone Surfaces	0.57	0.24	0.12	0.079	0.052	0.041
Breast	0.54	0.22	0.11	0.068	0.043	0.034
Skin	0.49	0.20	0.10	0.060	0.037	0.030
Brain	0.29	0.13	0.09	0.078	0.072	0.070
Other Tissues	0.59	0.25	0.13	0.083	0.052	0.042

Note1: Assumptions on the bio distribution based on data from Gallager et al. (JNM 18:10, 990-996) and Jones et al. (JNM 23:7, 613-617).

Note 2: The dynamic bladder model with a uniform voiding frequency of 1.5 hours was used.

2.4.4.4.4.9 Supply and storage

Fluorodeoxyglucose F-18 injection is supplied in a multi-dose, septum capped 30 ml glass vial containing between 148-1480 MBq/ml (4-40 mCi/ml) of no carrier added 2-deoxy-2-[^{18}F] fluoro-D-glucose, at end of synthesis, in approximately 16 ml.

Fluorodeoxyglucose F-18 should be stored upright in a lead shielded container at controlled room temperature. Storage and disposal of Fluorodeoxyglucose F-18 should be in accordance with the regulations and a general license, or its equivalent, of an Agreement State or a Licensing State. (Fowler, 1986)

2.4.4.4.4.10 Expiration date and time

The expiration date and time are provided on the container label. Fluorodeoxyglucose F-18 should be used within 8 hours from the time of the end of synthesis. (Fowler, 1986)

2.5 Radiation Safety and Dosimetry

In medical imaging, it is essential to be on familiar terms with radiation terminology. Those who are not will find themselves on unsteady ground either when reading the literature or discussing the particulars of a computed tomography (CT) scan with patients. The numerous terms used to describe radiation dose contribute substantially to the confusion, and I believe the first step to a solid understanding is to use only two or three terms for dose measurement. Otherwise, you will eventually get lost by using the full range of units e.g. Roentgen, rad, rem, Gray, Sievert, and their respective conversion factors. (Alexander C. M 2013)

2.5.1 Technical Factors Affecting Patient Radiation Dose:

1. The factors affecting CT patient radiation dose can be divided into the following categories:

a. System configuration.

b. User settings.

2. The individual technical configuration of a CT system determines several characteristics that may affect patient dose:

a. Source–detector distance: As the distance from the x-ray tube to the detectors decreases, dose increases.

b. Filtration within the CT x-ray tube varies between approximately 6 and 9 mm aluminum (Al) or equivalent material. Filtration acts to remove the unwanted, "low-quality" portion of the x-ray beam that adds to the patient radiation dose while failing to yield useful acquisition data. Beam-shaping or bow-tie filters are also added to the x ray tube to compensate for the non-cylindrical nature of most body shapes. Additional filtration material along the periphery of the x-ray beam absorbs radiation where it is not necessary, thereby reducing the overall patient dose.

c. Detector efficiency plays an important role in patient radiation dose and can be described in several ways:

• The inherent absorption efficiency of each detector element describes the ability of the detector to capture transmitted x-ray quanta and produce the appropriate response. Inefficiency here can result in the loss of data and a subsequent compensatory increase in patient dose.

• The geometric efficiency of a detector array describes the spatial arrangement of detector elements, including the amount of interspace material required between adjacent elements. The interspace material absorbs transmitted radiation but yields

no response. This results in a loss of acquisition data (signal) and requires an increase in radiation dose to compensate. This is of particular importance in MSCT, in which the complex arrangement of multiple rows of detectors requires increased interspace material, resulting in a reduction in geometric efficiency.

d. In order to expose the widened detector array equally, MSCT utilizes a cone-shaped beam, instead of the fan-shaped beam traditionally used by single-slice CT (SSCT) systems. All detectors of the array must be exposed to x-radiation of equal intensity. The beam must be expanded even further to avoid exposing the detectors to undesirable "penumbra." This process is referred to as over-beaming. CT image data are acquired from only a portion of the exposed detector array. This results in a radiation dose to the patient that does not contribute to the formation of the CT image. Some CT manufacturers employ focal spot tracking systems to finely control the position of the x-ray beam on the detectors, reducing over-beaming and subsequent radiation exposure.

e. Over-arranging occurs when radiation dose is applied before and after the acquisition volume to ensure sufficient data collection for the interpolation algorithms inherent in spiral CT. Up to a half-rotation both before and after the spiral scan are common and add to the patient radiation dose.

f. Noise reduction algorithms, or adaptive filters, are employed during the reconstruction process to reduce displayed noise within the CT image. Reduction of displayed noise allows for lower mAs (milliampere-seconds) settings during data acquisition.

3. Use of an MSCT rather than an SSCT system is associated with several technical pitfalls with the potential to increase the patient radiation dose. Dose can be considerably higher with MSCT because of:

a. Decrease in the focal spot–detector distance.

b. Use of a cone beam instead of a more z-axis– collimated fan beam.

c. Increases in the number of phases of acquisition enabled by decreased scan times.

d. Use of thinner section widths for improvement of three-dimensional and multi-planar reformation (MPR) images.

4. Scanning parameters should be routinely adjusted in an effort to minimize patient radiation dose.
Adjustments should consider the exam indication, region(s) of interest, and patient's age and body habitus.

5. Protocol optimization is the process of adjusting parameters such as mA/kVp, slice thickness, and pitch for the purpose of reducing patient radiation dose while maintaining adequate image quality.

6. In certain applications, such as pediatric scanning and CT angiography, reduced kVp settings may be used without a loss in image quality, resulting in a dose reduction.

7. There is a directly proportional relationship between the milliampere (mA) setting, scan time, and patient radiation dose. For example, if the mAs value is doubled, the patient radiation dose is doubled.

8. During CT data acquisition, the section of the patient exposed to radiation may be referred to as the dose profile. As measured at the iso center of the gantry, the longitudinal (z-axis) dimension of the dose profile is directly controlled by collimation of the x-ray beam.

9. When only a single slice is scanned, an increase in collimation (thinner section width) will result in a decrease in patient radiation dose. However, CT examinations rarely consist of a single slice.

10. Within the context of the standard CT examination, collimation may indirectly affect patient radiation dose. Increases in collimation (i.e., thinner slices) yield images with more noise. Although usually unnecessary, it is common practice for the user and/or system to compensate for the resultant noise generated by thin sections with an increase in mA, thereby increasing patient dose.

11. During multi-detector CT (MDCT), wider collimation results in improved dose efficiency because less over-beaming occurs. Narrow beam widths, i.e., thin slices, increase over-beaming and reduce dose efficiency.

12. Although reconstruction algorithm (kernel) and window width and level settings are not primary controllers of patient radiation dose, they can play an indirect role. Noise levels in the CT image are a function of dose: Decreased dose typically yields an increase in image noise. Displayed noise can be reduced with the utilization of an appropriate reconstruction algorithm, or kernel. Also, displaying the reconstructed image with the correct window settings can help reduce the low image qualities inherent with noise. Both of these solutions are alternatives to increasing the patient dose.

13. Image noise is directly related to patient size. As a patient size decreases, noise decreases. Protocol optimization should include size-based dose (mAs) adjustments. For example, optimal scans in children can be acquired with a substantially lower radiation dose than scans in larger patients.

14. The clinical indication for a CT study should also be considered in the attempt to reduce patient radiation dose. For example, during renal stone survey scans of the abdomen and pelvis, more noise can be tolerated because of the high inherent contrast of the pathology in question.

15. Overall scan length and repeat scans, including multiple phases, should be kept to a minimum.

16. During SSCT, pitch values greater than 1 allow for the acquisition of a given scan volume in a shorter time, resulting in a reduction in patient radiation dose.

17. However, an increase in pitch during MSCT results in a marked increase in image noise. It is typically compensated for by an increase in mA, yielding little net improvement in patient radiation dose.

18. The modern CT scanner comes equipped with a form of automatic exposure control (AEC) to manage patient radiation dose on the basis of the size, density, and overall attenuation of the part being examined. Automatic tube current modulation (ATCM) can occur as either:

a. Angular (x- and y-axis) tube current modulation, whereby the mA setting is adjusted according to the difference in thickness of the part as the tube rotates. For

example, during imaging of the oval torso, mA can be reduced as the beam passes from anterior to posterior. Less attenuation occurs in the AP path than in the lateral path through the patient.

b. Longitudinal (z-axis) tube current modulation, which allows for the adjustment of the mA setting as the scan proceeds along the z-axis of the patient. Differences in attenuation as the body thickness and tissue density change from the chest to the abdomen, and so on, are met with appropriate adjustments in mA, resulting in an overall reduction in radiation dose.

19. Radiation dose reduction is maximized in CT scanners that employ both the angular and longitudinal current modulation techniques.

20. During MSCT cardiac studies, prospective gating can be used to reduce the patient radiation dose. ECG-triggered tube current modulation allows for pulses of x-ray energy rather than continuous exposure to be used.

21. Tube current is reduced during the cardiac phase not utilized for image reconstruction.

22. The potential radiation dose savings gained with ECG-triggered tube current modulation depend on the patient's heart rate. As heart rate increases, the radiation dose savings decrease.

2.5.2 Radiation Protection:

1. Radiation protection in CT should follow the ALARA (as low as reasonably achievable) concept.

2. Radiation protection of the CT patient should also encompass three general principles:

a. Strict clinical indication.

b. Protocol optimization.

c. Shielding.

3. Limiting CT examination to strict indications is the best way to reduce radiation exposure.

4. Scan lengths should be limited to the clinically indicated region(s).

5. Multiple phase acquisitions should be held at a minimum.

6. An optimized protocol is one that acquires CT images with acceptable levels of noise at the lowest possible dose.

7. Lead shielding should be utilized during CT whenever clinically possible.

8. Shielding of radiosensitive tissues, such as the eye lenses, breasts, and gonads, is critical.

9. Shielding must be applied both above and below the patient, to account for the rotational nature of the exposure in CT.

10. In-plane bismuth shielding of particularly radiosensitive areas, such as the orbits, thyroid, and breast tissue, can substantially reduce the effective radiation dose.

11. Scatter radiation does occur in the immediate area surrounding the CT scanner.

12. Room shielding requirements must be evaluated by a qualified radiologic health physicist.

13. Consideration for shielding requirements should account for exam workload, scanner position, and construction of doors, windows, and so on.

14. When it is clinically necessary to have the patient accompanied by a guardian or family member during a CT procedure, or when other health personnel remain in the room during scanning, the guardian/ family member or health personnel must wear appropriate lead shielding (Daniel N. DeMaio 2011).

Deterministic Effects

Radiation sickness leading to death is the most severe of the immediate or deterministic effects of radiation and is usually associated with nuclear warfare or reactor accidents. There are rare exceptions, however. For example, about 5 years ago, Alexander Litvinenko, a former officer in the KGB, died from radiation sickness after being intentionally poisoned with polonium 210. His cause of death was initially overlooked since polonium kills with alpha particles, not gamma rays, making it very difficult to detect if this poison is not suspected.

In clinical practice, deterministic effects are only rarely encountered because the absorbed dose of a diagnostic scan is so far below the threshold for effects. However, it is not uncommon to see skin and hair changes from radiation after prolonged interventional procedures or in patients who have multiple high-dose imaging procedures during a single hospitalization. In addition, it is very important for anyone involved with CT imaging to be aware of the possibility of deterministic

effects and know what they look like. For example, it was reported that some patients who experienced hair loss after improperly administered CT scans were initially sent to dermatologists because the connection between the recent CT scan and their symptom of hair loss was not initially recognized.

Effective Dose

The effective dose is measured in units of Sieverts or milli-Sieverts (mSv), named for physicist Rolf Sievert. It is a measurement of dose that, unlike absorbed dose, takes into account the sensitivity of the tissues that receive the radiation. For example, while CT imaging of the head requires a relatively large radiation dose, its effective dose is only 2mSv. That is less that the average individual's effective dose from background radiation in the United States (3mSv). The reason the effective dose of a head CT is so low is that the brain is relatively insensitive to radiation. Compare that with a chest CT that has a much lower absorbed dose but an effective dose that is three to five times more than a head CT.

That is because the organs included in the chest CT, such as breast and esophagus, are much more sensitive to radiation, and this is reflected its high effective dose.

Stochastic Effects

The effective dose is use to predict the late or stochastic effects of radiation. The word "stochastic" is not commonly used in medicine apart from this circumstance. Its meaning in this situation is usually taken to be "randomly determined" but its derivation is attributed to the Greek word skokhos, "to aim," although some would say more aptly from the word stokhazesthai , "to guess." The magnitude of the stochastic effect for diagnostic radiation remains unclear, but it is generally accepted that the late adverse effects of diagnostic radiation may appear years after radiation exposure. What remains uncertain to this day is the precise level of radiation exposure necessary to even entertain the possibility of these late effects. The authors

of an article on virtual colonoscopy using CT wrote, “An estimated 70 million CT scans are performed in the U.S. every year, up from three million in early 1980s, and as many as 14,000 people may die every year of radiation induced cancers as a result.” A more recent paper in the Lancet suggested that just three CT scans of the head incurred prior to age 15 will increase the risk of brain cancer in that patient by several fold. These are just estimates and difficult to confirm since it is almost impossible to determine which cancers are related to radiation, among the many that occur every year.

There is little doubt, however, that late effects can occur from a long exposure to high doses of radiation. It is worthwhile for anyone involved in medical imaging to read about those who died from radiation as a result of early medical or scientific investigations. Perhaps the most famous example is Marie Curie. She is credited in some share with introducing the term “radioactivity” and with the discovery of polonium (named after her homeland Poland) and, later, radium. Her tireless work to isolate the element radium required long exposures to pitchblende, a radioactive ore. She died in 1934 from aplastic anemia that seems undoubtedly the result of her prolonged exposure to radiation.

The American Association of Physicists in Medicine (AAPM) in December 2011 took the position that, for diagnostic tests with an effective dose of 50mSv or less, when incurred in a single exposure, or 100mSv in multiple exams over a short time, the late effects may be “nonexistent” (their word). It is also important to keep in mind that medical radiation has a purpose, and the expectation is that the risk should be offset by the benefits of the exam for the patient. Since the actual risk of low-dose radiation is unknown, and a small risk is reasonable for a large gain, it is very difficult to know how much concern should be attached to a single CT exam. However, common sense would indicate that less radiation is better, and many patients are having multiple CT scans. These are the best reasons why medical

imagers must be attentive to using the smallest amount of radiation necessary to make the diagnosis using CT or any other X-ray device.

This idea is captured in the term ALARA (As Low As Reasonably Achievable) and should be our goal whenever considering the necessary dose for medical imaging (Alexander C. M 2013).

2.5.3 Dose Measurement:

1. Slice sensitivity profile (SSP) may be used to describe the reconstructed CT section.

2. However, the section of tissue exposed to ionizing radiation, or dose profile, is greater in width than the SSP. The accurate calculation of CT patient radiation dose must take this fact into account.

3. Exposure is the term used to describe the ability of x-rays to ionize a volume of air. It is measured in roentgens (R).

4. Absorbed dose describes the amount of x-ray energy absorbed in a unit of mass. It is measured in grays (Gy) (Daniel N. DeMaio 2011).

The absorbed dose is the measure of ionizing radiation deposited into a specific volume of tissue. Although absorbed dose does not take into account the behavior of that tissue or provide an estimate of the risk of radiation, it does correlate well with the immediate or deterministic effect s of radiation.

The units of absorbed dose in common use are the Gray (Gy) and milli-Gray (mGy) named for the physicist Louis Harold Gray. The actual absorbed dose can be quite difficult to determine since it depends on the energy of the X-rays, their total number, and the nature and depth of tissues involved. Although it is easiest to

measure dose at the skin surface, it is the total absorbed dose that is of interest, and so this number for CT is always an estimate.

The absorbed dose can be used to predict whether the radiation was likely to be the cause of reddening of the skin or even hair loss in a particular patient. Just so you have some benchmark values, keep in mind that the absorbed dose of a head CT is about 50mGy and temporary hair loss occurs at a dose of 3Gy at the skin. Thus, it would take over 50 diagnostic head CT scans to cause temporary hair loss, assuming there is a cumulative effect. There are reports of hair loss after a single CT brain perfusion scan in patients who also had more than one cerebral angiogram, thus supporting the concept of cumulative effect of diagnostic radiation (Alexander C. M).

5. Kerma may also be used to describe absorbed dose. Air kerma describes the amount of radiation absorbed in a quantity of air.

6. Effective dose accounts for the type of tissue that the radiation is deposited in. Different tissues are assigned weighting factors based on their individual radio sensitivity. Effective dose approximates the relative risk from exposure to ionizing radiation. It is measured in Sieverts (Sv).

7. The CT dose index (CTDI) is an approximate measure of the dose received in a single CT section or slice.

8. CTDI is calculated for the central slice in a series that is surrounded by seven slices on each side.

9. CTDI is measured by performing scans of both head- and body-sized CT phantoms using specific technical parameters. A thermo luminescence dosimeter (TLD) is placed within each phantom during the scans.

10. The exposure measured by the TLD is used to calculate the CTDI for each acquisition.

11. Exposure from the scan is measured by the TLD, and the CTDI is calculated from those measurements.

12. $CTDI_{100}$ is a fixed measurement taken with a 100- mm-long pencil ionization chamber and makes no reference to a specific number of slices.

13. Because of absorption, dose varies within the CT image across the acquired field of view. $CTDI_w$ is an internationally accepted, weighted dose index. It is calculated by summing two-thirds of the exposure recorded at the periphery of the field with one third of the centrally recorded dose. This weighting yields a more accurate dose approximation.

14. $CTDI_w$ is calculated from measurements made with TLDs positioned at the center and periphery of the phantom to account for the variance in dose distribution.

15. The $CTDI_w$ is measured utilizing a conventional step-and-shoot mode of axial CT scanning and does not account for the effects of helical scanning on patient radiation dose.

16. $CTDI_{vol}$ is used to approximate the radiation dose for each section obtained during a helical scan (Daniel N. DeMaio 2011).

A number of CT dose measurements have been used over time, and these are variations of a term called CT dose index or CTDI. Some that are no longer in common use are CTDI FDA, $CTDI_{100}$, and $CTDI_{w}$. Fortunately, there is only one you should be familiar with now, the measurement CTDI volume ($CTDI_{vol}$) since it is calculated on most commercial CT scanners and is widely used in the literature.

The meaning of CTDI has changed over time in response to advances in CT technology. The measurement of $CTDI_{vol}$ is performed in a phantom and incorporates some weighting of the peripheral dose compared with the lower central dose, as well as the pitch used for helical scanning. Keep in mind, however, that $CTDI_{vol}$ for a CT scan is just a calculated value based on X ray tube settings.

Although it does account for the specific features of the scanner, such as beam filtration, when reported by the scanner at the end of a scan, it is not at all a direct measurement of the dose delivered to a particular patient. It is in truth a measurement of the X-ray tube output and is based on specific scan parameters, including mA, kV, and pitch, as well as dose modulation. It can be quite helpful as long as one recognizes that in some situations it may not accurately reflect the actual patient dose, and CT brain perfusion has been cited as one example.

Although $CTDI_{vol}$ is by no means a perfect measure of dose it is useful in day-to-day CT operations. Many find it helpful whenever they want to see how the modification of one scan parameter will influence patient dose because that change will be reflected in the $CTDI_{vol}$. This number also allows comparison of the dose of the same scan performed on different machines even when they are from different manufacturers. And, by just glancing at the dose report, now available for each patient exam, one can determine whether a specific exam falls within both the ACR's and your own institutional guidelines. For example, if the dose page from a

head CT scan shows a $CTDI_{vol}$ of 90mGy, it should serve as a warning that there is a problem with the scan protocol that should be addressed immediately (Alexander C. M 2013).

17. It corresponds to the axially acquired $CTDI_w$ divided by the helical pitch, as follows:

$$\textbf{CTDIvol} = \frac{\textbf{CTDIw}}{\textbf{Pitch}}$$

18. As the pitch increases, the dose per section ($CTDI_{vol}$) decreases.

19. $CTDI_w$ approximates dose along the x- and y-axes of the acquired CT image. $CTDI_{vol}$ also includes the dose along the z-axis of the scan acquisition; it is given in units of milligrays (mGy).

20. $CTDI_{vol}$ is similar in principle to an older term used for conventional step-and-shoot scanning, multiple scan average dose (MSAD).

21. MSAD is a calculation of the average cumulative dose to each slice within the center of a scan consisting of multiple slices.

22. The MSAD is higher than the dose from an acquisition of a single slice, because of the contribution of scatter radiation.

23. The doses at the beginning and end slices in a series are slightly less, owing to the lack of dose from their outer sides.

24. MSAD may be calculated for axial scanning as follows:

$$\text{MSAD} = \frac{T}{I} \times \text{CTDI}$$

Where T is slice thickness and I is increment or image spacing.

25. MSAD accounts for the effects of image spacing or bed index on the patient dose during axial scanning.

26. During axial scanning, overlapping scans increase the patient radiation dose, whereas gaps between slices decrease it.

27. MSAD increases when slice thickness is greater than image spacing—overlapping scans.

28. MSAD decreases when slice thickness is less than the bed index—noncontiguous scans.

29. When slice thickness equals the bed index, MSAD is equal to CTDI.

30. During spiral or helical scanning, MSAD is controlled by pitch, as follows:

$$\text{MSAD} = \frac{\text{CTDI}}{\text{Pitch}}$$

Where pitch is the amount of table travel per tube rotation divided by the collimation (Daniel N. DeMaio 2011).

The choice of pitch is always a compromise among scan speed, patient dose, and image resolution.

It is useful to consider using a pitch of 1 as a starting point. Pitch 1 means that there are no gaps in the path covered by the X-ray beam, and no tissue is exposed more than once. Increasing the pitch above 1 means that gaps will appear in coverage by the X-ray beam so that some tissue receives much less radiation. Although this would result in complete gaps in imaging when using axial mode scanning, because of the interpolation of data these gaps in the helical scan simply mean that the estimations are less accurate. In principle, this can be used to reduce dose as long as adequate image quality is preserved, and increasing pitch allows faster coverage of the anatomy. For example, this is a good option to consider for CTA of the chest, where resolution demands are less than for brain CTA but rapid coverage of a large section of anatomy is necessary.

With the exception of cardiac imaging, it is uncommon to use a pitch of less than 1, but it may be helpful for high-detail exams such as temporal bone scans. With low pitch, there is actually overlap of the X-ray path over the body. This results in increased dose in those areas, but, this oversampling allows a more accurate measurement of attenuation values and lower noise. Low pitch also requires more time to cover the same anatomy (Alexander C. M 2013).

31. MSAD is most accurate at the center of a scan series. At either end of an acquisition, MSAD tends to overestimate patient radiation dose.

32. Both $CTDI_{vol}$ and MSAD are used to approximate average radiation dose within a scan volume. Total scan length along the z-axis is not considered. Therefore, neither provides an estimate of the total dose along a given scan volume.

33. Dose length product (DLP) is expressed in the units of mGy-cm. Its determination is really quite uncomplicated; it is simply the calculated $CTDI_{vol}$ multiplied by the length of the scan, from head to foot, in centimeters. But this simple calculation has been demonstrated to provide a remarkably accurate measure of effective dose when compared with the much more sophisticated Monte Carlo simulation. Although sounding very James Bond-ish, this method uses a mathematical representation of the body with approximate shapes of organs and their estimated radiation sensitivity to predict the effects of radiation. It has been demonstrated that multiplying the DLP by a predetermined constant for a specific body part will provide a value for effective dose in mSv that is a surprisingly close to the calculated effective dose using the Monte Carlo simulation.

Dose length product (DLP) for brain imaging, that constant is .002 mSv/mGy-cm. Since the average head CT has a $CTDI_{vol}$ of under 70mGy and a DLP of about 1,000 mGy-cm, the calculated effective dose of a head CT is 2mSv (.002mSv/mGy-cm × 1,000mGy-cm). Now, if we were to use the exact same imaging parameters for a CT scan of the neck and assume it has the same DLP of 1,000 mGy-cm, we would then use a larger constant (.005 mSv/mGy-cm) to predict effective dose because of the increased sensitivity to radiation of the tissues in the neck. The conversion factor for chest CT is even higher, .018 mSv/mGy-cm, because the tissues there are even more sensitive to the effects of radiation (Alexander C. M 2013).

Dose Length Product is an internationally accepted measure of CT patient dose defined as:

DLP = MSAD x slice width (cm) x No. of slices in scan volume

where slice again equals the pre-patient collimator setting and not the reconstructed slice thickness.

34. The DLP can also be illustrated as the product of $CTDI_{vol}$ and scan length and is given in units of milligrays-centimeters (mGy-cm), as follows:

$$\mathbf{DLP = CTDI_{vol} \times scan\ length}$$

35. When evaluating patient radiation dose from a MDCT study, one must bear in mind that $CTDI_{vol}$ is still controlled by the pre-patient collimator setting, regardless of the number of reconstructed slices.

36. Because direct measurement of effective dose from CT is not possible, estimations must be made on the basis of exposure to a phantom. Once the air kerma or absorbed dose in a phantom is measured, an estimate of effective dose can be calculated.

37. $CTDI_{vol}$ and DLP are displayed on many CT scanners to help the technologist achieve protocol optimization.

38. It is important to remember that $CTDI_{vol}$ and DLP do not account for patient size and so overestimate the radiation dose to the larger patient and underestimate the dose to the smaller patient.

39. $CTDI_{vol}$ and DLP may also be expressed by the newer terms computed tomography air kerma index (Ca) and air kerma length product (klp), respectively (Daniel N. DeMaio 2011).

2.5.4 Patient Radiation Dose Reduction:

One of the most difficult challenges for the diagnostic imager is to determine the "optimal dose" for CT imaging. This is in part due to the very subjective nature of this assessment, which can vary widely among individuals based on their experience and expertise. It is important to keep in mind at all times that the goal is not just to

produce exquisite CT images. It should be to use just enough radiation to provide images as good as they need to be in order to establish the diagnosis. And, keep in mind that when we talk about “radiation cost,” it is the patient paying the price. That is why the CT user needs to find a reasonable compromise between patient dose and image quality. Although it is tempting to create images of extraordinary quality—and even if you find them easier to interpret—if this requires a higher dose, it must be justified by the clinical question.

Another problem to consider when determining optimal dose for CT is our inability to perceive when a CT was performed using too much dose. Early X-ray images were no different from photographs taken with a film camera. Those early film negatives accurately reflected the relationship between the available light, the sensitivity of the film, and the camera settings. For example, if the aperture was set too wide on a sunny day, the picture would appear dark from overexposure. There was a time when making a high-quality X-ray image, in much the same way, required a good deal of judgment so that the proper settings of kV, mA, and exposure time were combined to give the correct exposure of the radiographic film. I still remember my discomfort when looking at the nearly black X-ray image that was taken of one of my children by a student radiographer many years ago. Both of us clearly recognized that too much radiation was used.

As many newly unemployed newspaper photographers well know, photography using digital cameras is much more forgiving because only a loose relationship remains between the exposure settings and the final image. That is due largely to the use of electronic detectors instead of fi lm in modern cameras. These can provide acceptable images under a wide range of lighting situations just by modifying the sensitivity of the sensor. Within reasonable limits of X-ray dose, modern CT scanners function the same way as digital cameras since they also provide acceptable images within a wide range of exposures.

In fact, when CT scans are performed with too much radiation there will be few complaints from imagers because the CT images actually look better—the higher the dose, the better the images.

Modern CT scanners therefore require that the user have a good understanding of the dose reports since image assessment alone can be misleading. Even when CT images are made with too little dose they might pass for a time as adequate if their poor quality is attributed to other confounding factors like motion (Alexander C. M 2013).

Years ago, a writer reflected that the most effective way to minimize travel time was to just stay home. In the same way, the simplest and most powerful way to minimize patient radiation dose is to not perform a CT scan at all. You must consider whether the patient will benefit from imaging and, if so, if CT is ideal for the diagnosis (since there are now many other options for imaging, such as magnetic resonance [MR] and ultrasound). Another strategy that immediately reduces dose, and one you may have more control over, is to severely restrict your use of high dose techniques such as multiphase CT. In most circumstances, there is no need for both pre- and post-contrast imaging of the brain or chest, for example. For sites that have access to a dual-source, dual energy CT scanner a technique called “virtual non-contrast” may be an option for dose reduction. For example, when obtaining a contrast enhanced brain CTA there can be substantial dose reduction for the patient by not performing a non-contrast head scan prior to the CTA. For example, with conventional CTA is difficult to determine whether there exists subarachnoid hemorrhage without a non-contrast exam.

But, by using the imaging characteristics of iodine and blood at the different energies it becomes possible to provide a “virtual” non-contrast scan from the CTA data by removing the contrast enhancing structures.

Critical evaluation of the need for CT scanning does not require canceling all exams, just a thoughtful approach and some humility when considering whether our patient's health has improved in proportion to the increased use of CT over the past 15 years (Alexander C. M 2013).

1. A dose gradient exists across the field of view (FOV) of the CT image.

2. Dose at the periphery can be markedly greater than that at the center of the image, along the x- and y-axes.

3. The magnitude of this gradient is size dependent.

The difference in absorbed dose is greater in larger patients.

4. Smaller adults and pediatric patients exhibit little to no radial dose gradient.

5. For smaller patients, the entrance radiation and exit radiation are equal in intensity, resulting in a more uniform distribution of dose.

6. When all other technical factors remain constant, absorbed dose is greater in the smaller patient.

7. This difference in dose distribution illustrates the importance of dose reduction for the smaller, i.e., pediatric, patient.

8. Recommendations for the reduction of pediatric dose include:

a. Eliminate CT scans for inappropriate indication.

b. Reduce multiphase scanning (pre-contrast, delays, and so on).

c. Reduce mA.

d. Increase pitch.

9. Regardless of age, the CT protocol should be optimized on the basis of the individual patient's size and/or weight.

10. Patient size–based protocols should be developed for each specific CT system to include adjustments in mA, kVp, and pitch.

11. The Image Gently campaign was developed by the Alliance for Radiation Safety in Pediatric Imaging and sponsored by the Society for Pediatric Radiology (SPR). The widely recognized campaign offers guidelines to help reduce pediatric radiation exposure from CT imaging. Like the dose reduction techniques listed here, the Image Gently guidelines suggest that:

a. mA and kVp should be "child-sized."

b. One single-acquisition phase is often enough (Daniel N. DeMaio 2011).

mA and kV

There are many factors that you can alter to lower dose. These include X-ray tube kV and mA, tube rotation time, detector collimation, tube collimation, pitch, reconstructed slice thickness reconstruction kernel, and more. The two that are usually considered the most important contributors to total patient dose are the X-ray tube electrical current (mA) and the potential (kV).

Voltage and amperage are standard measurements of electrical current that acknowledge the contributions of Andre-Marie Ampere and Alessandro Volta to our understanding of electricity. If you have trouble understanding what these measures of electrical energy mean—and many do—you may find it is easier to picture water instead of electrical current. For example, you can consider that voltage is

equivalent to the water pressure at the end of a hose, whereas amperage indicates the actual volume of water flowing from the hose.

My grandfather explained this to me when I was child (which I suppose says a lot about my grandfather and my childhood) by using two streams of water emerging from holes in a large water tank. A large hole just below the top of the tank would allow a lot of water to escape but at very low pressure. This is comparable to the low voltage but high amperage current provided by a car battery.

Now visualize a very small hole near the bottom of the tank. That hole would allow a small, low-volume stream to shoot out of the tank but under tremendous pressure. In electrical terms, that stream would be equivalent to the high voltage and low amperage current typically used to drive the flash in your camera or phone. Static electricity, which we consider harmless, is measured in thousands of volts but with very low amperage.

When considering an X-ray tube, increasing the tube current (referred to in milliampere or mA) will result in more X-rays created at the anode, but the energy of those X-rays is determined by the electrical potential across the tube, which is measured in kilovolts (kV). A higher kV means a greater electrical potential across the tube, and that leads to higher mean energy X-rays emerging from the anode, with greater potential for tissue penetration. A change in kVp, however, alters both the energy of the X-rays emerging from the tube and their number.

Although we frequently talk about CT scans in terms of a single kV value (i.e., kV 120), you should keep in mind that this number represents the peak voltage across the X-ray tube and not the average energy of the X-rays. Although kV reflects the energy range of the X-rays, the beam is composed of

X-rays at multiple energies—it is poly-chromatic. The actual energy of the X-rays in the beam can be described in terms of thousand-electron volts or keV. At a kVp of 80, the lowest X-ray energies in the beam could be as low as 20keV, but no X-rays

will be higher than 80keV. The mean energy within this polychromatic X-ray beam is about one-third to one-half of the peak energy predicted by the kVp.

The use of specially shaped metal filters between the X-ray source and the patient can substantially alter the energy range of the beam. It is commonplace to use a filter that strips out the very lowest energy

X-rays since these contribute to dose without contributing to the image. Another benefit t to using a filter is that by narrowing the range of X-ray energies in the beam, it reduces the beam hardening that occurs within the patient. The filter is also shaped to better suit the shape of the patient, to reduce the number of X-rays at the edges where there is usually less tissue to penetrate than at the center.

The magnitude of the tube current corresponds roughly to the number of X-rays emerging from the X-ray tube, and the imager should use no more and no less necessary for diagnosis. The dose relationship to mA is linear—lower the mA by half, and you cut the dose by half. But whenever you decrease mA by half, you need to remember that noise increases by about 40%. It is also important to recognize that tube current (mA) may be expressed in several different ways that can lead to some confusion when you are changing scan parameters. Tube current can be expressed as mA, mAs, or effective mAs. That last term incorporates the rotation time and tube current, as well as the scan pitch. An effective ma (mAs_{eff}) is simply the mAs divided by the pitch. For example, if the pitch is decreased from 1 to 0.5, the mAs_{eff} doubles.

Why do you need to know this? So that you are not surprised to fi nd that your scanner automatically decreased the tube current when you selected a pitch below l to improve the quality of your temporal bone exams. The scanner software may be set up to keep effective mAs constant, and you will find that the $CTDI_{vol}$ measure of the scan did not change with the alteration of pitch, nor do your scans look better.

That is why you need to check the values of mAs and dose for the resulting scans whenever you alter scan parameters.

The tube potential or kVp determines both the energy of the X-rays and also the number created at the anode of the X-ray tube. For many users, a kVp of 120 is adequate for nearly all scans, but this "one size fits all" approach is quite different from conventional X-ray imaging, in which the kV is frequently adjusted to suit the imaging task. Many believe that CT imaging should take more advantage of this approach since the ideal kV value should be based on the size of the patient, imaging goals, and whether

CT contrast is administered, since contrast has a powerful effect on radiation dose to the patient.

When to Increase kV

The choice of kV has a much larger impact on patient dose than does the choice of mA. That is because patient radiation dose increases proportionately to mA but increases approximately by the square of kV.

For example, an increase of kV from just 120 to 140 results in a 30% increase in patient dose. Although using low kV for CT is desirable when possible, since low-energy X-rays are attenuated more easily, it may be necessary in some circumstances to actually increase kV above 120. This is usually the case in large patients or in patients with implanted metal. Although it is reasonable to consider increasing mA first to accommodate requirements when imaging large patients, in some cases the tube limits may be exceeded by the requirements. And it does not seem reasonable to use more low-energy

X-rays when what is really required are higher energy X-rays that have better penetration. That is certainly the case when imaging patients with titanium aneurysm clips. Adding more low-energy X-rays in that situation makes little

difference toward minimizing artifacts since they are related to photon starvation, and this is best addressed by using X-rays with better penetration. And keep in mind that using a lower kV does not mean there will be a decrease in X-ray dose in all cases. Because noise increases as kV decreases, it is possible that the additional X-rays needed to offset the increased noise may result in a net increase in patient dose. This is more likely to occur in large patients and with non-contrast CT scans.

New scanner software that incorporates both kV, mA adjustments based on the scout view, and not just tube current as nearly all AEC does now, should help the user optimization these two factors.

When to Decrease kV

Adequate low-kV CT imaging is frequently possible when performing body imaging in children and thin adults. This is because the quality of penetration of high-kV X-rays may not be necessary for that patient population. Although decreasing kV is accompanied by an increase in image noise and beam hardening artifacts, the improvement in contrast conspicuity whenever using iodinated contrast in most circumstances offsets these disadvantages. You should recall that iodine is more evident on low-kV CT scans because of the photoelectric interaction of low-energy X-rays with iodine. Since

X-ray beams are polychromatic, the X-ray beam generated using kV 80 will contain many X-rays close to the k-edge of iodine, around 30keV. The increased noise at low kV can be made less evident with an increase in mA while still providing a lower total dose. Although brain imaging is nearly always performed with kV 120, for high-dose exams like brain perfusion, this property of iodine allows adequate imaging using kV 80. Although not commonly considered in practice, the increased conspicuity of iodine should also allow the use of less contrast for some applications.

This could prove to be an advantage for patients with marginal renal function (Alexander C. M 2013).

Axial Versus Helical Scans

An important starting point when designing a scan protocol is the decision of whether to use axial or helical mode imaging. In general, axial imaging will prove to be slower and have inferior reconstructions compared with helical mode, but, at the same time, it offers better control of the dose distribution and, in many cases, produces fewer artifacts. Other factors may not be immediately apparent as you consider these two options for brain imaging. For example, the use of helical mode means that the gantry cannot be tilted on some scanners.

But for those CT scans that must be fast, such as chest imaging and CT angiography (CTA), helical mode is the better choice. With regard to dose distribution, there are two terms you need to understand when considering the choice between axial and helical: overbeaming and overranging (Alexander C. M 2013).

Overbeaming and Overranging

On all CT scanners, the shape of the X-ray beam that emerges from the tube is modified using metal plates called collimators. On the old single-slice CT scanners, the fan beam width was the same or less than the width of the detector row and so the entire X-ray dose was utilized in some fashion to create the image. If we choose to discount differences in detector sensitivity, this arrangement provided a very high "dose efficiency."

This is not the case in multi detector scanners, where the beam width must always be wider than the detectors. That is because the X-ray beam must cover all the active detector rows evenly. Since the X-ray beam diverges from a point on the anode, a portion of the X-ray beam must always fall outside the end detectors in the array,

and this dose is effectively wasted since it does not contribute to the image. The portion of the beam that extends beyond the detectors is called the penumbra, and this effect is called overbeaming. It is important to recognize that this extra dose occurs over the entire length of the detector array and, on average, this adds about 1.5mm of extra tissue radiation on either side of the array. While seemingly small, this extra radiation adds up quickly when using a scanner with a narrow detector array since it will require many rotations to cover the chest and abdomen, for example. However, overbeaming can be discounted for scanners using 32 rows or more since they require so many fewer rotations to cover the same anatomy.

As the number of detector rows increased, however, another source of added dose became more significant called overranging. Because of the very nature of helical image reconstruction, the X-ray beam must begin and end its path outside the region of interest. This bit of extra scanning is necessary to provide the data points needed for interpolation on the end slices. This added dose, unlike overbeaming, is not really wasted since it is necessary for reconstruction, but it is easy to overlook when considering patient dose. The magnitude of this added dose from overranging increases with beam collimation, number of detector rows, and the pitch value.

In practice, the proportion of the total dose from overranging diminishes as the scan length gets longer since overranging at the ends is the same whether the scan length is short or long. This means that overranging can add significantly to total dose on focused exams like temporal bone scans, but its contribution is considered insignificant on studies that cover a lot of anatomy, such as chest-abdomen-pelvis scans.

In cases where the dose contribution from overranging is considered substantial, you should consider using axial mode imaging to better constrain the dose. It may be hard to really gauge the impact of overranging, however, since some of the current generation of large-array scanners can limit the added dose from overranging

through sophisticated collimation at both ends of the scan range. And, for some scanners with very wide detector arrays, helical imaging is not even necessary for head scans since they can be performed with a single axial rotation that eliminates overranging altogether (Alexander C. M 2013).

Tube Rotation Time

Rotation time and mA are interdependent and are sometimes combined in the term milliampere seconds (mAs). That is because the number of X-rays produced is a function of the magnitude of the tube current and the amount of time the tube is turned on. Since the tube is generally on the entire time it is moving, the mAs can be decreased both by using a lower tube current and by spinning the gantry faster so that the rotation is completed faster.

On some scanners, however, decreasing the tube rotation time will cause the scanner to automatically increase the tube current to offset the shorter time the tube is on. This results in no net change in mAs and, as a result, there is no dose reduction and little impact on image quality. But the faster rotation speed may prove to be an advantage since, for CTA, it can increase the chances of imaging the contrast during the arterial phase in the brain. But for detailed imaging, like temporal bone exams or routine brain imaging, where there is usually no advantage to decreasing the total scan time from 10 seconds to 5 seconds, it is usually better to use a longer rotation time since it provides better a signal-to-noise ratio (SNR) at equivalent dose (Alexander C. M 2013).

Detector Collimation and Slice Reconstruction

It is preferable to use narrow detector collimation to improve resolution and decrease artifacts, as long as sufficient dose is utilized. Since there are fewer photons collected per detector when using detector collimation of less than 1mm

compared with say 2mm detector collimation the SNR reflected on images will be lower. Noise can be estimated as 1/[square root of slice thickness]. This means that a 10mm slice has three times less noise than a 1mm slice.

In practice, the primary use of thin detector collimation proves to be less of a problem than one might expect. That is because the data from each thin detector can be combined with three or more neighbors to provide image reconstructions at 5mm; with considerably more SNR than if images were reconstructed at a displayed slice width of 0.625mm. However, whenever the very thin sections are used primarily for diagnosis, the mAs will need to be increased as detector collimation decreases to preserve image quality.

A variation of using thin detectors and thick reconstructions that preserves SNR and some of the benefits of viewing the thin sections directly is to reconstruct relatively thick images but at a smaller increment than the displayed slice thickness. For example, you have the option of generating 2mm reconstructions but at 0.5 mm intervals. The only real disadvantage of this approach is that it increases the total number of slices necessary for storage and review.

You might wonder: “If I am going to combine data from detector rows, and SNR is better with thicker detector collimation, why use thin detector collimation at all?” First, keep in mind that if you perform the scan using thick detector collimation you cannot later go back later and reconstruct thinner sections. There are other benefits of thin detector collimation, however. It decreases the artifacts from partial volume that may appear as indistinct edges of structures on helical reconstructions and volume averaging. It also reduces the beam hardening artifacts that degrade posterior fossa imaging on brain CT.

Filter or Kernel

The terms filter and kernel are used interchangeably and refer to the method of raw data reconstruction after the scan is acquired. There is potentially less confusion if you use the word “filter” to refer to the metal plate that is designed to optimize the X-ray beam and use “kernel” to refer to your choice of image reconstruction algorithm.

The choice of kernel proves to be significant in any dose reduction project since apparent image noise will influence decisions regarding the dose necessary for adequate scanning. So, although the reconstruction technique is not commonly considered a dose reduction tool, you should at least be aware of how this parameter may influence your perception of image quality.

Automatic Exposure Control

It is one thing to select ideal scan parameters when examining a small part of the anatomy, such as the temporal bones, but quite another when performing a scan that includes several body parts of very different thickness, shape, and composition, such as chest and abdomen. The problem with these parts of the anatomy that have wide variations in shape and thickness is that the ideal choice of kV and mA for one portion of the exam will prove to be either too much or too little for another portion covered during the same scan. For example, the appropriate choice for tube current in the chest will be insufficient for imaging the abdomen. Even within a single slice through the chest, what may be an appropriate dose in the anterior to posterior (AP) direction may prove to be insufficient to penetrate side to side across both shoulders. This has become a more commonplace problem as helical imaging has allowed coverage of long sections of the body in a single scan.

To better allow the scanner to match the tube current to the requirements of varying anatomy, most manufacturers offer some variation of automatic exposure control

(AEC) on their scanners. This dose reduction tool is based on one or two scanogram that are created at the start of the exam.

Automatic exposure control usually modifies only the tube current (i.e., mA) during the scan, not the kV. That is why it is sometimes called tube current modulation. By modifying the dose during the scan to match the attenuation of that part of the body, both from slice to slice and within the same slice, significant dose reduction is possible without image degradation. Automatic exposure control should be considered for CT imaging whenever the scan covers a portion of the body where there are significant variations in thickness or attenuation. On some scanners continuous adjustments are made even during a single rotation. This technique is called angular adjustment and it provides more X-rays during the part of the rotation from side to side through the shoulders than when imaging from front to back. The use of that software tool can provide a lower overall dose with better quality, assuming the reference values are correctly set.

There are four important things you need to understand about AEC to use it properly. First, as suggested by the word “automatic,” the user needs to recognize that they have given up a small degree of control over the scan parameters and therefore the final patient dose.

Second, you need to understand that AEC does not “automatically” lower dose. All it does is match tube current to the anatomy based on some target value, such as noise level or mAs equivalent.

It is up to the user to pick an appropriate mA or noise value in order to provide acceptable images but at the lowest possible dose. Third, when imaging thin patients and children, is very important to decide on the appropriate tube voltage first. Automatic exposure control on nearly all scanners will only modify tube current. For thin patients and children, first consider decreasing kV for body imaging since that has a more substantial impact on dose than does AEC. When modifying kV,

keep in mind that AEC quality settings are commonly relevant for only one kV selection. For example, if you choose to decrease tube voltage and also activate AEC, the increase in noise at the lower kV may lead to the AEC to apply a much higher mA value than necessary. Fourth, keep in mind that AEC is intended to accommodate changing anatomy. One instance where AEC may result in excessive patient dose is when it is used during continuous imaging such as CT brain perfusion. In one hospital, it was reported that 200 patients received unusually high doses of radiation during CT perfusion exams in part because AEC was turned on for the brain perfusion studies. This was selected with the intent to reduce dose, but the software "automatically" provided a very high dose. The images were very likely of excellent quality, which may explain why this problem went undetected for so long.

Shielding

Since X-ray dose at diagnostic energies is much higher in superficial tissues, there has been some interest in using radiation shields over particularly sensitive tissues like breast, thyroid, and eyes.

These shields are usually made of bismuth, which has desirable attenuation characteristics compared with lead, for example (i.e., X-ray attenuation without significant metal artifact). These shields are not in widespread use in part because they add cost when used for eyes (eye shields are one-time use), and they add to exam time elsewhere in the body since they need to be applied after the scanogram but before the scan. This is important to keep in mind whenever AEC is used with shields since it is the scanogram that is used to select the tube current on most scanners. If the shield is put in place prior to the scanogram, say at the beginning of the scan, the software would direct the AEC to increase tube current at the level of the shield and that would effectively offset any benefit to shielding. In spite of these

current limitations, shielding should at least be considered as part of any comprehensive dose reduction program.

Iterative Reconstruction

The first CT scans used a purely mathematical reconstruction of the collected data to create images.

That was found to be too slow for clinical imaging and all current scanners routinely use some variety of back-projection. With increasing concern about patient dose from CT and the decreasing cost of computer hardware, it has become commonplace for vendors to offer some variety of mathematical reconstruction called iterative reconstruction. By referring back to the source data, and in some versions accounting for the fixed noise in the system, iterative reconstruction can improve the imaging

SNR and that can be used for better images at the same dose or equivalent imaging at a lower dose.

Although there is no question it can help with dose reduction, its impact on diagnosis is still uncertain.

With any new reconstruction tool, it would be expected that new artifacts may appear, and altered image contrast may alter sensitivity. Early reports, however, indicate that dose reductions of at least 50% for body CT imaging and 10–20% for brain imaging are to be expected once iterative reconstruction is fully integrated into clinical scanners. It seems highly likely that some version of pure mathematical reconstruction or a blend of back-projection and iterative reconstruction will become routine for CT reconstructions (Alexander C. M 2013).

2.6.1 Radiation Dose and Units

The term radiation dose, or simply dose, is defined carefully in terms of two key concepts: (a) the energy deposited per gram in an absorbing medium, principally tissue, which is the absorbed dose, and (b) the damaging effect of the radiation type, which is characterized by the term effective dose equivalent. A related term is radiation exposure, which applies to air only and is a measure of the amount of ionization produced by x-rays and gamma radiation in air. Each of these is defined in the conventional system of units, which in various forms and refinements has been used for several decades, and in the newer SI system, which is gradually re- placing the conventional units. This presentation uses both sets, but for the most part emphasizes conventional units, which are firmly embedded in governmental standards and regulations, at least in the USA (James E. Martin 2006)

2.6.2 Radiation Absorbed Dose

The absorbed dose is defined as the amount of energy deposited per unit mass. The conventional unit for absorbed dose is the rad (radiation absorbed dose), and is equal to the absorption of 100 erg of energy in 1 g of absorbing medium, typically tissue:

1 rad = 100 erg/g of medium

The SI unit of absorbed dose is the gray (Gy) and is defined as the absorption of 1 J of energy per kilogram of medium:

1Gy=1J/kg = 100 rads

A milligray (mGy) is 100 m rads, which is about the amount of radiation one receives in a year from natural background, excluding radon. This is a convenient relationship for translating between the two systems of units since the annual radiation dose due to natural background (equal to 1 mGy

or 100 m rads) is a convenient reference point for radiation dose received by a person. The rate at which an absorbed dose is received is quite often of interest. Common dose rates are rad/s, m rad/h, etc. In SI units, dose rates may be expressed as Gy/s, mGy/h, etc., and because the Gy is such a large unit compared to many common circumstances, the unit l Gy/h is often used (James E. Martin 2006).

2.6.3 Radiation Dose Equivalent

The definition of dose equivalent is necessary because different radiations produce different amounts of biological damage even though the deposited energy may be the same. If the biological effects of radiation were directly proportional to the energy deposited by radiation in an organism, the radiation absorbed dose would be a suitable measure of biological injury, but this is not the case. Biological effects depend not only on the total energy deposited, but also on the way in which it is distributed along the path of the radiation. Radiation damage increases with the linear energy transfer (LET) of the radiation; thus, for the same absorbed dose, the biological damage from high-LET radiation (e.g., alpha particles, neutrons, etc.) is much greater than from low-LET radiation (beta particles, gamma rays, x-rays, etc.). The dose equivalent, denoted by H, is defined as the product of the absorbed dose and a factor Q, the quality factor that characterizes the damage associated with each type of radiation:

H (dose equivalent) = D (absorbed dose) C Q (quality factor)

In the conventional system of units, the unit of dose equivalent is the rem which is calculated from the absorbed dose as:

Rem= rad C Q

The value of Q varies with the type of radiation: Q = 1.0 for x-rays, gamma rays, and electrons, Q = 20 for alpha particles and fission fragments, and Q = 2–10 for neutrons of different energies. The SI unit of dose equivalent is the Sievert (Sv) or Sieverts = Gy C Q. The Sievert, as is the gray, is a very large unit, corresponding to 100 rem in conventional units, and it is often necessary to abbreviate it to mSv or in some cases to l Sv to describe the radiation dose equivalent (or rate) received by workers and the public. (James E. Martin 2006)

2.6.4 Radiation Exposure

The term exposure is used to describe the quantity of ionization produced when x-rays or gamma rays interact in air because it can be conveniently measured directly by collecting the electric charge, whereas that which occurs in a person cannot be. The roentgen (R) is the unit of radiation exposure; it is defined only for air and applies only to x-rays and gamma rays up to energies of about 3 MeV. A milli-roentgen (mR) is 0.001 R. Exposure rates are often expressed as roentgens per unit time, e.g., R/s, mR/h, etc. Since the roentgen is determined in air, it is not a radiation dose but with appropriate adjustment it can be converted to dose. The roentgen was originally defined as that amount of x-radiation or gamma radiation such that the associated corpuscular emission produces in 0.001293 g of air (1 cm 3 of air at atmosphere pressure and 0 EC) 1 electrostatic unit (1 esu =3.336 C l0–10 C) of charge of either sign. The ionization produced by the associated corpuscular emissions is due to photoelectric, Compton, and, if applicable, pair production interactions.

The modern definition of the roentgen is based on this value; i.e., 1 R is that amount of x-radiation or gamma radiation that produces 2.58 C 10 C of

charge in 1 kg of air. The roentgen is not included in the SI system of units; the SI unit for exposure is the X unit, defined as the production of 1 C coulomb of charge in 1 kg of air, or:

X = 1 C/kg of air

The X unit corresponds to deposition of 33.97 J in 1 kg of air, and is equal to 3876 R. The X unit is a huge unit, and consequently most exposure measurements are made and reported in R which seems appropriate for the discoverer of x-rays. Exposure and exposure rate do not apply only to x-rays and gamma rays and only in air, and the roentgen nor the X unit is appropriate for describing energy deposition from particles or for energy deposition in the body. Energy deposition per roentgen is an important relationship because the deposition of energy in air is readily calculated. The amount of charge produced in air varies with energy, but is approximately linear for photons between about 70 keV and 3 MeV such that the amount of energy required producing an ion pair is 33.97 ev on average. The roentgen thus corresponds to an energy deposition in air, the absorbing medium, of 87.64 erg/g of air (James E. Martin 2006)

2.6.5 Radiation Dose Calculations:

Radiation dose can be calculated by a three-step procedure as follows:

1. First establish the number of radiation pulses (particles or photons) per unit area entering a volume of medium of known density.
2. Next, establish the mass of medium in which the energy is dissipated. For particles, this is just the depth of penetration. For photons, it is necessary to use a unit depth (e.g., 1 cm) due to the probabilistic pattern of interactions.

3. From the pattern(s) of interaction probabilities, determine the amount of energy deposited.

All emitted radiations must be considered in this process, and adjustments should be made for any attenuating medium between the source and the point of interest. Since different radiations penetrate to different depths in tissue, radiation dose has been specified in regulations for three primary locations:

1. The shallow dose, which is just below the dead layer of skin that has a density thickness of 7 mg/cm, or an average thickness of 70 lm;
2. The eye dose just below the lens of the eye with a density thickness o 300 mg/cm
3. The deep dose, which is located at a depth of 1 cm in tissue or at a density thickness of 1000 mg/cm, primarily to account for highly penetrating radiation such as x-rays or gamma rays or neutrons. A precise determination of absorbed energy at these depths requires an adjustment for any diminution in the flux due to energy losses in the overlying tissue layer. Since energy deposition is dependent on the radiation type, its energy, and the absorbing medium, it will, for the sake of clarity, be discussed in the context of the interaction mechanisms of each type of radiation. (James E. Martin 2006)

2.6.6Methods used to quantify ionizing radiation

The Methods used to quantify ionizing radiation are summarized in Table 2. 3:-

Method	Conventional unit	SI unit
Radiation dose	Rad	Gray (Gy)
Equivalent dose	REM	Sievert (Sv)
Effective dose	Effective dose equivalent (Sv)	Sievert (Sv)
Computed tomography dose index	-	Milligray (mGy)
Dose length product	-	Milligray centimeter (mGy.cm)
1 Gy = 1 J/kg. 1 rad = 100 Gy. 10 mSv = 1 REM (1 mSv = 100 m REM).	-	-

2.6.7 Radiation Risks

Adverse radiation effects are usually divided into two categories: stochastic and deterministic effects. Stochastic effects most commonly refer to the radiation induction of neoplasms or hereditary effects. These effects are due to unrepaired or misrepaired DNA damage. The probability of incurring these effects is a direct function of dose and there is no known threshold below which these effects do not occur. However, at low doses the probability of the effects may be so small as to be impossible to find using epidemiological or population studies. The severity of stochastic effects is dose independent. Epidemiological studies have shown that the mean latent period, the time from exposure to clinical appearance is 7–10 years for leukemia and about 20 years for solid tumours (FAO 1996, Mettler et.al

1996). Deterministic effects are mostly due to cell killing. If only a few cells in a given tissue are killed, no effect will be apparent. If enough cells are killed, there will be an obvious clinical effect. An example of a deterministic effect is skin necrosis. Thus for deterministic effects there is a threshold below which the clinical effect will not be apparent, and the severity of a deterministic effect is a direct function of dose. The title of this paper broadly refers to radiation risks associated with the practice of medicine. Obviously there are potential risks to the patient, medical staff, families and possibly the public (Mettler et al 1996).

2.7 Previous studies

Mathew R. et al. (2005) reviewed Utility of ^{18}F-FDG PET in evaluating cancers of lung; no one denied that PET has seen rapid progression in recent years, with applications in oncology leading the way. The glucose analog ^{18}F-FDG is the most commonly used PET radiopharmaceutical and has been shown to accumulate avidly in several different neoplasms, including cancers of the lung. They reviewed the physiologic basis for the uptake of ^{18}F-FDG in lung neoplasms and demonstrate the utility of ^{18}F-FDG PET in lung cancer. A brief review of other PET radiopharmaceuticals in lung cancer imaging, and dual-modality PET/CT scanners, were presented. Upon completion of this article, the reader should be able to describe the pharmacokinetics of ^{18}F-FDG and discuss the efficacy of ^{18}F-FDG PET scans in the evaluation of solitary pulmonary nodules, disease staging, and monitoring response to therapy. Additionally, the reader should be able to compare ^{18}F-FDG PET with conventional anatomic imaging and describe some of the technical challenges of PET/CT fusion imaging. In spite of that PET has seen rapid progression in recent years, from a research tool to routine clinical use. Much of the increased use of PET

can be attributed to applications in oncologic imaging and the increased availability of the radiopharmaceutical ^{18}F-FDG, which is the most extensively, used PET radiopharmaceutical. ^{18}F-FDG has been shown to be taken up by several neoplasms, including cancers of the lung. Lung cancer has the regrettable distinction of being the most common cause of death by malignancy in both men and women. Approximately 3 million new cases arise each year. The mean survival time for untreated lung cancer is a mere 6 month, with a 5-y survival rate of 13%. Even after surgical resection of tumor tissue, the 5-y survival rate is _40%. Common metastatic sites in lung cancer include the liver, bone, and adrenal glands. Non–small cell lung cancer (NSCLC) accounts for 80% of bronchogenic malignancies and is often amenable to surgery, especially in patients with stage I and stage II disease. Conversely, small cell lung carcinomas have a more dismal prognosis, as they generally present with widespread disease that is not amenable to surgical resection. The mean survival is _1 y even when treated aggressively the vast majority of the literature surrounding ^{18}F-FDG PET of the lungs has focused on patients with NSCLC, in whom local and distant spread of disease can change staging and therapy. The uptake of ^{18}F-FDG in NSCLC has been shown to be several folds greater than that of normal tissue. Small cell lung cancer also exhibits high ^{18}F-FDG uptake, and preliminary studies have shown ^{18}F-FDG to be of use in this imaging as well. Despite the high cost of ^{18}F-FDG PET, it has been proven to be an economical tool in the evaluation of lung cancer. ^{18}F-FDG PET has the potential to alter the staging of disease, reduces the number of futile thoracotomies, and thus may be cost-effective in this indication. The following discussion will focus primarily on the utility of ^{18}F-FDG PET in NSCLC. The role of ^{18}F-FDG PET in diagnosis, staging, and evaluating response to treatment as well as some of the limitations of this technique will be discussed. Finally, a brief look at new developments and future directions of PET in lung cancers will be presented. **Conclusion** The accumulation of the glucose analog ^{18}F-FDG in lung neoplasms has

been well documented. ^{18}F-FDG PET is a highly advanced molecular imaging technique that has been shown to be of great utility in lung cancer and can facilitate noninvasive, in vivo quantification of tumor status. ^{18}F-FDG PET has a significant role to play in the diagnosis, staging, and evaluation of response to therapy in lung carcinoma. PET has the advantage of better identifying loco-regional and distant metastases than conventional anatomic imaging such as CT or MRI. This has the potential to change both the staging and therapeutic management of lung carcinoma and, in the case of upstaging, decreases the number of futile and invasive interventions. Though it is not without limitations, the advantages of ^{18}F-FDG PET over invasive and surgical assessment of lung cancer and the anatomic imaging modalities have already been shown to alter the management strategies of many patients with lung cancer. ^{18}F-FDG PET is now a widely accepted imaging modality for the evaluation of patients with lung cancer. The rapid technologic advances in PET, including research with new PET radiopharmaceuticals and the advent of integrated PET/CT scanners, will serve to keep PET at the forefront of lung cancer imaging in the future.

Nestle et al. (2005) did a comparison of different methods for delineation of ^{18}F-FDG PET–positive tissue for target volume definition in radiotherapy of patients with Non–Small Cell Lung Cancer, 25 patients with NSCLC were analyzed. They had ^{18}F-FDG PET during initial tumor staging. Then, another PET of the thorax in treatment position was done, followed by planning CT. CT and PET images were co registered, and the data were then transferred to the treatment planning system (PS). Sets of 4 GTVs were generated for each case by 4 methods: visually (GTV_{Vis}), applying a threshold of 40% of the maximum standardized uptake value (SUV_{Max}; GTV_{40}), and using an iso-contour of SUV=2.5 around the tumor ($GTV_{2.5}$). By phantom measurements we determined an algorithm, which rendered the best fit comparing

PET with CT volumes using tumor and background intensities at the PS. Using this method as the fourth approach,(GTV_{Bg})was defined. A subset of the tumors was clearly delimitable by CT. Here, a GTVCT was determined. Finally they found substantial differences between the 4 methods of up to 41% of the GTV_{vis}. The differences correlated with SUV_{max}, tumor homogeneity, and lesion size. The volumes increased significantly from GTV40 (mean 53.6 mL) _ GTV_{bg} (94.7 mL) _ GTV_{vis} (157.7 mL) and $GTV_{2.5}$ (164.6 mL). In inhomogeneous lesions, GTV_{40} led to visually inadequate tumor coverage in 3 of 8 patients, whereas GTV_{bg} led to intermediate, more satisfactory volumes. In contrast to all other GTVs, GTV_{40} did not correlate with the GTVCT. **Conclusion:** The different techniques of tumor contour definition by ^{18}F-FDG PET in radiotherapy planning lead to substantially different volumes, especially in patients with inhomogeneous tumors. Here, the GTV_{40} does not appear to be suitable for target volume delineation. Also there are more complex methods, such as system-specific contrast-oriented.

Hatt et al. (2011) studied the impact of tumor size and tracer uptake heterogeneity in ^{18}F-FDG PET and CT in Non–Small Cell Lung Cancer tumor delineation. They had Twenty-five NSCLC cancer patients with ^{18}F-FDG PET/CT was considered. Seventeen underwent surgical resection of their tumor, and the maximum diameter was measured. Two observers manually delineated the tumors on the CT images and the tumor uptake on the corresponding PET images, using a fixed threshold at 50% of the maximum (T50), an adaptive threshold methodology, and the fuzzy locally adaptive Bayesian (FLAB) algorithm. Maximum diameters of the delineated volumes were compared with the histopathology reference when available. The volumes of the tumors were compared, and correlations between the anatomic volume and PET uptake heterogeneity and the differences between delineations were investigated. Results: All maximum diameters measured on PET and CT images significantly

correlated with the histopathology reference (r. 0.89, P, 0.0001). Significant differences were observed among the approaches: CT delineation resulted in large overestimation (132% 6 37%), whereas all delineations on PET images resulted in underestimation (from 215% 6 17% for T50 to 24% 6 8% for FLAB) except manual delineation (18% 6 17%). Overall, CT volumes were significantly larger than PET volumes (55 6 74 cm3 for CT vs. from 18 6 25 to 47 6 76 cm3 for PET). A significant correlation was found between anatomic tumor size and heterogeneity (larger lesions were more heterogeneous). Finally, the more heterogeneous the tumor uptake, the larger was the underestimation of PET volumes by threshold-based techniques. **Conclusion**: Volumes based on CT images were larger than those based on PET images. Tumor size and tracer uptake heterogeneity have an impact on threshold-based methods, which should not be used for the delineation of cases of large heterogeneous NSCLC, as these methods tend to largely underestimate the spatial extent of the functional tumor in such cases. For an accurate delineation of PET volumes in NSCLC, advanced image segmentation algorithms able to deal with tracer uptake heterogeneity should be preferred.

Biehl et al. (2006) reviewed ^{18}F-FDG PET Definition of Gross Tumor Volume for Radiotherapy of Non–Small Cell Lung Cancer: Is a Single Standardized Uptake Value Threshold Approach Appropriate?, Data for patients who had peripheral NSCLC with well-defined borders on CT and SUV_{Max} of greater than 2.5 were reviewed. PET/CT datasets were reviewed, and a volume of interest was determined to represent the GTV. The CT_{GTV} was delineated by using standard lung windows and reviewed by a radiation oncologist. The PET_{GTV} was delineated automatically by use of various percentages of the SUV_{Max}. The PET_{GTV}-to-CT_{GTV} ratios were compared at various thresholds, and a ratio of 1 was considered the best match, or the optimal threshold. They reached to twenty peripheral NSCLCs with volumes

easily defined on CT were evaluated. The SUV_{Max} (mean 6 SD) was 12 6 8, and the mean CT_{GTV} was 198 cm3 (97.5% confidence interval, 5–1,008). The SUV_{Max} were 16 6 5, 13 6 9, and 3.0 6 0.4 for tumors measuring greater than 5 cm, 3–5 cm, and less than 3 cm, respectively. The optimal thresholds (mean 6 SD) for the best match were 15% 6 6% for tumors measuring greater than 5 cm, 24%69%for tumors measuring 3–5 cm, 42% 6 2% for tumors measuring less than 3 cm, and 24% 6 13% for all tumors. The PET_{GTV} at the 40% and 20% thresholds underestimated the CT_{GTV} for 16 of 20 and 14 of 20 lesions, respectively. The mean difference in the volumes (PET_{GTV} minus CT_{GTV} [$PET_{GTV} - CT_{GTV}$]) at the 20% threshold was 79 cm3 (97.5% confidence interval, 2922 to 178). The PET_{GTV} at the20% threshold overestimated the CT_{GTV} for all 4 tumors measuring less than 3 cm and underestimated the CT_{GTV} for all 6 tumors measuring greater than 5 cm. The CT_{GTV} was inversely correlated with the $PET_{GTV} - CT_{GTV}$ at the 20% threshold (R250.90, P, 0.0001). The optimal threshold was inversely correlated with the CT_{GTV} (R2 5 0.79, P, 0.0001). **Conclusion**: No single threshold delineating the PET_{GTV} provides accurate volume definition, compared with that provided by the CT_{GTV}, for n the majority of NSCLCs. The strong correlation of the optimal threshold with the CT_{GTV} warrants further investigation.

H Yan et al. (2011) did a measurement of tumor volume by PET to evaluate prognosis in patients with advanced non-small cell lung cancer treated by non-surgical therapy. They reviewed 120 patients with pathologically proven NSCLC (61 squamous cell carcinomas and 59 adenocarcinomas) who underwent pretreatment ^{18}F-FDG PET. MTV and maximum standardized uptake value (SUV_{Max}) for the primary tumors were measured by ^{18}F-FDG PET. Pretreatment variables (age, sex, American Joint Committee on Cancer [AJCC] stage, histological type, SUV_{Max}, and MTV) were analyzed to identify their correlation with two-year

survival. To further evaluate and compare the predictive value of PET parameters, MTV, and SUV_{Max}, time-dependent receiver-operating characteristic curve (ROC) analysis was used. Finally in the uni-variation analysis, AJCC stage, histological type, MTV, and SUV_{Max} of primary tumor were significant predictors of survival. On multivariate analysis, independent prognostic factors associated with decreased two-year survival were AJCC stage (hazard ratio [HR] 2.236, P ¼ 0.003), histological type (HR 2.038, P ¼ 0. 004), and MTV (HR 1.016, P ¼ 0.001). SUV_{Max} was not a significant factor (HR 0.96, P ¼ 0.490). On time-dependent ROC analysis, MTV showed good predictive performance for two-year survival consistently better than SUV_{Max}. **Conclusion**: MTV, a volumetric parameter of ^{18}F-FDG PET, is an important independent prognostic factor for survival and a better predictor of survival than SUV_{Max} for the primary tumor in patients with advanced NSCLC.

Pawinee et al. (2013) quantified metabolic tumor volume (MTV) on PET reduced more than gross tumor volume (GTV) on CT during radiotherapy in patients with non-small cell lung cancer treated with 3D conformal radiotherapy (3DCRT) or stereotactic body radiotherapy (SBRT). They took patients with stage I–III NSCLC treated with a definitive course of RT ± chemotherapy were eligible for this prospective study. FDG-PET/CT scans were acquired within 2 weeks before RT (pre-RT) and at about two thirds of total dose during-RT. PET metabolic tumor volumes (PET-MTVs) were delineated using a method combining the tumor/aorta ratio auto segmentation and CT anatomy based manual editing. Data are presented as mean (95 % confident interval). They approached that the MTV delineation methodology was first confirmed to be highly reproducible by comparing volumes defined by different physicians and using different systems (co efficiency>0.98). Fifty patients with 88 primary and nodal lesions were evaluated. The mean ratios of MTV/GTV were 0.70 (−0.07~1.47) and 0.33 (−0.30~0.95) for pre-RT and during-

RT, respectively. PET-MTV reduced by 70 % (62– 77 %), while CT-GTV by 41 % (33–49 %) ($p<0.001$) during-RT. MTV reduction was 72.9 % and 15.4 % for 3DCRT and SBRT, respectively ($p<0.001$). **Conclusion** PET-MTV reduced more than CT-GTV during- RT, while patients treated with 3DCRT reduced more than SBRT. RTOG1106 is using during-RT PET-MTV to adapt radiation therapy in 3DCRT.

Gregoire et al. (2007) studied the molecular imaging and they proved that molecular imaging, in particular, PET, has brought an additional dimension to management for patients with cancer. ^{18}F-FDG, which is the most widely available tracer, has been shown to be of value for the selection of target volumes in radiation oncology. Depending on its sensitivity and specificity, ^{18}F-FDG has been shown to influence the selection of target volumes for non–small cell lung cancers (NSCLC) or for esophageal tumors. On the other hand, for tumors such as head and neck squamous cell carcinomas (HNSCC) and rectal carcinomas, convincing data on the value of ^{18}F-FDG for target volume selection are still lacking. For target volume delineation, given that an adequate method is used for volume segmentation, the added value of ^{18}F-FDG has been demonstrated for HNSCC and NSCLC. For both types of tumors, modifications in target volume delineation translated into differences in dose distribution compared with the results of CT scan–based plans. Studies are in progress for rectal tumors. Novel markers of tumor hypoxia or proliferation have the potential to modify the delineation of target volumes, allowing for ‘‘dose painting’’ in selected sub volumes. Finally, variations in tumor volume and viability during radiotherapy also are under intense investigation, potentially paving the way for so-called ‘‘Theragnostic’’ or adaptive dose distribution during treatment. This review discusses how PET/CT might modify the current state of the art of radiotherapy planning **Conclusion** In summary, the introduction of PET images into the

treatment planning procedure remains a challenging issue. The use of ^{18}F-FDG PET for target volume selection should be considered within the framework of its sensitivity and specificity for various tumor types. Given the considerable ranges of accuracy of PET across different tumor types, its role will not be identical in different tumor locations. The use of PET for target volume delineation requires specific tuning of parameters, such as image acquisition, processing, and segmentation, and these parameters may vary among tumor sites. Theragnostic PET/CT with various molecular imaging probes is an emerging field; however, its clinical implementation would be premature given the paucity of clinical outcome data. In conclusion, before proper validation of the use of various PET tracers has been performed and all methodological aspects have been fully optimized, it is reasonable to state that the use of PET for treatment planning should not be routine but should remain in the clinical research arena.

Sahiner et al. (2014) evaluated the use of PET in lung cancer , they found that positron emission tomography (PET) using 2-(^{18}F)-flouro-2-deoxy-D-glucose (FDG) has emerged as a useful tool in the clinical work-up of lung cancer. This review provides an overview of applications of PET in diagnosis, staging, treatment response evaluation, radiotherapy planning, recurrence assessment and prognostication of lung cancer. Lung cancer is the most common form of cancer and despite major advances in prevention and treatment; it is still the leading cause of cancer related death throughout the world. Non-small cell lung cancer (NSCLC) constitutes more than 85% of the cases and small cell lung cancer (SCLC) constitutes the rest. Imaging techniques play a crucial role in the diagnosis, staging and follow-up of patients with lung cancer. Although presence of good physical performance, absence of weight loss and female gender predicts better prognosis; the most important prognostic indicator is the stage determined based on tumor,

node, and metastasis (TNM) classification. Besides its prognostic value, staging is of great importance in deciding the treatment plan. Staging in NSCLC is performed according to TNM staging system, which was updated in 2009 by the International Union against Cancer and American Joint Committee on Cancer with the proposals of International Association for the Study of Lung Cancer (IASLC). Although TNM staging is applied occasionally, a more simplified method is used in the evaluation of SCLC; classifying the disease as limited or extensive. Positron emission tomography/computerized tomography (PET/CT) using 2-(^{18}F)-flouro-2-deoxy-D-glucose (FDG) has emerged as a useful tool in the clinical work-up of lung cancer with its accuracy in diagnosis , staging, evaluation of response to chemotherapy and/or radiotherapy and differentiation of fibrosis versus viable tumor. FDG PET scan is superior to other noninvasive imaging modalities in detecting mediastinal nodal involvement, thus in N staging of lung cancer. Moreover distant metastasis to bones, adrenal glands, liver and soft tissues, which are the most common sites of spread in lung cancer, can be evaluated in a single examination with good accuracy. The prognostic value of FDG PET derived metabolic parameters such as maximum standard uptake value (SUV_{Max}), metabolic tumor volume (MTV) and total lesion glycolysis (TLG) have been demonstrated in lung cancer in various studies**.** **Conclusions** PET using FDG has become a commonly used modality in routine clinical workup of lung cancer by being both accurate and noninvasive. Widespread availability of PET/CT scans has revolutionized both the staging and radiotherapy planning process of lung cancer. It provides valuable information by means of response evaluation early after therapy with high accuracy in assessment of recurrences. In addition to that, FDG PET scan provides information about biologic aggressiveness of the tumor and prognosis.

P. M Price et al. (2011) worked in an era in which it is possible to deliver radiation with high precision, there is a heightened need for enhanced imaging capabilities to improve tumor localization for diagnostic, planning and delivery purposes. This is necessary to increase the accuracy and overall efficacy of all types of external beam radiotherapy (RT), including particle therapies. Positron emission tomography (PET) has the potential to fulfill this need by imaging fundamental aspects of tumour biology. The key areas in which PET may support the RT process include improving disease diagnosis and staging; assisting tumour volume delineation; defining tumour phenotype or biological tumor volume; assessment of treatment response; and in-beam monitoring of radiation dosimetry. The role of PET and its current developmental status in these key areas are overviewed in this review, highlighting the advantages and drawbacks. Positron emission tomography (PET) is the most specific and sensitive means of imaging molecular pathways and molecular interactions in humans; it provides unique functional in vivo imaging data that are not made available by other modalities. PET exploits the physics of positron decay after injecting a patient with a positron emitting tracer or ‘‘probe’’, i.e. a molecule of interest linked to a positron-emitting radioisotope such as fluorine-18 (^{18}F), carbon-11 (^{11}C) or oxygen-15 (^{15}O). Each single emitted positron combines with an electron, up to a few millimeters away from the point of emission, forming a positronium. This is immediately annihilated, producing two photons of equal energy (511 keV), which are simultaneously emitted at 180^0 to each other. An external PET scanner, which is essentially a circular array of scintillation detectors, detects both of these photons and associates them using a coincidence filter. After correction for attenuation of the annihilation photons in the surrounding tissues of the body by transmission scan, the resulting PET data directly describe the three-dimensional (3D) localization of the radiation event, thereby revealing the position of the source probe within the patients’ body. PET scan data may be acquired either

statically or dynamically. Subsequent analysis of PET imaging data can be qualitative, by subjective visualization; alternatively, qualitative analysis may be carried out following manual definition or automatic segmentation to define regions of interest (ROI). Using subsequent modeling techniques, the spatial and temporal variation of the radiolabeled compound(s) may be determined in specific tissue with exquisite sensitivity (Pico molar resolution). For example, one commonly used semi quantitative method involves determining the standardized uptake value (SUV) of tumor tissue by measuring the radioactivity present at a specific time, usually normalized against injected radioactivity and body surface area. **Conclusion** Research to date has shown that PET is a useful aid for diagnosis and staging in many tumor types; its substantial clinical use could impact an estimated one third of cancer patients. For GTV delineation, the situation is less clear. PET may assist GTV delineation in areas of uncertainty in some tumor types, but it is constrained by spatial resolution, specificity and sensitivity. The definition of tumour volumes is also significantly affected by technical and methodological variations in PET modeling techniques, which may be improved by additional research. Greater awareness of these limitations is required in the clinic, and further research is necessary to examine whether or not the use of PET in defining GTV has clinical benefits. In assessments of RT response, PET is poised as a potentially useful tool that is effective in monitoring change. Nevertheless, for the therapeutic clinician, the real ‘‘value’’ of PET in tumor diagnosis and staging, GTV delineation and assessing RT response is often limited or obscure, especially when other modalities are sufficient. For example, by implication, two-thirds of cancer patients are not affected by PET for tumor diagnostic purposes; and using PET may not aid GTV delineation, for example, owing to false-negative PET findings in esophageal cancer. This can lead the clinician who is aware of PET’s limitations to conclude that, in many instances, it only adds time and complexity to clinical processes rather

than adding utility to therapy planning decisions. For PET-determined RT response in particular, the value of PET scanning is restricted by the availability of efficacious alternative or salvage treatment options, with the result that the managing radiation oncologist is unable to act on PET information for the patients benefit. This highlights two important conclusions: there is a need to recognize the advantages and drawbacks of PET for current clinical applications and apply it more judiciously; and there is a requirement for more effective treatments. Ongoing and future multidisciplinary research advances that use PET's greatest strengths—in BTV or phenotype definition, in RT response and in-beam PET for true in vivo dose monitoring—promise to improve external beam RT, particularly for particle therapies. This may well lead to the development of truly 3D, radio biologically optimized adaptive radiation therapy, in which treatment may be selected, optimized. Beam on-line positron emission tomography system mounted on a rotating gantry port (BOLPs RGp). This system is used in the treatment room immediately following proton therapy to detect the position and intensity of resulting positron activity.

De Geus-Oei et al. (2007) focused in ^{18}F FDG in NSCLC and reported that for several years, molecular imaging with ^{18}F-fluorodeoxyglucose positron emission tomography (FDG-PET) has become part of the standard of care in pre surgical staging of patients with non-small-cell lung cancer (NSCLC), focusing on the detection of malignant lesions at early stages, early detection of recurrence, and metastatic spread. Currently, there is an increasing interest in the role of FDGPET beyond staging, such as the evaluation of biological characteristics of the tumor and prediction of prognosis in the context of treatment stratification and the early assessment of tumor response to therapy. In this systematic review, the literature on the value of the evolving applications of FDG-PET as a marker for prediction (i.e.,

therapy response monitoring) and prognosis in NSCLC is addressed, divided in sections on the predictive value of FDG-PET in locally advanced and advanced disease, the prognostic value of FDG-PET at diagnosis, after induction treatment, and in recurrent disease. Non-small-cell lung cancer (NSCLC) is the leading cause of cancer- related death in both men and women. Surgery with curative intent represents the best chance for cure, but is only an option in patients with stages I, II, and selected cases of stage III. However, only 30% of NSCLC cases present at early stages. Even if a complete curative resection can be performed, about 50% of patients will recur without adjuvant chemotherapy treatment. The majority of these recurrences occur at distant sites. Hence, each pathological stage consists of a heterogeneous population containing individuals at much higher risk of recurrence and death than others. Therefore, there is a need for noninvasive functional imaging modalities that could play a role in further characterization of NSCLCs.

Another major clinical problem in the treatment of NSCLC is therapy response monitoring; because the morphologic information provided by chest radiographs and computed tomography (CT) cannot reliably distinguish necrotic tumor or fibrotic scar from residual tumor tissue. Response evaluation with these morphological imaging methods does not correlate well with pathologic response, or with changes at the cellular level or with tumor viability. Indeed, final treatment outcome will be determined more by the biological aggressiveness of residual tumor than by its volume. Examination of biopsy material also has its limitations, because it can be inconclusive because of sampling difficulties, it provides information at a single time point only, and is not suitable for sequential assessment. A potential noninvasive molecular imaging tool that could be helpful in solving these problems is positron emission tomography (PET). The most frequently used tracer in PET is ^{18}F-fluorodeoxyglucose (FDG). FDG-PET localizes tumors by identifying cells in the body that have increased glucose uptake and metabolism. FDG is transported

into cells analogous to glucose and is converted to FDG-6-phosphate. This metabolite is trapped in the cell, as it will not be processed in the glycolytic pathway, and hence will accumulate preferentially in those cells with high glucose uptake, such as tumor cells. The introduction of the combined use of FDG-PET and CT has had a major impact on the diagnosis and staging of lung cancer. FDG-PET has been used to evaluate unclassified pulmonary nodules for malignancy. Furthermore, it provides noninvasive mediastinal staging and reduces the number of futile thoracotomies and mediastinal scopes. This imaging modality detects unsuspected extra thoracic metastases in 14% to 17% of patients otherwise considered potentially respectable. Recently, FDG-PET has also demonstrated its value in radiation treatment planning and detection of recurrent disease. Because FDG-PET relies on the detection of metabolic alterations of cancer cells, this examination yields data independently of associated structural characteristics, and therefore allows the detection or monitoring of specific metabolic changes that are not associated with or precede the anatomical changes. One of the great advantages of this technique is that it cannot only observe but can also quantify FDG uptake to distinguish metabolically highly active from less active tumor tissues and therefore offers an opportunity for noninvasive, in vivo tissue characterization. Hence, the number of clinical applications for FDG-PET in NSCLC continues to increase. This comprehensive review aims to discuss the potential future applications in the management of patients with NSCLC. The literature is reviewed on the value of FDG-PET in identifying tumor response to anticancer therapies at an early phase of treatment and in identifying subsets of patients with poor outcome**. Conclusions** It has been shown that the degree of FDG uptake is of prognostic value at initial presentation, after induction treatment before resection, and in case of recurrence. At initial presentation, as well as post treatment, FDG-PET is a better predictor of survival than TNM system staging or CT response. Agreement Prognostic Value of

FDG-PET in Recurrent Disease Year n* Histology Stage Treatment Survival/Hazard ratio P Reference 2001 63 Squamous 57% Recurrent disease 67% Resection 48% 1-y survival .012 84 Adeno 30% No relapse 33% Radical radiotherapy 52% Positive FDG-PET 55% Large-cell 11% Negative FDG-PET 84% Other 2% Hazard ratio positive FDG-PET 2.95 .012 2006 62 Squamous 53% Recurrent disease 70% Resection 31% Median survival, mo. <.01 86 Adeno 30% Second primary 19% Nonsurgical 69% SUV_11 9 Large-cell 2% No relapse 11% SUV<11 18 BAC 8% Carcinoid 2% Undetermined 5% SUV indicates standardized uptake value; PET, positron emission tomography; FDG, ^{18}F-fluorodeoxyglucose. * Number of patients. Prognostic Value of FDG-PET in NSCLC/de Geus-Oei et al. 1661 on methods of scanning, SUV measurement, and the best cutoff values is needed before this technique can be fully exploited in clinical medicine to select patients for adjuvant treatments. In future multicenter trials standardization of acquisition, reconstruction, and ROI methods is preferred for SUV quantification. Further research in this field is of great importance because it may induce a change in the therapeutic concept of patients with NSCLC. FDG-PET could separate patients with a good prognosis from those with a poor one, which may help in deciding on the most appropriate treatment and which may be of particular value in stratifying patients for clinical trials. FDG-PET is also of value in predicting outcome of induction therapy and it probably also has a predictive value early in the course of first-line therapy in the case of advanced disease. There are indications that FDG-PET can predict response and patient outcome as early as after 1 course of (induction) chemotherapy. However, monitoring tumor response with FDG-PET is still in its infancy. The methods of measurement of FDG uptake currently are diverse and timing with respect to anticancer therapy and used thresholds to define response are variable. Therefore, further study is required to deal with these major issues before it is possible to draw definite conclusions on FDG-PET as a tool for

therapy response monitoring. If the results of the reviewed studies can be confirmed, FDG-PET could shorten the track of early clinical trials that assess new antineoplastic agents and could also improve patient management by reducing morbidity, efforts, and costs of ineffective treatment in non-responders.

Pieterman et al. (2000) evaluated the PET in the lung cancer; they reached to determining the stage of non–small cell lung cancer often requires multiple preoperative tests and invasive procedures. Whole-body positron emission tomography (PET) may simplify and improve the evaluation of patients with this tumor. They prospectively compared the ability of a standard approach to staging (computed tomography [CT], ultrasonography, bone scanning, and, when indicated, needle biopsies) and one involving PET to detect metastases in mediastinal lymph nodes and at distant sites in 102 patients with resectable non– small-cell lung cancer. The presence of mediastinal metastatic disease was confirmed histopathologically. Distant metastases that were detected by PET were further evaluated by standard imaging tests and biopsies. Patients were followed postoperatively for six months by standard methods to detect occult metastases. Logistic-regression analysis was used to evaluate the ability of PET and CT to identify malignant mediastinal lymph nodes. They found that the sensitivity and specificity of PET for the detection of mediastinal metastases were 91 percent (95 percent confidence interval, 81 to 100 percent) and 86 percent (95 percent confidence interval, 78 to 94 percent), respectively. The corresponding values for CT were 75 percent (95 percent confidence interval, 60 to 90 percent) and 66 percent (95 percent confidence interval, 55 to 77 percent). When the results of PET and CT were adjusted for each other, only PET results were positively correlated with the histopathology findings in mediastinal lymph nodes ($P<0.001$). PET identified distant metastases that had not been found by standard methods in 11 of 102 patients. The sensitivity and

specificity of PET for the detection of both mediastinal and distant metastatic disease were 95 percent (95 percent confidence interval, 88 to 100 percent) and 83 percent (95 percent confidence interval, 74 to 92 percent), respectively. The use of PET for clinical staging resulted in a different stage from the one determined by standard methods in 62 patients: the stage was lowered in 20 and raised in 42. **Conclusions** PET improves the rate of detection of local and distant metastases in patients with non–small-cell lung cancer.

Behzadi et al. (2009) studied The potential use of positron emission tomography (PET) imaging in patients with Non–small cell lung cancer (NSCLC) is broadly divided into 5 categories: management of solitary pulmonary nodule, mediastinal lymph node evaluation, detection of metastases, and evaluation of response to chemo-radiation and detection of recurrence. The purpose of this review is to discuss the current clinical applications of ^{18}F-fluorodeoxyglucose PET in patients with NSCLC and to discuss future applications and developments of this technology. Despite many advances in the diagnosis, staging and treatment of non–small cell lung cancer (NSCLC), the overall 5-year survival rate of patients with resectable NSCLC is less than 50%. This suboptimal survival rate is likely due to many factors, including the aggressiveness of the specific phenotype, locally advanced disease at presentation and inaccurate pretreatment staging. It is plausible that undetected loco-regional and distant micro metastatic disease at the time of presentation results in suboptimal or at times inappropriate treatment and, therefore, decreased stage-specific survival. Accurate clinical staging at the time of diagnosis has many important advantages, of which the following 3 have particular importance: • It allows for appropriate patient selection for potentially curative surgical and/or nonsurgical therapies, • It identifies patients who would benefit from neo-adjuvant therapy, and • It allows for more accurate follow-up assessment and

detection of loco-regional recurrences that might still be amenable to salvage treatment. In the management of NSCLC, ^{18}F-fluorodeoxyglucose (FDG) positron emission tomography (PET) is an imaging technology with evolving potential. The advantage of FDG-PET lies in its ability to detect metabolic changes in cancer cells even before the manifestation of the anatomic changes commonly identified by conventional imaging modalities such as computed tomography (CT), ultrasonography, magnetic resonance imaging (MRI) and bone scintigraphy. This advantage may help with more accurate staging than is possible with conventional imaging. It may also identify tumors at an earlier stage, assess their response to neo-adjuvant therapy and help with follow-up surveillance. The potential capability of PET in assessing the tumor responsiveness to chemotherapy can be used as a prognostic factor, thereby influencing the direction of further management. The optimal use of FDG-PET in the management of lung cancer continues to evolve. The overall poor prognosis of lung cancer and lack of optimal treatment for advanced stages of the disease have facilitated rapid integration of this imaging technology in the management of NSCLC. However, its financial burden on health care systems and individual payers has brought its widespread use into question. They discussed the current practical applications of FDG-PET in patients with NSCLC, summarizing clinically applicable data. A systematic review of the role FDG-PET in the diagnosis and staging of lung cancer has already been published by one of us **Conclusion** they had shown the potential applications of FDG-PET in patients with NSCLC. Positron emission tomography is a potentially powerful imaging technology, and clinicians need to determine how best to integrate this tool in the management of NSCLC to improve patient outcomes while maintaining the financial integrity of health systems care.

Bunyaviroch et al. (2006) studied the PET evaluation in lung cancer so they reported that in the last hundred years, lung cancer has risen from are portable disease to the most common cause of death from cancer in both men and women in developed countries. When descriptions of lung cancer were published in 1912, there were only 374 reported cases. In the 1950s, little more than the chest radiograph and sputum cytology analysis were available for lung cancer screening. Since then, the mortality from lung cancer has decreased, but the 5-y cure rates have barely improved. The annual number of deaths from lung cancer is greater than the numbers of deaths from breast, colon, and prostate cancers combined. More than 150,000 patients died of lung cancer in 2004. The 5-y survival rates currently are 16% in the United States and 5% in the United Kingdom. The association of lung cancer with tobacco smoking was initially reported in the 1950s and subsequently led to the determination by the U.S. Surgeon General that smoking is harmful to one's health. Further investigation has led to the discovery that this association is related to the type and amount of tobacco product used, the age at initiation, and the duration of use. Lung cancer often presents as a solitary pulmonary nodule on chest radiographs. Chest radiographs usually are performed for patients as a preoperative or physical examination screening test, often in the absence of symptoms. Few signs and symptoms are present at an early stage, leading to more advanced disease when patients present to their physicians. One third of lung nodules in patients more than 35 y old are found to be malignant. Over 50% of the radio graphically indeterminate nodules resected at throat scope are benign. It is clear that there is a need for the accurate diagnosis of these lesions. The use of PET has much promise as an aid to the noninvasive evaluation of lung cancer. ^{18}F-FDG PET currently is indicated for the characterization of lung lesions, staging of non–small cell lung carcinoma (NSCLC), detection of distant metastases, and diagnosis of recurrent disease. Furthermore, many institutions have found significant value in ^{18}F-FDG PET for

treatment monitoring. **Conclusion** As alluded to previously, there are multiple avenues of investigation that could be used to improve the ability of PET to diagnose and stage malignancies. One avenue that has received attention is improving the co-registration of lung tumors on PET/CT. In a study of 8 patients with 13 thoracic tumors, the researchers compared the SUVs of the tumors determined by attenuation correction with conventional helical CT (HCT) versus averaged CT with respiratory gating (ACT. A difference of greater than 50% in the maximum SUV was demonstrated between the HCT and the ACT data for 4 of the 13 tumors. A significant reduction in diaphragmatic miss-registration also was found with the ACT images. The researchers concluded that ACT provides a more accurate attenuation map for SUV quantitation. Further investigation is warranted, but it appears that respiratory gating provides potential improvements in quantitative and qualitative evaluations of thoracic malignancies. A second avenue of investigation involves image processing and display formats for enhanced reader detectability. In a study of 15 patients with 21 intraluminal tumors, the researchers compared the detectability and localization of these lesions by conventional PET/CT and PET/CT virtual bronchoscopy and colonography. The data demonstrated 100% detection of lesions on virtual 3-dimensional images versus axial images and demonstrated subjective improvements. This initial work shows the potential improvement that can be obtained in detectability and localization by use of 3-dimensional display modes with fused PET/CT images. A third avenue of investigation is the determination of the potential benefit of other PET radiotracers compared with the benefit of ^{18}F-FDG. Other radiotracers, such as ^{18}Ffluorothymidine (^{18}F-FLT) and ^{18}F-fluorocholine (^{18}F-FCH), are being investigated for use in lung cancer. Buck et al. compared the diagnosis and staging of lung cancer with ^{18}F-FDG and ^{18}F-FLT in 43 patients. They concluded that

^{18}FFLT had a higher specificity for malignant lung tumors; however, ^{18}F-FLT was less accurate for N staging and M staging.

Cobben et al compared ^{18}F-FLTand ^{18}F-FDG in 17 patients with NSCLC. ^{18}F-FLT demonstrated a significantly lower maximum SUV in NSCLC than did ^{18}F-FDG. They concluded that ^{18}F-FLTwas not useful in the staging or restaging of NSCLC. Similarly, ^{18}F-FCH has been compared with ^{18}F-FDG as a potentially useful tumor imaging agent. Tian et al. compared ^{18}F-FCH and ^{18}F-FDG in 38 patients with various tumors, including 6 patients with lung cancer. They found similar radiotracer uptake in the known tumors, without clear improvement with ^{18}F-FCH over ^{18}F-FDG. Neither ^{18}F-FLT nor ^{18}F-FCH has shown clear improvement over ^{18}F-FDG at this time; therefore, they have no role at present.

Pöttgen et al. (2006) studied the Value of 18F-Fluoro-2-Deoxy-D-Glucose-Positron Emission Tomography/Computed Tomography in Non-Small-Cell Lung
Cancer for Prediction of Pathologic Response and Times to Relapse after Neo-adjuvant Chemo radiotherapy, so they reached to that to determine the value of combined positron emission tomography/computed tomography (PET/CT) during induction chemotherapy (CTx) followed by chemo radiotherapy (CTx/ RTx) for non - small-cell lung cancer to predict histopathology response in primary tumor and mediastinum and prognosis of the patient. Experimental Design: Fifty consecutive patients with locally advanced non - small-cell lung cancer received induction therapy and, if considered resectable, proceeded to surgery (37 of 50 patients). Patients had at least two repeated ^{18}F-2-fluoro-2-deoxy-D-glucose (FDG)-PET/CT scans either before treatment (t0) or after induction CTx (t1) or CTx/RTx (t2).Variables from the PET/CT studies [e.g., lesion volume and corrected maximum standardized glucose uptake values ($SUV_{Max,\ corr}$)] were correlated with

histopathology response (graded as 3, 2b, or 2a: 0%, >0-10%, or >10% residual tumor cells) and times to failure. Results: Primary tumors showed a percentage decrease in $SUV_{Max,\ corr}$ during induction significantly larger in grade 2b/3 than in grade 2a responding tumors (67%versus 34%at t1,73%versus 49% at t2; both P < 0.005). $SUV_{Max,\ corr}$ at t2 was significantly correlated with histopathology response in tumors smaller than the median volume (7.5 cm3; r =_0.54, P =0.02). In the mediastinal Lymph nodes, $SUV_{Max,\ corr}$ values at t2 predicted any pN0 status with a sensitivity and specificity of 7 3% and 89%, respectively ($SUV_{Max,\ corr}$ threshold of4 .1, r = _0.54, P = 0.0005). Freedom From extra cerebral relapse was significantly better in grade 2b/3 patients (86%at16months versus 20%in2aresponders;P =0.003) and in patients with a greater percentage decrease in $SUV_{Max,\ corr}$ in the primary tumor at t2 in relation to t0 than in patients with lesser response (83% at16 months versus 43%; P = 0.03 for cutoff points between 0.45 and 0.55). Conclusions: $SUV_{Max,\ corr}$ values from two serial PET/CT scans, before and after three chemotherapy cycles or later, allow prediction of histopathology response in the primary tumor and mediastinal lymph nodes and have prognostic value.

Abravan et al.(2017) assed the effects of radiotherapy (RT) and erlotinib on pulmonary glucose uptake using 2-deoxy-2-(^{18}F) fluoro-D-glucose (^{18}F-FDG) positron emission tomography (PET) during and after treatment of non-small cell lung cancer (NSCLC) and to identify associations between serum cytokine levels and lung glucose uptake. There were Twenty-seven patients with advanced NSCLC, receiving RT alone or concomitant RT and erlotinib therapy, were examined by ^{18}F-FDG PET before, during, and after treatment. A total of 57 ^{18}F-FDG PET scans were analyzed. Pulmonary ^{18}F-FDG uptake and radiotherapy dose mapping were used to acquire dose-response curves for each patient, where subsequent linear regression gave a glucose uptake level in the un-irradiated parts of the lungs (SUV0)

and a response slope (DSUV). Serum cytokine levels at corresponding time points were assessed using a multiplex bioassay. Correlations between the most robust cytokines and lung ^{18}F-FDG dose response parameters were further investigated. They found that from the dose response analysis, SUV0 at post-therapy was significantly higher ($P < 0.001$) than at mid- and pre-therapy (45% and 58%, respectively) for the group receiving RT + erlotinib. Also, SUV0 at post therapy was higher for patients receiving RT + erlotinib compared to RT alone (42%; $P < 0.001$). No differences in DSUV were seen with treatments or time. SUV0 was positively associated ($r = 0.47$, $P = 0.01$) with serum levels of the chemokine C–C motif ligand 21 (CCL21) for patients receiving RT + erlotinib.

Conclusions: Concomitant RT and erlotinib causes an elevation in pulmonary 18F-FDG uptake post treatment compared to RT alone. Pulmonary glucose uptake is associated with an up regulation of a chemokine (CCL21) involved in inflammatory reactions.

Gigirey et al assed diagnostic accuracy of PET/CT for intra thoracic lymph node staging in patients with non-small cell lung carcinoma, by comparing those findings with pathology results and/or mediastinascopy. To determine positive and negative predictive values of PET/CT in the staging of mediastinal lymph nodes in lung cancer. To compare our results with those from international studies. They retrospectively selected 31 patients with NSCLC in whom PET/CT was performed for initial staging. TNM staging of disease was performed by CT; patients were found to be in stage I, II and III A. PET/CT images were evaluated separately by two different physicians for each imaging method. In all patients' mediastinascopy, video thoracoscopy and/or surgical resection with radical lymph node resection were performed. In our series, PPV for PET/CT was 72.7 % and NPV, 66.6 %. While PPV approaches the value of international series, the NPV was even lower.

Conclusions: The use of dual modality PET/CT significantly increases the number of correctly staged NSCLC patients and therefore has a positive effect in patient management. ^{18}F-FDG PET/CT has a higher overall performance than all the other imaging techniques put together, especially for N and M staging. This is of particularly evident in mediastinal studies.

Yan et al. (2017) experimented the low dose 18F-FDG PET imaging and its potential use for lung cancer screening. Lung cancer is the most common cause of death among both men and women from cancer worldwide. Overall, less than 20% of patients with lung cancer are still alive 5 years after diagnosis although there are significant improvements of treatment. The low survival rate could most likely be due to the low early detection. Most lung cancers are first diagnosed based on symptoms and regular chest X-rays. Symptoms of lung cancer are not very specific and generally reflect damage to the lungs' ability to function normally. In addition, chest X-rays are not reliable enough to find lung tumors in their earliest stages due to their low sensitivity and specificity. Recently, the National Lung Screening Trial (NLST) showed that low-dose computed tomography (LDCT) could reduce mortality rate due to lung cancer by 20% compared to chest X-rays screening for the current or former smokers with age of 55 to 74. However, due to its limited specificity, LDCT screening also detected more than 18% of all lung cancers which were indolent and led to over diagnosis in screening for lung cancer. Moreover, although LDCT could reduce lung cancer mortality for patients at the high risk in the NLST study, however, 24.2% of the patients were tested positive, but 96.4% of them were false positives. Further investigations are needed to introduce 18F-FDG PET/CT for lung cancer screening. First, a larger number of lesions with size less than 1 cm are warranted. Only 12 lesions were included in the current work. It may be inadequate to train observer models. Secondly, volume of interest (VOI) was

obtained by a simple threshold method on the full statistics images and the resulting VOIs were copied to the images at the lower count levels. Accurate delineation of lesions is very challenging due to limited spatial resolution and high noise in PET images, and this will be more challenging when there is no high-count image in low dose cancer screenings. Thirdly, one challenge of PET quantification for lung cancer imaging is respiratory motion, which leads to blurring of lesions and can cause an underestimation of standardized uptake values (SUV) and overestimation of lesion volume. Respiratory motion could be mitigated by breath-hold methods, post-processing methods and PET raw data-driven respiratory motion correction. Fourthly, the optimal reconstruction settings including post-reconstruction smoothing filters vary with quantitation tasks. In the work, OSEM reconstruction with PSF and TOF using default settings for iteration number, subset number and post-reconstruction smoothing filter was employed, which may not be optimal for different count level. Fifthly, attenuation correction (AC) is a prerequisite for PET imaging and quantification. X-ray-based AC is now the most commonly used method and its accuracy depends on voltage and tube current. The effect of LDCT based AC on quantitative PET lung imaging should be evaluated in the future. Sixthly, the different count statistics or injected doses were produced by simulated by randomly discarding events in the PET list mode data stream. However, due to the biology washout effect, this kind of simulation may not be the same as reducing the FDG dose at the beginning. The effect of reducing injected dose on lung lesion quantification and detectability is worthwhile for prospective investigation. Finally, the cost and benefit of low dose 18F-FDG PET/CT for lung cancer screening should be justified. We believe study such as the one reviewed here represent a promising step in the right direction.

Massaccesi et al. (2012) evaluated the metabolic changes on ^{18} F-fluoro-2-deoxyglucose positron emission tomography integrated with computed tomography (^{18} F-FDG PET-CT) performed before, during and after concurrent chemo-radiotherapy in patients with locally advanced non-small cell lung cancer (NSCLC); to correlate the metabolic response with the delivered radiation dose and with the clinical outcome. They took twenty-five NSCLC patients candidates for concurrent chemo-radiotherapy underwent ^{18} F-FDG PET-CT before treatment (pre-RT PET-CT), during the third week (during-RT PET-CT) of chemo-radiotherapy, and 4 weeks from the end of chemo-radiotherapy (post-RT PET-CT). The parameters evaluated were: the maximum standardized uptake value (SUV_{Max}) of the primary tumor, the SUV_{Max} of the lymph nodes, and the Metabolic Tumor Volume (MTV). They ended in SUV_{Max} of the tumor and MTV significantly ($p=0.0001$, $p=0.002$, respectively) decreased earlier during the third week of chemo-radiotherapy, with a further reduction 4 weeks from the end of treatment ($p<0.0000$, $p<0.0002$, respectively). SUV_{Max} of lymph nodes showed a trend towards a reduction during chemo-radiotherapy ($p=0.06$) and decreased significantly ($p=0.0006$) at the end of treatment. There was a significant correlation ($r=0.53$, $p=0.001$) between SUV_{Max} of the tumor measured at during-RT PET-CT and the total dose of radiotherapy reached at the moment of the scan. Disease progression free survival was significantly ($p=0.01$) longer in patients with complete metabolic response measured at post-RT PET-CT. **Conclusions**: In patients with locally advanced NSCLC, ^{18} F-FDG PET-CT performed during and after treatment allows early metabolic modifications to be detected, and for this c is the more sensitive parameter. Further studies are needed to investigate the correlation between the metabolic modifications during therapy and the clinical outcome in order to optimize the therapeutic strategy. Since the metabolic activity during chemo-radiotherapy

correlates with the cumulative dose of fractionated radiotherapy delivered at the moment of the scan, special attention should be paid to methodological aspects, such as the radiation dose reached at the time of PET.

Nieves Gómez León et al. (2014) reviewed ^{18}F-Fluorodeoxyglucose Positron Emission Tomography/Computed Tomography Accuracy in the Staging of Non-Small Cell Lung Cancer and Cost-Effectiveness, because Lung cancer is the most common fatal neoplasm in developed countries. Non-small cell lung cancer (NSCLC) is responsible for 80% of all deaths from this neoplasm. Despite all efforts to improve early diagnosis, survival rates remain very low (about 18% at 5 years). The stage at which NSCLC is detected is the most important of all prognostic factors and the only one that determined treatment options in our study before targeted therapy was administered. The TNM classification of malignant tumors for staging NSCLC is internationally accepted and validated. CT is currently the most commonly used technique in tumor staging. However, results, which are based on normal lymph node size, have limited value. In contrast, PET provides valuable functional information because it can detect metabolically active tumor cells. Over the last 10 years, PET has become an important tool for staging lung cancer, given its high sensitivity in the detection of lymph node involvement and distant metastasis and its current use in pre-surgical stratification of NSCLC. The combination of CT and PET makes it possible to visualize anatomical and metabolic images together, thus minimizing the limitations and maximizing the benefits of each technique individually. They aimed to compare the accuracy of PET/CT and of PET and CT alone for staging NSCLC, with histological examination as the gold standard; and to determine the cost-effectiveness of PET/CT in staging of NSCLC. They used 103 patients with histologically confirmed NSCLC. All patients were examined using PET/CT with intravenous contrast medium. Those with disease

stage ≤IIB underwent surgery (= 40). Disease stage was confirmed based on histology results, which were compared with those of PET/CT and positron emission tomography (PET) and computed tomography (CT) separately. 63 patients classified with ≥IIIA disease stage by PET/CT did not undergo surgery. The cost-effectiveness of PET/CT for disease classification was examined using a decision tree analysis. So compared with histology, the accuracy of PET/CT for disease staging has a positive predictive value of 80%, a negative predictive value of 95%, a sensitivity of 94%, and a specificity of 82%. For PET alone, these values are 53%, 66%, 60%, and 50%, whereas for CT alone they are 68%, 86%, 76%, and 72%, respectively. Incremental cost-effectiveness of PET/CT over CT alone was €17,412 quality-adjusted life-year (QALY). **Conclusion** In our clinical study, PET/CT using intravenous contrast medium was an accurate and cost-effective method for staging of patients with NSCLC.

Usmanij et al. (2013) detected the ^{18}F-FDG PET Early Response Evaluation of Locally Advanced Non–Small Cell Lung Cancer Treated with Concomitant Chemo-radiotherapy. So For 28 patients, ^{18}F-FDG PET was performed before treatment, at the end of the second week of treatment, and at 2 week and 3 month after the completion of treatment. Standardized uptake value (SUV), maximum SUV, metabolic tumor volume (MTV), and total lesion glycolysis (TLG) were obtained. Early metabolic changes were defined as fractional change (DTLG) when ^{18}F-FDG PET at the end of the second week was compared with pretreatment ^{18}F-FDG PET. In-treatment metabolic changes, as measured by serial ^{18}F-FDG PET, were correlated with standard criteria of response evaluation of solid tumors by means of CT imaging (Response Evaluation Criteria in Solid Tumors. Parameters were analyzed for stratification in progression-free survival (PFS). They ended in when

compared with early metabolic non-responders, a DTLG decrease of 38% or more was associated with a significantly longer PFS (1-y PFS 80% vs. 36%, P 5 0.02). Pretreatment TLG was found to be a prognostic factor for PFS. **Conclusion**: The degree of change in TLG was predictive for response to concomitant chemo-radiotherapy as early as the end of the second week into treatment for patients with locally advanced NSCLC. Pretreatment TLG was prognostic for PFS.

Chapter Three

3.1 Materials

All patients examined on General Electrical medical system company (GE) Discovery 710 and 690 PET/CT (64 slice), PET detectors: (9x6 lyso), CT gantry (64 slice), in Kuwait Cancer Control Center (KCCC), Kuwait city, Kuwait.

3.1.1 Patient:

156 patients are included in this study

3.1.2 Machine:

PET/CT: General Electrical medical system company (GE) Discovery 710 PET/CT (64 slice), PET detectors: (9x6 lyso), CT gantry (64 slice).

Discovery PET/CT 710 is one of the first double-digit sensitivity PET/ CT scanners, with an absolute sensitivity of 10cps/kBq1. That means the scanners are designed to collect a large number of counts and deliver fast and detailed scans at a low dose.

CT : General Electrical medical system company GE Light Speed VCT (64 slice), Whole-Body CT, 0.4 Sec Scan 64 Row (Solid State Array) HI Light Detectors Slice Widths- (mm): 1.25, Light speed (Air-Cooled) Gantry Specifications, 70cm Aperture with ± 30 Tilt Carbon Fiber Patient Couch, Laser Positioning Lights Performix Pro-Hercules 8.0MHu X Ray Tube Generator (kW): 85k/100, EXTREME Operators Console

3.2 Methods:

3.2.1 Material used to collect the data:

PET/CT: General Electrical medical system company (GE) Discovery 710 PET/CT (64 slice), PET detectors: (9x6 lyso), CT gantry (64 slice).

CT : General Electrical medical system company GE Light Speed VCT (64 slice)

3.2.2 Design of the study:

Descriptive cross sectional study where data will be collected prospectively

3.2.3 Population of the study:

The target population of this study is male and female patients with Non-small cell Lung carcinoma presented at the area of the study, age range from 20 to 90 years.

3.2.4 Sample size and type:

The data of this study consisted of 100 patients chosen conveniently

3.2.5 Place of the study:

This study will be achieved in Kuwait Cancer Control Center (Kuwait)

3.2.6 Method of data collection (technique):

PET scan: The patient receive an intravenous injection of ^{18}F-FDG according to BMI of the patient, after an initial uptake phase of an approximately one hour, a CT scan without oral or IV contrast, without breath holding at low mA level is acquired for attenuation correction and localization purposes only, arms is hold up. Subsequently PET images from vertex to mid-thigh is obtain, CT, PET and fused images are reconstructed in trans-axial, coronal and sagittal projection and interpreted from a workstation.

The CT scan used for treatment planning was acquired first using the multi-slice helical CT portion of the scanner. Axial scan will be done in all patients in supine position with different acquisition parameters to generate cross sectional views; the acquisition of FDG-PET data was then acquired without repositioning the patient.

The PET and CT data sets were transferred to a processing unit where the data sets were fused automatically using DICOM coordinates.

By comparing the effectiveness and difference between CT and PET in treatment planning system patient will do CT and we will use it in treatment planning system to localize the target volume and gross target volume and also patient will do PET and we will use it in treatment planning system to localize the target volume and gross target volume after that we will calculate the percentage of change.

3.2.7 Variable of the study:

- Patient age

-Patient body mass index (BMI)

- Patient staging include length, width, and depth and TNM classification method

- Patient gender

- Tumor grading

3.2.8 Method of data analysis:

The images are retrieved from the PACS and viewed by Clarity DICOM viewer, then the images in DICOM format were converted to JPEG image to suit IDL manipulation, then the image was read by IDL in JEPG format and the user clicks on areas represents the Tumor, Sub mucosal extension, Cardiac and lungs. The data will be analyzing by using Statistical Package for Social Studies (SPSS). CT and PET images will be analyzed by drawing ROI around the GTV, then estimate the GTV difference between them.

3.2.9 Image interpretation

The data will be analyzing by using Statistical Package for Social Studies (SPSS). CT and PET images will be analyzed by drawing ROI around the GTV, then estimate the GTV difference between them using the IDL program.

LANGUAGE IDL

IDL is the programming language of choice for many scientists and engineers because it's easy to learn, easy to use, and requires fewer lines of code than other programming languages, making it easier and faster to go from data to discovery.

The dynamically typed nature of IDL gives you more flexibility in your programming than a static language, saving you valuable time and allowing you to focus on data analysis and visualization, rather than on programming details. Because the IDL language is based on intuitive and easy-to-learn rules and conventions, you can create visualization programs and even full-blown applications with fewer lines of code. With an extensive library of prebuilt analysis and visualization routines, IDL is the choice for programmers of any experience level.

IDL is a flexible and extensible visualization, analysis, and development environment that easily integrates with the other software tools you use. IDL provides a host of ways to import code and functionality from other programming

languages and advanced methods for exporting IDL capabilities to your applications written in other languages.

IDL provides built-in support for the data sources, data types, file formats, and file sizes you use. Receive data from remote servers or write files to a disk at a remote location using common protocols. IDL acts as a client to HTTP and FTP servers, and provides access to common Open Geospatial Consortium (OGC) servers such as Web Map Service (WMS) and Web Coverage Service (WCS).

The scriptable nature of IDL makes it easy to quickly create powerful graphic visualizations, ranging from 2D plots, contours, maps, and image displays to complex, interactive 3D representations. The powerful IDL graphics engine leverages OpenGL hardware acceleration for rapid rendering. This means IDL can efficiently handle large data sets and output the graphics you need

The interactive IDL graphics system allows you to customize how your graphics look. Whether you need to include multi-byte characters (Japanese, Chinese, or Korean) or include TeX-like formatting for math and Greek annotations, IDL is suitable for creating graphics for office presentations or international publications. While other programming languages require you to reprogram or regenerate results

to make a change, with IDL you can modify line styles, symbols, annotation, font style, and color on the fly.

Programmatically or interactively output to a variety of standard image formats, like GIF, JPEG, PNG, TIFF, EPS etc. or import graphics into PowerPoint, Keynote, or HTML presentations. Additionally, graphics can be output to PostScript or PDF for inclusion in a journal article, LaTeX, or Word Document. With so many standardized output options, you can easily share your findings with colleagues for review, secondary analysis, or a verification study.

IDL MODULES

Advanced Math & Stats Module

Quickly add advanced mathematical and statistical functionality to an IDL application with the IDL Advanced Math and Stats Module. This add-on solution combines advanced data visualization and analysis capabilities with the comprehensive mathematical and statistical routines of the IMSL™ C Numerical Library — a set of pre-written mathematical and statistical algorithms that can be embedded into your program. The IDL Advanced Math and Stats Module give you the ability to directly access nearly 200 proven algorithms and routines from within the IDL environment. Additionally, you can easily call these mathematical and statistical functions from new or existing IDL applications and immediately visualize the results.

IDL Data-miner Module

IDL Data-miner is an easy-to-use add-on module to IDL that provides the technology you need for accessing, querying and editing information from common databases, including Oracle, Sybase, MySQL and more. IDL Data-miner makes IDL an even more convenient, flexible tool for scientists, engineers and application developers who do not have the time or expertise to write their own database access routines. Yet it is still advanced enough for power users to design their own SQL queries.

This ODBC (Open Database Connectivity) compliant module is an off-the-shelf solution with pre-made routines for calling databases. Now you can get the data you need, regardless of your experience level with ODBC or SQL queries.

- Retrieve the data you need without interrupting your IDL
- Create, delete, query tables
- Access, analyze, and visualize data using one tool
- Query and edit information from multiple databases simultaneously
- Automatically convert records to IDL data types
- Use a consistent API across platforms – Works with Windows and Unix

IDL Virtual Machine

The IDL Virtual Machine (IDL VM) is designed to provide IDL users with a simple, no-cost method for distributing IDL applications. This execution mode of IDL allows you to easily distribute IDL application SAVE files to your colleagues or your customers, without requiring them to own an IDL runtime license.*

IDL DICOM/Medical Solutions

IDL has played an integral part in medical imaging technology, beginning with analysis and visualization solutions for some of the first imaging modalities, and continuing with advancements today. Sophisticated software solutions developed with IDL are packaged with leading medical imaging instruments, including PET, CT, ultrasound, and MRI. Programming flexibility and advanced visualization and analysis capabilities have allowed IDL to play an integral role in medical research advances by the world's foremost laboratories and hospitals.

As a medical imaging professional, DICOM (Digital Imaging and Communications in Medicine) provides a standardized data management approach for today's medical imaging workflow, where images and data can be exchanged across hospitals or clinics or around the world in a consistent manner.

IDL offers an off-the-shelf solution that not only supports medical standards, but that also meets your medical image analysis and software development needs. IDL

offers everything you need for medical image visualization and analysis - a dynamic programming environment for application development, high-end image processing functionality, and robust, DICOM specific modules that integrate seamlessly with your current workflow.

With two add-on modules available to suit your needs - the IDL DICOM Toolkit and the IDL DICOM Network Services Module - IDL is your DICOM solution. So, whether you need to simply read and write DICOM files, or you need to add advanced network access, IDL gives you the functionality you need (Harrisgeospatial.com/Software-Technology/IDL #language).

Chapter Four

Results

	Mean	Median	STD	Min	Max	3d Quartile
Age	60.13	60.50	11.35	31	85	69
BMI	26.61	26.8	4.69	16.1	37.6	30.48
Dose	5.26	5	2.52	2	14	5

DOSE (mci) * GENDER Crosstabulation

DOSE(mci)	GENDER		Total
	Female	Male	
2	2	1	3
3	5	9	14
4	16	35	51
5	8	42	50
6	1	11	12
7	0	2	2
8	1	1	2
9	0	1	1
10	0	1	1
11	3	1	4
12	3	2	5
13	1	2	3
14	0	2	2
Total	40	110	150

LOBE * GENDER Crosstabulation

LOBE	GENDER		Total
	Female	Male	
Right	21	73	94
Left	19	37	56
Total	40	110	150

Number of lesion * GENDER Crosstabulation

Number of lesion	GENDER		Total
	Female	Male	
1	28	70	98
2	9	30	39
3	3	9	12
Total	40	109	149

Table 4.1 Show demographic information for all patients:

Variables	Male	Female
Age	61.29 ± 10.40	57.28 ± 13.52
BMI	26.69 ± 4.89	27.98 ± 6.81

demographic information for all patients according to their gender presented as mean ± STD, for the age the mean was 61.29 ± 10.40 and 57.28 ± 13.52 years for male and female respectively, and the Body mass index for male was 26.69 ± 4.89 and for female 27.98 ± 6.81 kg/cm2.

Table 4.2 shows parameters of scan and the activity dose:

Variables		Variables	
Tube Potential	120 or 140	Collimation	16 or 32
Tube current	93.72 ± 35.81	Turn	4.9 ± 0.9
Table feed	16.43 ± 1.5	$CTDI_w$	4.43 ± 1.94
Pitch	1.02 ± 0.09	$CTDI_{vol}$	4.17 ± 1.83
Slice thickness	2.5 or 5	DLP	177 ± 71.62
Scan length	80.57 ± 14	Activity	5.35 ± 2.48

The parameters of scan divided to dose and table movement, the dose parameters such as tube potential, tube current, $CTDI_w$, $CTDI_{vol}$ and dose length product, and the table movement parameters the scan length, table feed and pitch. Were the data presented as mean ± standard deviation? For tube potential, tube current, table feed, pitch, slice thickness, scan length, collimation and the turn was 120 or 140, 93.72 ± 35.81, 16.43 ± 1.5, 1.02 ± 0.09, 2.5 or 5,80.57 ± 14, 16 or 32 and 4.9 ± 0.9 respectively. The dose parameters was $CTDI_w$, $CTDI_{vol}$ and DLP was 4.43 ± 1.94, 4.17 ± 1.83 and 177 ± 71.62 respectively. While the activity was 5.35 ± 2.48 mCi.

The average effective dose from computed tomography examinations was 3.17 mSv and for male and female was 2.89±1.13 and 3.93±1.71 mSv respectively. For dose internally administered ^{18}F-FDG was 3.75 and for male and female was 3.78±1.79 and 3.71±1.63 respectively. While the internally administered ^{18}F-FDG for the whole-body PET/CT examination was 6.93 mSv and for male and female was 6.66±2.38 and 7.64±2.42 mSv respectively.

CT			PET			Total		
Male	Female	Total	Male	Female	Total	Male	Female	Total
2.89 ± 1.13	3.93 ± 1.71	3.17 ± 1.39	3.78 ± 1.79	3.71 ± 1.63	3.75 ± 1.74	6.66 ± 2.38	7.64 ± 2.42	6.93 ± 2.42

Table 4.3: The average effective dose from computed tomography examinations and PET

Organ	Male		Female		Total	
	Mean	Std. Dev	Mean	Std. Dev	Mean	Std. Dev
Thyroid	6.653	2.8530	3.432	1.7018	5.786	2.9492
Breasts	.044	.4688	7.412	3.4563	2.028	3.7392
Esophagus	6.253	2.6652	6.875	3.1950	6.420	2.8115
Lungs	6.655	2.8274	7.230	3.3572	6.810	2.9695
Liver	5.032	1.8604	5.903	2.5691	5.267	2.0954
Stomach	4.717	1.6216	5.603	2.3674	4.955	1.8794
Kidneys	4.055	1.1827	5.097	2.0133	4.335	1.5141
Gall bladder	4.502	1.7810	5.331	2.3963	4.725	1.9855
Heart	5.823	2.4736	6.164	2.8668	5.915	2.5720

Table 4.4: Organs absorbed dose and difference between male and female.

Since the range is from apex of the lung end at upper of abdomen, a number of organs received substantial dose. A detailed assessment of organ dose distribution within the human body for whole body is given in Table 4.4. Focusing on thyroid and breast were the average was 5.78 and 2.03 respectively.

With the increasing use of ionizing radiation in the nuclear medicine and radio-diagnostic examinations, estimates of patient (absorbed) dose receives greater seem to have any threshold [1,2]. Since the estimated patient dose is dependent on several factors viz. machine parameters,

The features extracted from PET/CT images using Second order statistic and All these features were calculated for all images and then the data were ready for discrimination which was performed using step-wise technique in order to select the most significant feature that can be used to classify the lung cells from PET/CT images and the results show that:

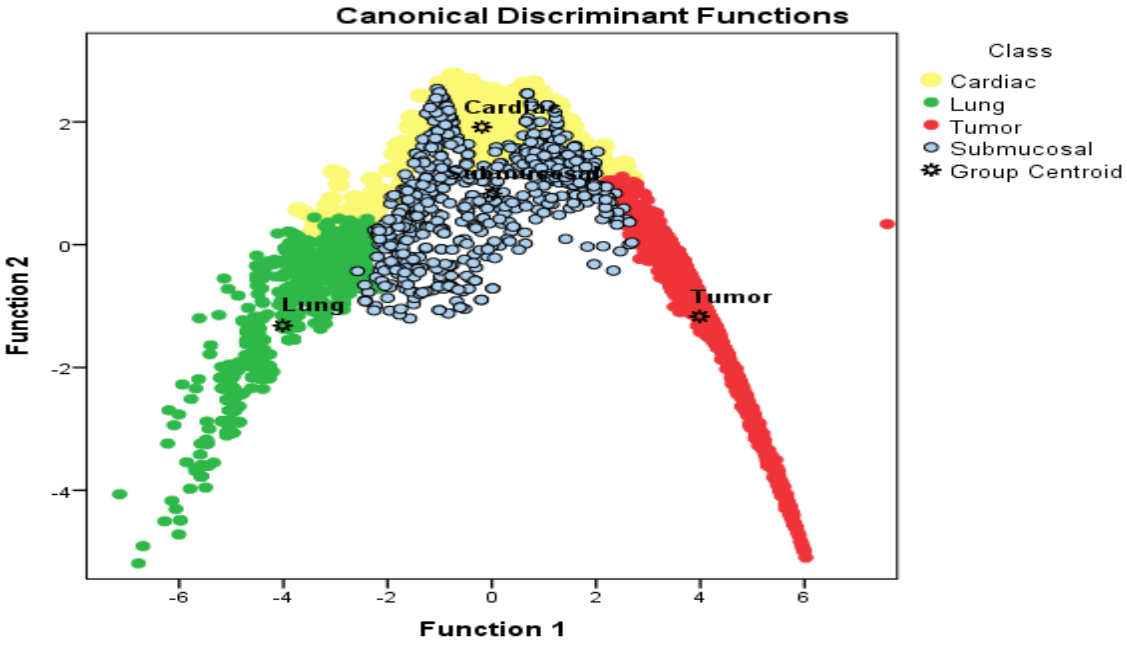

Figure 4.1: Scatter plot generated using discriminate analysis function for four classes represents: Cardiac, lung, tumor, submucosal

The classification showed that the lung cells were classified well from the rest of the tissues although it has characteristics mostly similar to surrounding tissue.

Table 4.5: Showed the classification accuracy of the lung cells using linear discriminant analysis:

Classes		Predicted Group Membership				Total
	Original groups	Cardiac	Lung	Tumor	Submucosal	
%	Cardiac	91.6	7.4	0.1	0.9	100.0
	Lung	0.0	100.0	0.0	0.0	100.0
	Tumor	0.1	.0	99.6	0.4	100.0
	Submucosal	4.8	3.7	0.3	91.2	100.0

96.0% of original grouped cases correctly classified

Table (1) show classification score matrix generated by linear discriminate analysis and the overall classification accuracy of lung cells 96.0%, were the classification accuracy of cardiac 91.6%, lung accuracy 100%, the tumor 99.6%, While the submucosal showed a classification accuracy of 91.2%.

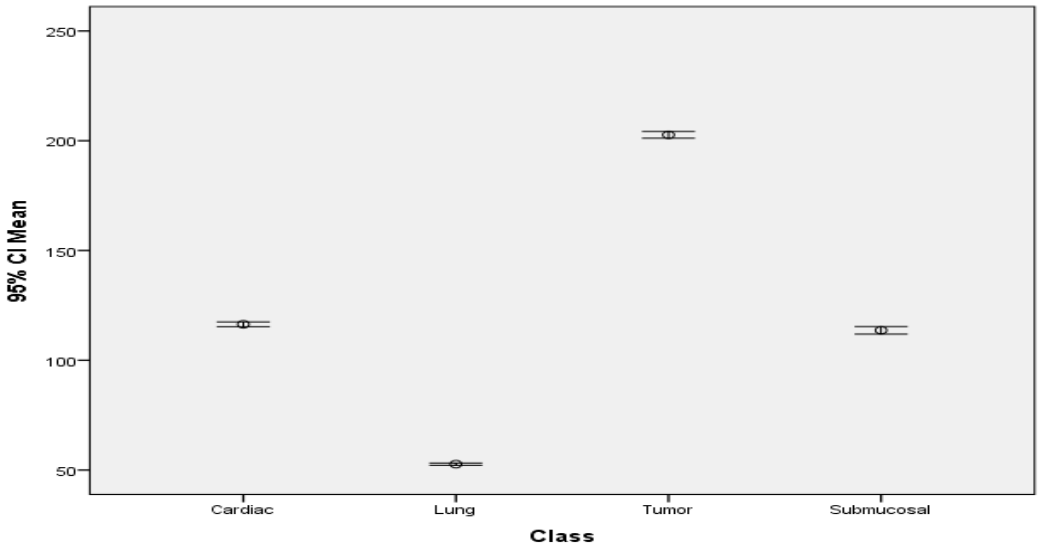

Figure 4.2 show error bar plot for the CI mean textural features that selected by the linear stepwise discriminate function to discriminate between all features. From the discriminate power

point of view in respect to the applied features the mean can differentiate between all the classes successfully.

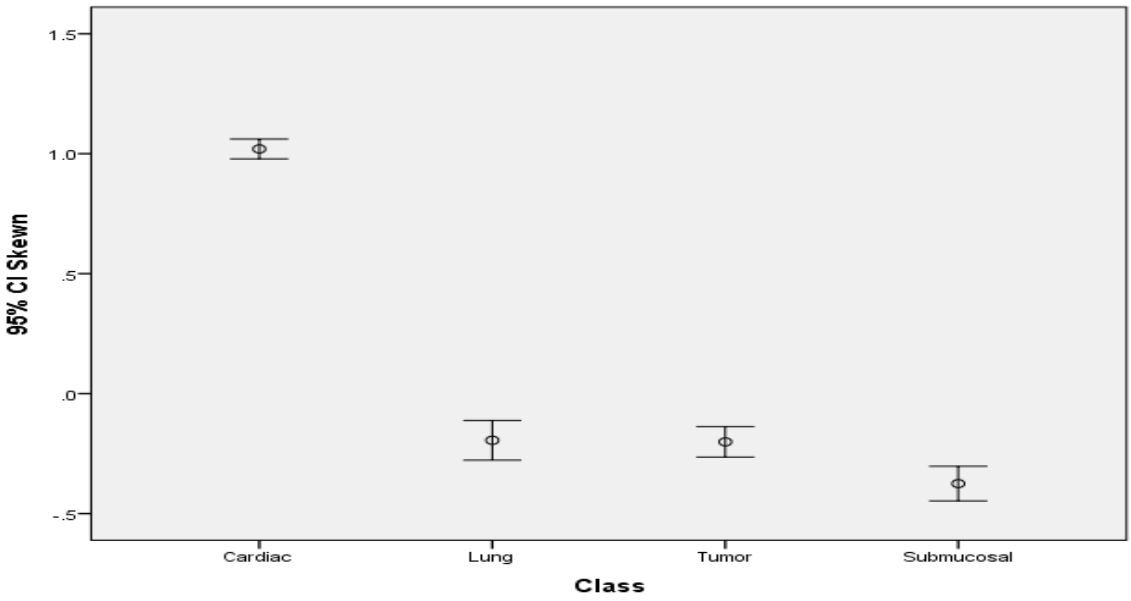

Figure 4.3 show error bar plot for the CI skewness textural features that selected by the linear stepwise discriminate function to discriminate between all features. From the discriminate power point of view in respect to the applied features the skewness can differentiate between all the classes successfully**.**

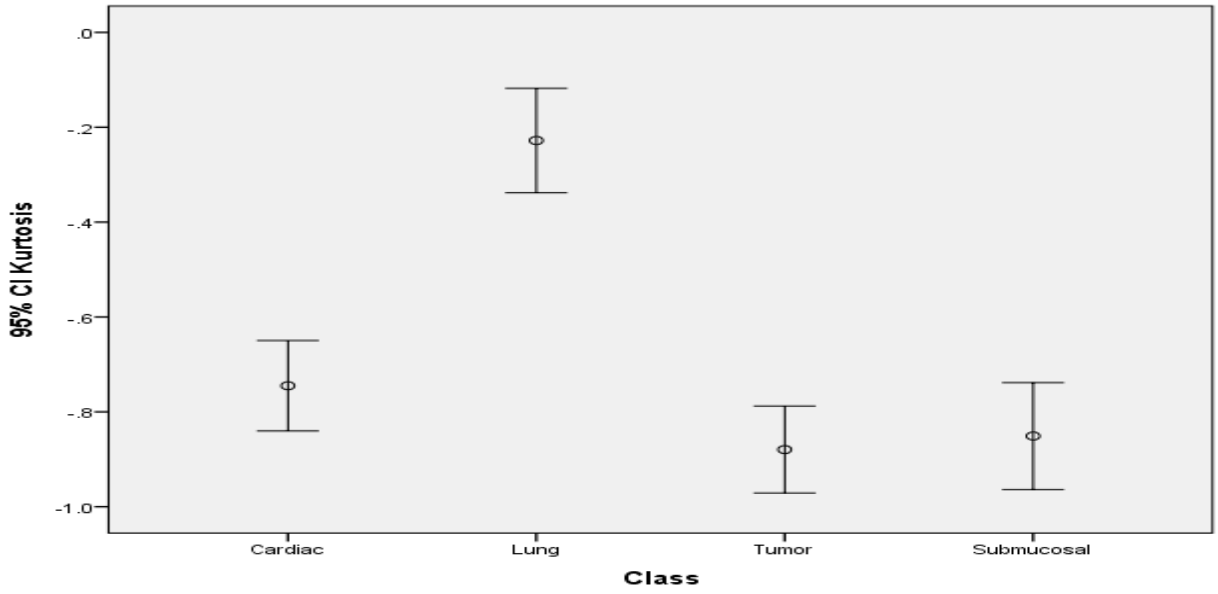

Figure 4.4 show error bar plot for the CI kurtosis textural features that selected by the linear stepwise discriminate function as a discriminate feature where it discriminate between all features.

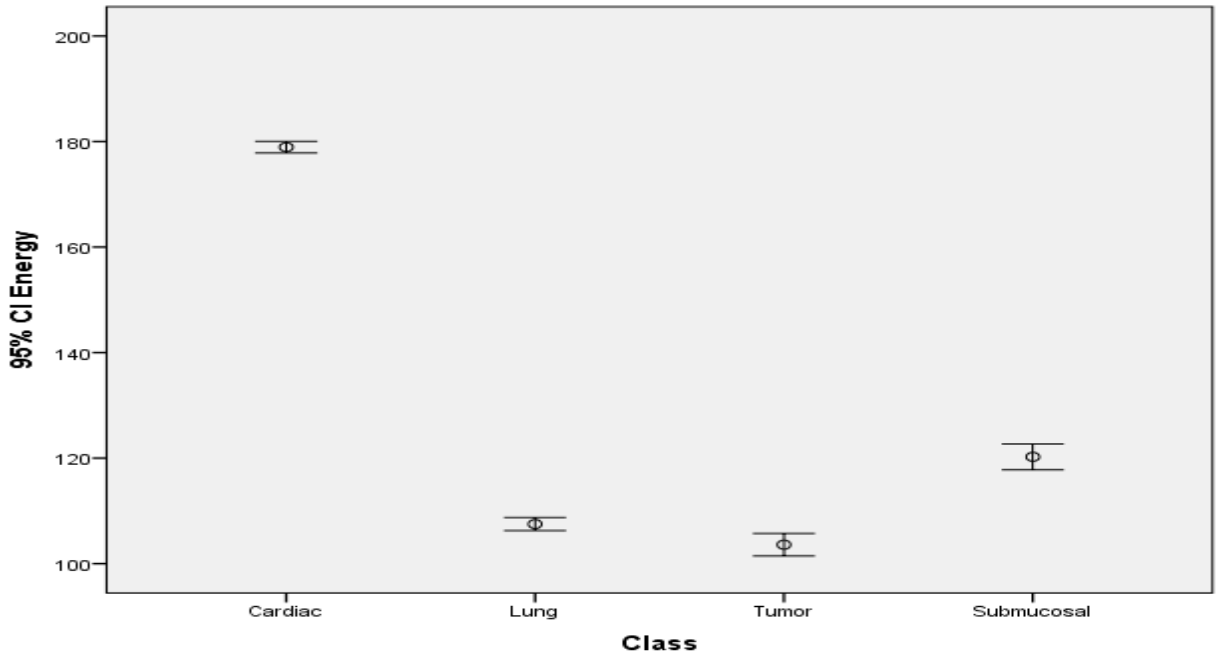

Figure 4.5 show error bar plot for the CI energy textural features that selected by the linear stepwise discriminate function where it discriminate between all features.

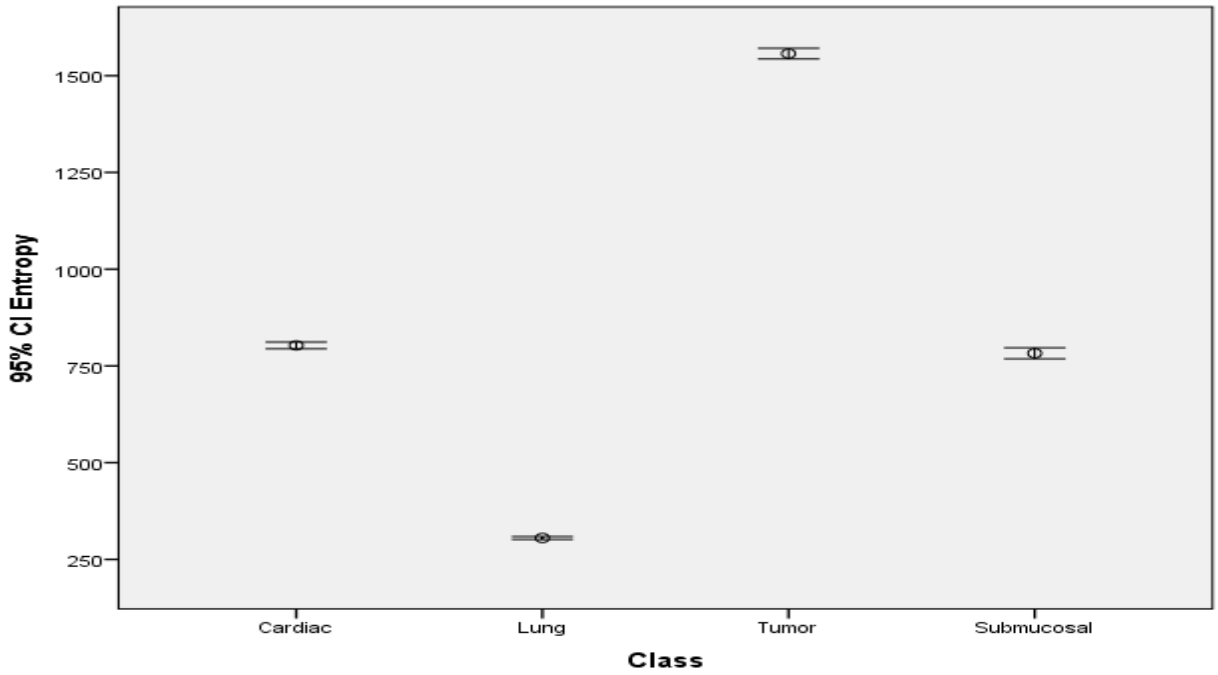

Figure 4.6: show error bar plot for the CI entropy textural features that selected by the linear stepwise discriminate function as a discriminate feature between all features.

From the discriminate power point of view in respect to the applied features the entropy can differentiate between all the classes successfully. comparable with previous study in texture analysis; Suhaib Alameen et al 2017 [10], Characterization of Hepatocellular Carcinoma in CT Images using Gray Level Run Length Matrix Several texture features are introduced from (GLRLM) and the classification accuracy of hepatocellular carcinoma 98.8%, liver accuracy 85.2 %, While the spine and ribs showed a classification accuracy of 75.3 % respectively. Total classification accuracy 85.4%

Einas M. Ahmed 2017 [11] discussed the assessment of Quality Control Uniformity & linearity of SPECT Gamma Camera using Image Processing, and the result showed that the resolution for minimum object used 4mm was 70% and increased with object size increased to reach 100% resolution for an object size of 10 mm i.e. 100% resolution corresponds to the coordinate of the MTF at 10% and frequency of 0.05cycle /mm. In conclusion the developed algorithm can be used objectively and improved as required without looking for expertise from other country, as well it can be made to check the acceptance of the device performance regardless the built-in programs.

Texture analysis depending on the relative attenuation coefficient of tissues and can used to avoid invasive technique if the base line for individual tissues being determined and algorithmic aided computer have been applied.

Chapter Five

5-1 Discussions:

No one denies the big need of radiological examination to stage and follow up the cancer patients, among that the PET/CT is playing a great role in diagnosis and staging the cancer and efficiency of treatment.

Radiotherapy is one of important choice for treatment of non-small cell lung carcinoma and the radiotherapy planning using the PET/CT is adding a huge values and precision to treatment efficiency.

In this study, performed for 150 patients, male and female with diagnosis of Non-Small Cell Carcinoma who are presented for PET/CT whole-body either for staging or follow-up.

Table 4-1 shows the final statistics and the study variable which include the age, the Body Mass Index (BMI), Fasting Blood Sugar (FBS), the dose of Fluorodeoxyglucose (FDG) and Standard Uptake Values (SUV).

Table 4-2 present patient's gender distribution, show that the male patient has higher rate 26.7:73.3 % female to male.

Table 4-3 shows the percentage of affected lung lobe among the NSCLC patients, which shows that right lobe has the higher rate 62.7:37.3 % right lobe to left lobe of lung.

Table 4-4 shows the values of Fasting Blood Sugar (FBS) in mg/dl of the patients which is checked before starting the PET/CT procedure, and it ranges from 4 till 16 mg/dl, put in mind that FBS has great effect in the distribution and absorption of FDG dose.

Table 4-5 shows the percentage of injected FDG dose values and its frequency between the patients which range between 2 mCi till 14 mCi, most patients injected according to Body Mass Index (BMI). Also in other way Figure 4-5 shows scatter plot generated using discriminate analysis function of dose in mCi and BMI, $y = 0.1739x + 0.6542$.

Table 4-6 shows the percentage of number of lesions per every patient and its frequency, which vary 1, 2 and 3 lesions with percent of 65.3, 26, 8 % respectively

Table 4-7 and figure 4-1 shows the comparison and variance between the injected FDG doses which varies between 2 mCi (millicurie) to 14 mCi and patient gender (male or female), high doses goes to male.

Table 4-8 is LOBE-GENDER cross tabulation and Figure 4-2 which shows the comparison and occurrence between the affected lobe of lung and patient gender, for female 52.5%, 47.5% is for right and left lobe respectively, for male 66.3%, 33.7% is for right and left respectively.

Table 4-9 is FBS*GENDER cross tabulation and Figure 4-3 which shows variance of FBS (Fasting Blood Sugar) in mg/dl which varies from 4mg/dl to 14mg/dl versus patient gender and high FBS level is among male more than female.

Table 4-10 is NUMBER OF LESION*GENDER cross tabulation and the figure 4-4 which shows the variance of number of lesion through patient gender.

Figure 4-6 is a scatter plot generated using discriminate analysis function shows the relation between the Standard Uptake Value (SUV) and the BMI, $y = 0.0927x + 14.498$.

Figure 4-7 is scatter plot generated using discriminate analysis function which demonstrates the relation of Body Mass Index (BMI) in Fasting Blood Sugar (FBS), $y = 0.0163x + 6.5282$, $R^2 = 0.0012$.

Figure 4-8 is scatter plot generated using discriminate analysis function of FDG dose and patient's age, $y = 0.0128x + 4.5156$, $R^2 = 0.0034$.

Figure 4-9 is scatter plot generated using discriminate analysis function relationship between the patient's age and Fasting Blood Sugar (FBS),

$y = 0.0587x + 3.4298$.

Figure 4-10 is scatter plot generated using discriminate analysis function of Standard Uptake Value (SUV) and patients age, $y = 0.0658x + 8.0756$.

5-2 Conclusions:

The classification processes of non-small cell lung carcinoma gross target volume with fluorine-18 fluorodeoxyglucose in KCCC were defining the lung area to cardiac, lung, tumor and submucosal and carried out using Interactive Data Language (IDL) program as platform for the generated codes. The result of the classification showed that the lung tissues were classified well from the rest of the tissues although it has characteristics mostly similar to surrounding tissue.

Several texture features are introduced from Gray Level Co-occurrence Matrix (GLCM) and the classification score matrix generated by linear discriminate analysis and the overall classification accuracy of image regions 96%, and the classification accuracy of cardiac 91.6%, lung 100%, tumor 99.6%, while the submucosal showed accuracy 91.2%.

Using linear discrimination analysis generated a classification function which can be used to classify other image into the mention classes as using the following multi regression equation;

Cardiac = (Mean * 11.905) + (Skewness * -3.887) + (Energy *-0.004) + (Entropy * 1.363) - 145.247
Lung = (Mean * 9.401) + (Skewness * -4.229) + (Energy *-0.034) + (Entropy * 1.344) -81.525
Tumor = (Mean * 11.964) + (Skewness * -3.968) + (Energy *-0.104) + (Entropy * 1.344) - 162.757
Sub-mucosal = (Mean * 12.565) + (Skewness * -5.213) + (Energy *-0.079) + (Entropy * 1.441) - 147.494

On the other hand an estimate of patient's dose from ^{18}F-FDG Whole-Body is done, the dose calculations using RADAR Medical Procedure Radiation Dose Calculator to estimate the effective dose, for 156 patients (110 male and 40 female) were examined by Discovery PET/CT 710, GE Medical Systems in Kuwait Cancer Control Center using ^{18}F-FDG Whole-Body PET/CT.

The results provide that there is no difference demonstrates in the effective dose from ^{18}F-FDG in male and female patients. And recommended that all the clinical practice should be justify and be careful about the concept risk-benefit ratio to any and efforts ^{18}FDG whole-body PET/CT scan.

5-3 Recommendations:

1-PET/CT should be introduced in Sudan.

2-More research should be done in same topic with more data so the results will be more accurate and the variance will be good.

References:

Abdullah Behzadi; Yee Ung; Val Lowe; Claude Deschamps: The role of positron emission tomography in the management of non–small cell lung cancer. Canadian Medical Association, Canadian *Journal of Surgery*, Vol. 52, No. 3, (June 2009).

Alexander C. Mamourian; CT IMAGING PRACTICAL PHYSICS, ARTIFACTS, AND PITFALLS, (2013), New York.

Anna Person: Anatomy and Physiology of the Respiratory Tract Current Clinical Practice: Disorders of the Respiratory Tract: Common Challenges in Primary Care By: M. L. Mintz © Humana Press, Totowa, NJ (2006).

Ann Barrett, Jane Dobbs, Stephen Morris, Tom Roques; Practical Radiotherapy Planning, Fourth edition (2009). UK London, ISBN 978 034 0927731.

Azadeh Abravan; Hanne Astrid Eide; Ingerid Skjei Knudtsen ; Ayca Muftuler Løndalen ; Åslaug Helland ; Eirik Malinen: Assessment of pulmonary 18F-FDG-PET uptake and cytokine profiles in non-small cell lung cancer patients treated with radiotherapy and erlotinib. Clinical and Translational Radiation Oncology, *European Society for Radiotherapy and Oncology* (2017) 2405-6308.

Christoph Po¨ ttgen; Sabine Levegru¨n;DirkTheegarten; SimoneMarnitz; Sara Grehl; Roman Pink; Wilfried Eberhardt; Georgios Stamatis; Thomas Gauler; Gerald Antoch; Andreas Bockisch; Martin Stuschke: Value of 18F-Fluoro-2-Deoxy-D-Glucose-Positron Emission Tomography/Computed Tomography in Non-Small-Cell Lung Cancer for Prediction of Pathologic Response and Times to

Relapse after Neo-adjuvant Chemo-radiotherapy. American Association for Cancer Research, Clinical Cancer Research (2006) 10.1158/1078-0432.CCR-05-0510.

Daniel N. DeMaio; MOSBY'S EXAM REVIEW FOR COMPUTED TOMOGRAPHY, SECOND EDITION (2011) 978-0-323-06590-0.

Edwin A. Usmanij; Lioe-Fee de Geus-Oei; Esther G.C. Troost; Liesbeth Peters-Bax; Erik H.F.M. van der Heijden; Johannes H.A.M. Kaanders; Wim J.G. Oyen; Olga C.J. Schuurbiers; and Johan Bussink: 18F-FDG PET Early Response Evaluation of Locally Advanced Non–Small Cell Lung Cancer Treated with Concomitant Chemo-radiotherapy. *THE JOURNAL OF NUCLEAR MEDICINE* • Vol. 54 • No. 9 • (September 2013). 54:1–7.

Elaine M. Zeman, Eric C. Schreiber, and Joel E. Tepper; Science of Clinical Oncology, Basics of Radiation Therapy, (2014) ISBN 978-1-4557-2865-7.

Food and agriculture organization of the United Nations, international atomic energy agency, international labor organization, oecd nuclear energy agency, pan American health organization, world health organization, international basic safety standards for protection against ionizing radiation and for the safety of radiation sources, safety series no. 115, iaea, vienna (1996).

Fowler, L. S, Wolf, A. P, *Applied, Radiation and. Isotopes*, 1986, 77, 663.

Gigirey,V; Servente, L; Fontes, M ; Escudero, B ; Campos, A; Durand, E; Alonso, O: EVALUATION OF ^{18}F-FDG PET/TC FOR MEDIASTINAL STAGING OF BRONCHOPULMONARY CARCINOMA. *Colegio Interamericano de Radiología*.

Harrisgeospatial.com/Software-Technology/IDL #language

Harsh Mohan: Textbook of pathology. Sixth edition Chandigarh New-Delhi- INDIA (2010).

Hongjiang Yan; Renben Wang; Fen Zhao; Kunli Zhu; Shumei Jiang; Wei Zhao; and Rui Feng: Measurement of tumor volume by PET to evaluate prognosis in patients with advanced non-small cell lung cancer treated by non-surgical therapy. *Acta Radiologica* 2011; 52: 646–650. DOI: 10.1258/ar.2011.100462.

James E. Martin; Physics for Radiation Protection: A Handbook. Copyright _ 2006 WILEY-VCH Verlag GmbH & Co. KGaA, Weinheim ISBN: 3-527-40611-5

Jianhua Yan; Zhifang Wu; Sijin Li: Extremely low dose 18F-FDG PET imaging and its potential use for lung cancer screening. Translational Cancer Research (2017); 6(Suppl 1):S99-S101, 10.21037/tcr.2017.01.22.

J. GORDON BETTS: Textbook Anatomy and Physiology by Rice University licensed under a Creative Commons Attribution 4.0 International License Open Stax publication Houston, Texas (March 6, 2013).

Karp JS, Daube Witherspoon ME, Hoffman EJ et al: Performance standards in positron emission tomography. Journal of Nuclear Medicine 32, 2342-50, 1991.

Kenneth J. Biehl; Feng-Ming Kong; Farrokh Dehdashti; Jian-Yue Jin; Sasa Mutic ; Issam El Naqa ; Barry A. Siegel; and Jeffrey D. Bradley :18F-FDG PET Definition of Gross Tumor Volume for Radiotherapy of Non–Small Cell Lung Cancer: Is a Single Standardized Uptake Value Threshold Approach Appropriate? *THE JOURNAL OF NUCLEAR MEDICINE* • Vol. 47 • No. 11, 47:1808–1812 (November 2006).

Ilgin Sahiner; Gulin Ucmak Vural: Positron emission tomography/computerized tomography in lung cancer. *Quantitative Imaging in Medical Surgery* (2014) 223-4292.

Lioe-Fee de Geus-Oei; Henricus F.M. van der Heijden; Frans H.M. Corstens; Wim J.G. Oyen: Predictive and Prognostic Value of FDG-PET in Non-small-Cell Lung Cancer. *American Cancer Society October* (2007) / Volume 110 / Number 8. 10.1002/cncr.22979.

Matthew. L. Mintz: Current Clinical Practice: Disorders of the Respiratory Tract: Common Challenges in Primary Care © Humana Press, Totowa, NJ) (2006).

Matthew R. Acker; Steven C. Burrell: Utility of 18F-FDG PET in Evaluating Cancers of Lung *JOURNAL OF NUCLEAR MEDICINE TECHNOLOGY* VOLUME 33, NUMBER 2, 33:69–74 JUNE 2005.

Mathieu Hatt; Catherine Cheze-le Rest; Angela van Baardwijk; Philippe Lambin; Olivier Pradier; Dimitris Visvikis: Impact of Tumor Size and Tracer Uptake Heterogeneity in ^{18}F-FDG PET and CT Non–Small Cell Lung Cancer Tumor

Delineation *THE JOURNAL OF NUCLEAR MEDICINE* • Vol. 52 • No. 11 • 52:1690–1697 November 2011.

Mariangela Massaccesi; Maria Lucia Calcagni; Maria Grazia Spitilli; Fabrizio Cocciolillo; Francesca Pelligrò; Lorenzo Bonomo; Vincenzo Valentini; and Alessandro Giordano: 18 F-FDG PET-CT during chemo-radiotherapy in patients with non-small cell lung cancer: the early metabolic response correlates with the delivered radiation dose. *Radiation Oncology* (2012), 7:106.

Mettler. Fred. A; Upton, Arthur. C, medical effects of ionizing radiation, 2nd edition, saunders publishing, philadelphia, pa (1996) ispn978-0721602004.

Michael E. Phelps: PET PHYSICS, INSTRUMENTATION, AND SCANNERS. (2006) 13: 978-0387-32302-2.

Michael I. Lewis, Robert J. McKenna; *Medical Management of the Thoracic Surgery Patient*, (2010), ISPN 978-1-4160-3993-8, Saunders publishing Philadelphia.

N. Hollings, P. Shaw: Diagnostic imaging of lung cancer. *European Respiratory Journals* 0903-1936 (2002).

Nieves Gómez León ; Sofia Escalona ; Beatriz Bandrés; Cristobal Belda; Daniel Callejo ; and Juan Antonio Blasco: 18F-Fluorodeoxyglucose Positron Emission Tomography/Computed Tomography Accuracy in the Staging of Non-Small Cell Lung Cancer: Review and Cost-Effectiveness. *Hindawi Publishing Corporation, Radiology Research and Practice* Volume 2014, Article ID 135934.

Pawinee Mahasittiwat ; Shuanghu Yuan ; Congying Xie ; Timothy Ritter ; Yue Cao ; Randall K. Ten Haken ; Feng-Ming Spring Kong : Metabolic tumor volume on PET reduced more than gross tumor volume on CT during radiotherapy in patients with non-small cell lung cancer treated with 3DCRTor SBRT. *Journal of Radiation Oncology* (2013) 2:191–202.

P M PRICE; M M GREEN: Positron emission tomography imaging approaches for external beam radiation therapies: current status and future developments. *The British Journal of Radiology*, 84 (2011. 10.1259/bjr/21263014.

REMGE M. PIETERMAN; JOHN W.G. VAN PUTTEN; JACOBUS J. MEUZELAAR; EDUARD L.MOOYAART; WILLEM VAALBURG; GERARD H. KOËTER; VACLAV FIDLER; JAN PRUIM; HARRY J .M. GROEN: PREOPERATIVE STAGING OF NON–SMALL-CELL LUNG CANCER WITH POSITRON-EMISSION TOMOGRAPHY. *The New England Journal of Medicine* (July 27, 2000) 343:254-61.

Sorensen J.A., Phelps M.E.: Physics in Nuclear Medicine, Second edition. Grune &Stratton, 1987.

Tira Bunyaviroch; R. Edward Coleman: PET Evaluation of Lung Cancer. THE *JOURNAL OF NUCLEAR MEDICINE* • Vol. 47 • No. 3 • (March 2006).

Ursula Nestle; Stephanie Kremp; Andrea Schaefer-Schuler,; Christiane Sebastian-Welsch,; Dirk Hellwig,; Christian Ru¨be; and Carl-Martin Kirsch: Comparison of Different Methods for Delineation of ^{18}F-FDG PET–Positive Tissue for Target Volume Definition in Radiotherapy of Patients with Non–Small Cell Lung Cancer.

THE JOURNAL OF NUCLEAR MEDICINE • Vol. 46 • No. 8 • 46:1342–1348 (Aug 2005).

Vincent Gr´egoire; Karin Haustermans; Xavier Geets; Sarah Roels; and Max Lonneux: PET-Based Treatment Planning in Radiotherapy: A New Standard. *Journal of Nuclear Medicine* (2007); 48:68S–77S.

Wienhard. K, Dahlbom. M, Eriksson L et al: The ECAT EXACT HR: Performance of a new high resolution positron scanner. *Journal of Computer Assist Tomographic* 18(1), 110-118, (1994).